0.7 Anomaly of Quantum Point Contacts
Treatment of Interaction with functional Renormalization Group

Florian Bauer

München 2008

0.7 Anomaly of Quantum Point Contacts
Treatment of Interaction with functional Renormalization Group

Florian Bauer

Erstgutachter: Professor Jan von Delft
Zweitgutachter: Professor Gerhard Buchalla

Contents

List of Figures

Deutsche Zusammenfassung

Diese Arbeit beschäftigt sich mit der 0.7 Anomalie im Leitwert von Quantenpunktkontakten (QPCen). Hierbei wird die Wechselwikung mit einer erst kürzlich entwickelten Methode, der Funktionalrenormierungsgruppe (fRG) behandelt.

Bei QPCen ist der Leitwert in Einheiten von $g_0 = \frac{2e^2}{h}$ quantisiert. Dies wurde schon 1957 von Landauer vorhergesagt und 1988 experimentell bestätigt [5, 10]. Zusätzlich zu dieser Quantisierung fand man 1996 eine Zwischenstufe bei $0,7g_0$ [6], die unter dem Namen 0.7 Anomalie bekannt wurde. Diese hängt in einer ganz bestimmten Art und Weise von der Gatterspannung, dem angelegten magnetischen Feld, der Temperatur und der Transportspannung ab, was in Kapietel 2 erläutert wird. Man ist sich einig, dass dieser Effekt auf Vielteilchenwechselwirkung zurückzuführen ist, jedoch wurde noch kein Modell gefunden, dass alle Aspekte dieses Effekts beschreiben kann.

In Kapitel 3 werden die fRG-Flussgleichungen hergeleitet, wobei ich mich im Wesentlichem auf das Vorlesungskript von Prof. Volker Meden [11] stütze und versuche alle Konventionen zu übernehmen. Die fRG-Methode basiert auf einem Infrarotcutuff im freien Propagators, bezüglich dessen Differentialgleichungen in der Selbstenergie und Vertexfunktionen höherer Ordnung hergeleitet werden. Die angewandten Vereinfachungen führen dazu, dass die numerischen Resultate nur im Limes von Null Temperatur und Transportspannung gültig sind. Daraufhin wird besprochen, wie fRG auf wechselwirkende Quantendrähte anzuwenden ist (Kapitel 4).

Bei den numerischen Ergebnissen in Kapitel 5 konzentriere ich mich zunächst auf Quantenpunkte (QDe) und untersuche die Gültigkeit der Methode im Vergleich mit numerischen Daten, die mit der quasi-exakten Numerischen Renomierungsgruppe erzeugt wurden. Schließlich werden numerische Ergebnisse füe QPCe vorgestellt, wobei der Kontakt mittels einer Barriere im Potential dargestellt wird. Es werden alle zu erwartenden Eigenschaften reproduziert. Im Einzelnen sind das: (i) Der pinch-off Wert in der Gatterspannung wird durch das magnetfeld kaum beeinflusst. (ii) Ausserdem ergibt sich für hohe Magnetfelder ein erhöter g-Faktor und (iii) der Rauschfaktor als Funktion des Leitwerts für verschiedene Magnetfelder zeigt qualitative Übereinstimmung mit dem Experiment. Das wichtigste Resultat ist jedoch, dass sich (iv) für kleine Werte der Zeemanenergie die nicht Spin-entartete Stufe im Leitwert von "oben herab" entwickelt. Dabei entsteht für bestimmte Werte des Magnetfeldes eine Zwischenstufe bei knapp $0,7g_0$.

Chapter 1

Introduction

In 1957 Landauer predicted that the electrical conductance of a narrow one dimensional wire is quantized in units of $g_0 = 2\frac{e^2}{h}$, where e is the electron charge and h is Planck's constant. It took over 30 years until the conductance quantization was first observed in 1988 simultaneously by van Wees et al. [5] and Wharam et al. [10].

Now, 20 years later, many body effects in short quantum wires, also called quantum point contacts (QPCs), are still an important issue. The most important is the so called 0.7 anomaly, an additional shoulder-like step at around $0.7g_0$, that arises in the conductance as the point contact is made so narrow that the last transport channel is closed, first observed in 1996 by Thomas et al. [6]. Although a huge number of prevailing phenomenological models have been proposed to explain this anomaly, and its rich and complex dependence on gate voltage, magnetic field, temperature and source-drain voltage, no consensus has yet been found. The most established models are the spontaneous spin polarization [12] and Kondo related models [7]. But, to the best of our knowledge, no attempt has yet been made to study the 0.7 anomaly with a theoretical tool sufficiently powerful to adequately incorporate all relevant ingredients, namely (i) electron-electron interactions (ii) the spin degrees of freedom (iii) spin-dependent correlations and (iv) the geometry (width, length, shape) of the quantum point contact, within a single, consistent, theoretical framework.

In this work we use an auspicious method, namely the functional Renormalization Group, which is able to treat interacting systems while taking into account microscopic details. This method is based on a functional field integral representation of the partition function with an additional infrared cutoff in the free propagator. Deriving an differential equation with respect to this cutoff leads to coupled flow equations of the self energy and higher order vertices. Solving this differential equation provides an effective noninteracting system.

We will show that a one dimensional interacting wire with potential barrier representing the QPC yields results for the dependence of the conductance on gate voltage and magnetic field that are in qualitative agreement with experiment. This leads us to conclude that the theoretical framework developed here is, in principle, appropriate for describing the 0.7 anomaly, although much further work theoretical will be required to also investigate its dependence on temperature and source-drain voltage.

The outline of this thesis is as follows:

- In chapter 2 we give a phenomenological overview of strong correlation effects for quantum dots and quantum point contacts. The former is included because of the Kondo related model of the 0.7 anomaly.

- In chapter 3 we develop the fRG flow equation for interacting systems, and state the approximations one has to make to implement the differential equations.

- How one can use the fRG method to describe one dimensional interacting QWRs with a smoothly varying local potential is described in chapter 4. We give an introduction to one dimensional tight binding chains, which we use to set up the flow equations. Furthermore we specify how the results can be used to calculate observables.

- We present results of the numerics in chapter 5. First we concentrate on QDs to sort out the validity of the approximations we made. In the last section we turn to QPCs and present details of the dependence of the conductance on gate voltage and magnetic field.

- In the last chapter we conclude the present work, and give an outlook an futur topics.

Chapter 2

Overview of the Physically relevant Aspects

In the last decades the progress in nano fabrication made it possible for experimentalists to study many body phenomena for geometries where the typical length scale is in order of the Fermi length. In such systems the electrons start to "feel" the boundaries: If in one of the three spatial dimensions, which usually defines the z-direction, electrons are trapped in a potential, so narrow that only the lowest resulting eigenstate (of the motion in the z-direction) is occupied, then the time evolution in z-direction is only affected by the lowest eigenenergy, which only produces some overall phase-factor. As a result, the dynamics of the system is essentially independent of the z-direction, and governed entirely by the motion in the other two dimensions. Such systems thus form a so-called two dimensional electron gas (2DEG). It is usually realized by a GaAs/AlGaA hetero structure. A constriction of the movement in one or both of the two remaining dimensions produces one and zero dimensional systems.

One-dimensional systems are called Quantum Wires (QWRs). Wires where the elastic mean free length l_e is much smaller then the length L are called diffusive. Electrons that pass such wires are scattered several times before they reach the other end. If $L \ll l_e$ the wire is called ballistic. It forms only a point-like contact between two reservoirs, hence it is called Quantum Point Contact (QPC). A good realization is a 2DEG with a top-gate geometry as the one in figure 2.4 left panel. The advantage over other structures is that one can control the effective width w of the wire via the applied gate voltage V_g.

Zero-dimensional systems are called Quantum Dots (QDs). If the charging energy E_C is comparable with the Fermi temperature they are also called Single Electron Transistors (SETs). One possibility to realize tunable QDs are lateral QDs. They are also defined by metallic gates on top of a 2DEG. The gates allow for a control of the tunnel barriers between the QD and the source and drain. QDs are also called artificial atoms, since their properties are similar to impurity atoms as we will discuss in the next section.

2.1   Quantum Dots

The energy of the electrons inside a QD is determined by three factors:

Firstly, the energy levels caused by the geometry of the dot are discrete, i.e. the level spacing is bigger than the width of the levels.

Secondly, the energy of the electrons is determined by the charging energy, which depends on the dot size. A good estimate for the level spacing δE and the charging energy U of a disc of diameter L is

$$\delta E \propto 1/L^2 \tag{2.1}$$

$$U = \frac{e^2}{2C} \approx \frac{e^2}{2\epsilon_0 L} \tag{2.2}$$

where C is the capacitance of the dot.

Thirdly, the energy is shifted by the potential of the gates. The transport through the dot at zero temperature $T = 0$ and small applied voltage $V_{sd} \approx 0$ only occurs when a level of the QD is aligned with the Fermi energy of the leads. This leads to resonances in the conductivity as a function of gate voltage V_g (see figure 2.1). These peaks are called Coulomb peaks. They are smeared if temperature is higher than the level width. Raising the applied voltage V_{sd} has the same effect. However if the applied voltage is big enough new levels can get involved. This leads do a jump in the conductance as a function of V_{sd}.
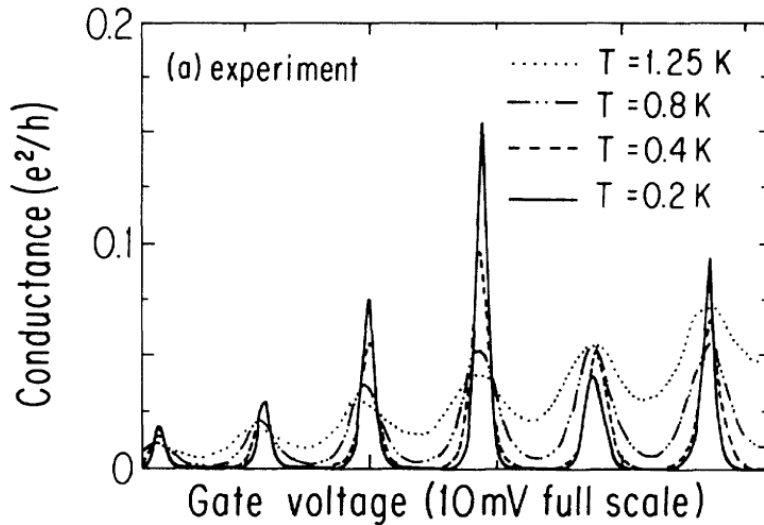
Figure 2.1: Linear conductance $G = \lim_{V \to 0} \frac{dI}{dV_{sd}}$ versus gate voltage V_g [1]. The peaks are separated alternately by U and $\delta E + U$.
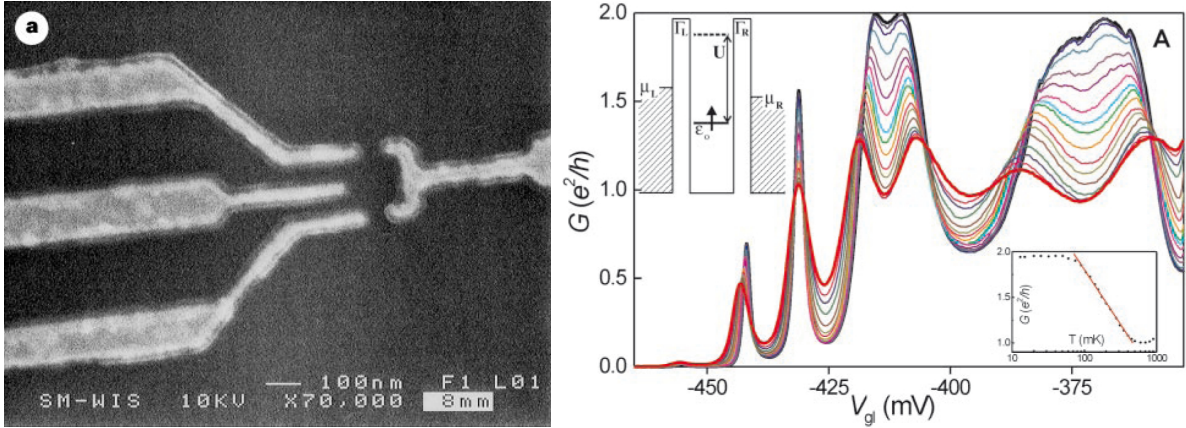
Figure 2.2: Left: Image of the QD device used by Goldhaber-Gordon et al. [2]. Right: Measurement of the linear conductance G vs. gate voltage V_g for temperatures higher than T_K (red curve) and temperatures lower than T_K (blue curve) [3].

2.1.1 The Kondo Effect in QDs

Under certain circumstances, which we will discuss in the following, the so called Kondo resonance can develop. As a consequence of this resonance the conductance through the dot is equal to one in units of $\frac{e^2}{h}$ for a wider range of gate voltage V_g. The origin of the Kondo resonance is the Kondo effect and was first associated with magnetic impurities in metals. For these magnetic impurities the Kondo resonance leads to an enhanced scattering of the electrons and thus to a lager resistivity, i.e. smaller conductivity for small temperatures. This effect was discovered by de Haas, de Boer and van den Berg [13] in 1934 and explained 30 years later in 1964 by Jun Kondo [14]. He found that if one takes into account spin flip events, the second term in the perturbation expansion leads to a logarithmic divergent of the resistivity as a function of temperature. These spin flip events lead to a many body resonance which is pinned at the Fermi surface, the Kondo resonance. The important energy scale for this effect is the Kondo temperature,

$$T_K = \sqrt{\Gamma U} e^{\pi \epsilon (\epsilon + U)/\Gamma U}, \tag{2.3}$$

where ϵ is the energy and Γ the width of a spin polarized level. The width of the resonance scales with T_K while the height scales with $1/\Gamma$ (compare figure 2.3 right panel). If the temperature is raised to values larger than T_K, the resonance is destroyed. T_K is more than just the temperature below which the Kondo resonance develops, it turns out that the resistivity is a universal function $f(T/T_K)$, i.e. the parameters U, Γ, ϵ enter the low-temperature properties only in the combination T_K and thus T_K is a universal scaling parameter, for low temperature behavior.

The simplest model for a magnetic impurity is the single impurity Anderson model

(SIAM)

$$H = \sum_{\sigma; k \in L,R} \epsilon_{k\sigma} \mathbf{c}_{k\sigma}^{\dagger} \mathbf{c}_{k\sigma} + \sum_{\sigma} \epsilon_{\sigma} \mathbf{d}_{\sigma}^{\dagger} \mathbf{d}_{\sigma} + U\mathbf{n}_{\uparrow}\mathbf{n}_{\downarrow} + \sum_{\sigma; k \in L,R} \left[V_{k\sigma} \mathbf{c}_{k\sigma}^{\dagger} \mathbf{d}_{\sigma} + H.c. \right] \qquad (2.4)$$

where $\mathbf{c}_{k\sigma}^{\dagger}(\mathbf{c}_{k\sigma})$ creates (annihilates) an electron in the bath with wave-vector k, spin σ and energy $\epsilon_{k\sigma}$, $\mathbf{d}_{\sigma}^{\dagger}(\mathbf{d}_{\sigma})$ creates (annihilates) an electron on the dot with spin σ and energy ϵ_{σ}. $n_{\sigma} = d_{\sigma}^{\dagger}d_{\sigma}$ counts the numbers of electrons on the dot with spin σ. A schematic sketch of this model can be seen in the left inset of figure 2.2.

The SIAM can also be used to describe a QD. Thus it was predicted that the Kondo effect also occurs in QDs, whenever they have a non-vanishing total spin,i.e. the total numbers of electrons on the dot is odd. Goldhaber-Gordan et al. [2] were the first to measure the Kondo effect in a highly controllable QD shown in figure 2.2, left panel.

The number of electrons on a QD is controlled via the gate voltage V_g. In the region of V_g where the total number of electrons on the dot is odd, the Kondo resonance develops, if the temperatures is below T_K. This leads to a transmission $\mathcal{T} = 1$. As a result the conductance has a plateau as a function of gate voltage, which develops into two peaks with increasing temperature (compare figure 2.2 right panel). If the the source-drain voltage V_{sd} becomes larger than the width of the resonance, which is small compared to Γ, the conductance reduces, as can be seen in figure 2.3. This feature is called zero bias anomaly (ZBA). The origin of the ZBA is quiet obvious if one takes the sharp peak in the spectral function (compare figure 2.3 right panel) into account. For nonzero frequency the spectral weight is almost zero, and thus averaging over frequencies leads to a small conductivity.

Applying a magnetic field the resonance splits into two peaks. This leads to a reduced transmission at zero source drain voltage. At higher voltage the separated peaks get involved and thus the conductance increases, in contrast to the ZBA at zero magnetic field. With increasing magnetic field the Kondo resonance gets more and more suppressed
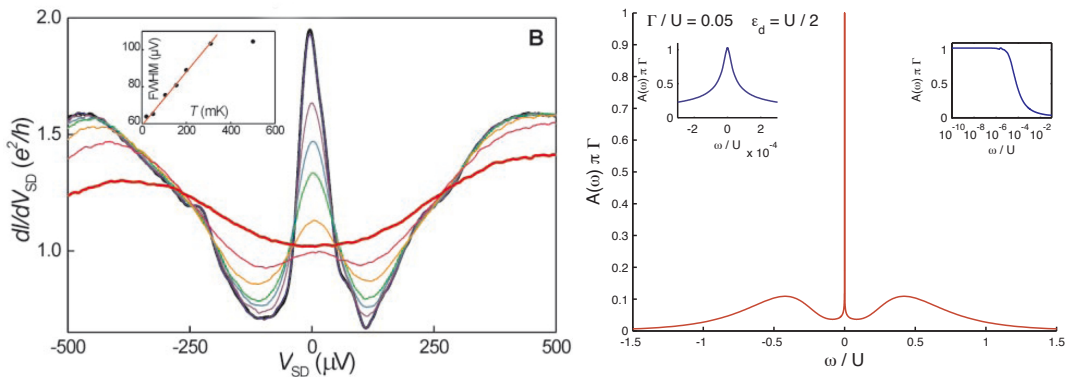
Figure 2.3: Left: Differential conductance dI/dV_{SD} versus V_{SD} of a QD for temperatures ranging from $15mK$ (blue line) up to $900mK$ (red line) [3]. Right: Spectral function of the SIAM with $\frac{\Gamma}{U} = 0.05$ and $\epsilon_d = \frac{U}{2}$ calculated with NRG.

since the condition for the Kondo resonance are two degenerate local levels.

Systems where the exchange energy of the Coulomb interaction is big enough to produce spin polarization at zero magnetic field are equivalent to systems with external magnetic field. The polarization increases with lower temperature, since fluctuations are lowered. Due to the intrinsic magnetic field the spin-flip events cost energy, and thus are less probable.

2.2 Quantum Point Contacts

2.2.1 Conductance quantization and Landauer formula

In QPCs the conductance is quantized in units of $2\frac{e^2}{h}$ as a function of the applied gate voltage (compare figure 2.4), where e is the electron charge and h is Planck's constant. Since a QPC is set up by a 2DEG we will describe it by the two dimensional time independent Schrödinger equation

$$E\psi(x,y) = -\frac{\hbar^2}{2m}(\partial_x^2 + \partial_y^2)\psi(x,y) + V(x,y)\psi(x,y) \tag{2.5}$$

where $V(x,y)$ is the potential that defines the geometry of the structure. One can think about $V(x,y)$ to be zero where the electrons can move and infinity elsewhere. If the width $w(x)$ of the structure x changes smoothly in x one can use the WKB-approximation and make the ansatz

$$\psi(x,y) = \phi_n(x,y) \exp\left[i \int_0^x k(x')dx'\right], \tag{2.6}$$
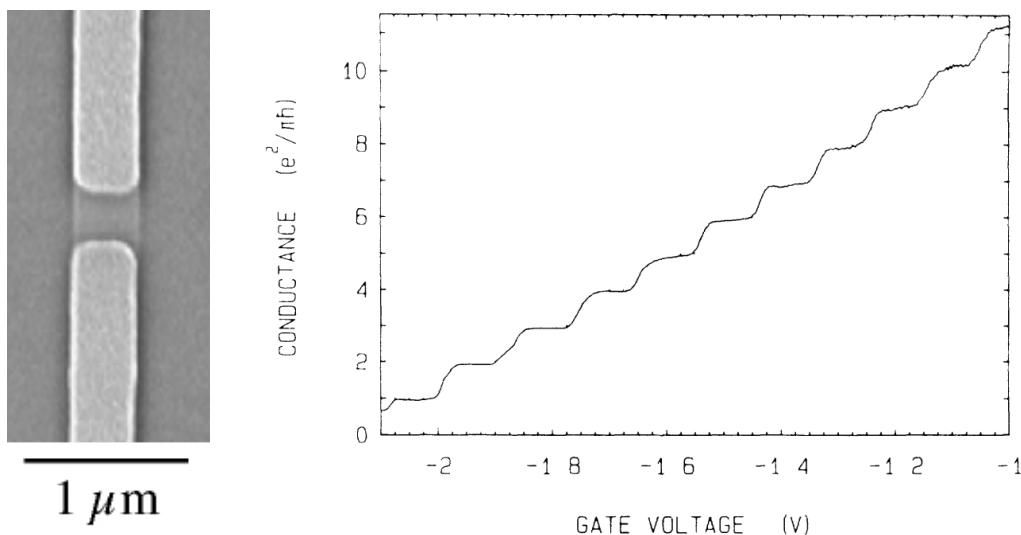
Figure 2.4: Left: Micrograph of a QPC-device [4]. Right: Conductance versus gate voltage V_g for a QPC [5].

where $\phi_n(x, y)$ solves the equation

$$E_n(x)\phi_n(x, y) = -\frac{\hbar^2}{2m}\partial_y^2\phi_n(x, y) + V(x, y)\phi_n(x, y). \tag{2.7}$$

If the potential goes discontinuously from zero to infinity at the border of the structure, $E_n(x)$ has the energy of an infinite square well, $E_n(x) = \frac{\hbar^2\pi^2}{2mw^2(x)}n^2$. This shows the qualitative behavior of E_n – it grows with decreasing $w(x)$. Inserting this in the Schrödinger-equation one gets

$$E = E_n(x) + \frac{\hbar^2 k^2(x)}{2m} \tag{2.8}$$

with

$$k(x) = \frac{1}{\hbar}\sqrt{2m(E - E_n(x))} \tag{2.9}$$

As a result $E_n(x)$ acts like an effective potential. For each n with $E_n < \epsilon_f$, where ϵ_f is the Fermi energy, one gets a one-dimensional quantum wire with the current

$$I = e \int dE \rho(E)v(E)\left[f_L(E) - f_R(E)\right] \tag{2.10}$$

where ρ is the density of states, v the velocity and $f_{L/R}$ the Fermi-Dirac-distribution on the left/right side of the structure. Using

$$\rho(E) = 2 \cdot \frac{1}{2\pi}\frac{dk}{dE} \tag{2.11}$$

(the 2 is due to spin degeneracy) and

$$v(E) = \frac{1}{\hbar}\frac{dE}{dk} \tag{2.12}$$

one gets

$$I = 2 \cdot \frac{e}{h}\int dE\left[f_L(E) - f_R(E)\right] \overset{T=0}{=} 2 \cdot \frac{e^2}{h}V_{SD} = g_0 V_{SD} \tag{2.13}$$

where $g_0 = 2 \cdot \frac{e^2}{h}$ is the conductance quantum and V_{SD} is the source-drain-voltage, not to be confused with the potential. So the conductance is

$$G = Ng_0, \tag{2.14}$$

where N is the number of channels that contribute to the current. Consequently G is a stepwise increasing function of the minimal width of the structure, w_{min}, which is controlled by the gate-voltage V_g. As a result the conductance quantization of QPCs can be completely understood in a noninteracting model.

2.2.2 The "0.7 structure" of QPCs

In addition to the conductance quantization at integer multiples of $\frac{2e^2}{h}$, Thomas et al. [6] found a shoulder-like step at about $0.7\frac{2e^2}{h}$, known as the 0.7 anomaly. It is generally agreed that the origin of this feature is the electron-electron interaction, but until now no theory has been presented that fully explains this effect.

Properties With Magnetic Field and Temperature Dependence

Applying an in-plane magnetic field parallel to the current the 0.7 anomaly develops smoothly towards the spin nondegenerated conductance quantization at $0.5g_0$ (see figure 2.5). This is far from being obvious, since for noninteracting electrons the step, that arises due to the energy splitting caused by the magnetic field, is at $0.5g_0$, independent of the strength of the field (compare figure 5.10).

The dependence of temperature is counterintuitive as well. With increasing temperature the 0.7 plateau gets more pronounced, even though the plateaus of the conductance quantization become weaker (see graphs in figure 2.5 and insets in figure 2.7). It is still visible at temperatures around $3K$ where the conductance quantization is totally smeared out. Furthermore for these high temperatures the conductance is almost independent of the magnetic field. I.e. the anomaly does not develop towards the spin-resolved step at $0.5g_0$ any more (see e.g. [9]). For small temperatures the anomaly gets less pronounced and in the limit $T \to 0$ it is expected to disappear completely (as argued, for example by Lunde [15], who calculated the interaction perturbatively).

In this work we present only calculations for the $T = 0$ case, where we do not expect
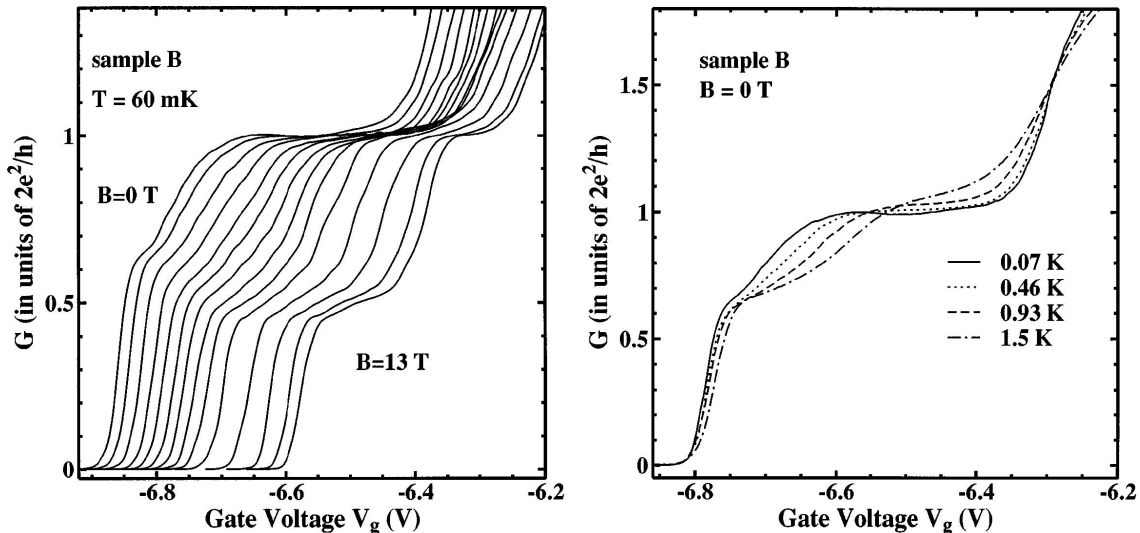
Figure 2.5: Left: Conductance versus gate voltage V_g of a QPC for different magnetic fields. Right: Conductance versus gate voltage V_g of a QPC for different temperatures [6].

to see the anomaly at zero magnetic field, so we will focus on studying the magnetic field dependence in detail.

Reduced Shot Noise - Indication of Spin Polarization?

In the 0.7-regime, measurements show a reduced shot-noise, as can be seen in figure 2.7. The shot noise can be calculated as follows (compare section 4.3.4)

$$S \propto \sum_n \mathcal{T}_n(1 - \mathcal{T}_n) \tag{2.15}$$

where $\mathcal{T}_n$ is the transmission of the nth channel. Consequently this is an indication that the current is carried mainly by one channel, and a second channel contributes only partially. So one explanation would be that in the 0.7-regime the exchange interaction is big enough to produce a spin polarization. This theory is strengthened by measurements of Rokhinson [16] who directly measured the spin polarization. However this is no prove for this theory since one has to apply a magnetic field to measure spin polarization, that in turn can produce it. This is likely, since Koop et. al. [9] measured an enhanced g-factor in the QPC up to three times higher than in the bulk 2DEG.

The idea of spin-polarization does not explain the counterintuitive temperature dependence. Spin polarization is lowered by fluctuations, and thus is expected to be enhanced with decreasing temperature.

Kondo related measurements

Cronenwett et al. [4] reported a zero bias anomaly (ZBA), as can be seen in figure 2.6, middle panel. Yet the comparison with the ZBA in the Kondo regime of QDs, as shown
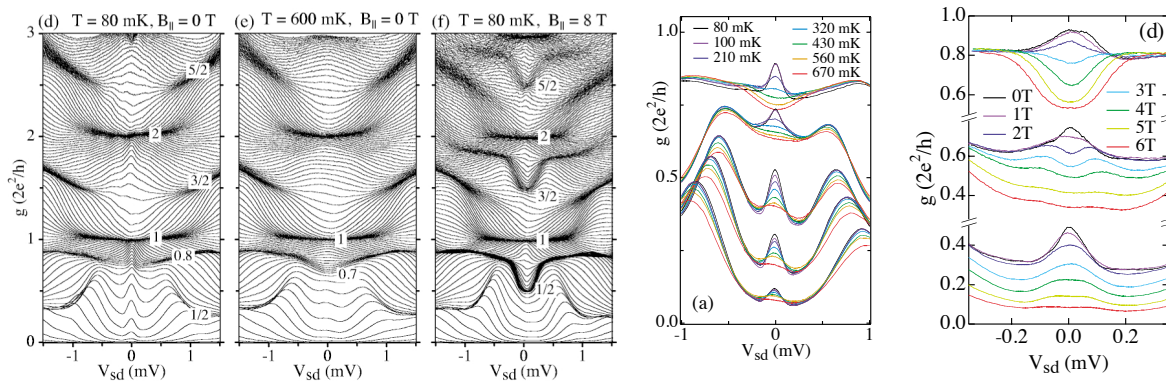
Figure 2.6: Left: Nonlinear differential conductance $g = dI/dV_{SD}$ versus V_{SD}, with each trace taken at a fixed gate voltage V_g [4]. Middle: Temperature dependence of the ZBA for different gate voltages, at temperatures from $80mK$ to $670mK$. Right: Evolution of the ZBA with in-plane magnetic field, at V_g corresponding to high, intermediate, and low conductance.

in figure 2.3, is an indication, that the 0.7 anomaly might be related to Kondo physics. An explanation for this assumption would be that the effective potential, which we have derived in the last section, can look like a square barrier. In the low density regime the borders of the barrier are less screened. Consequently electrons are reflected and a quasi-bound state is formed, similar to a QD with relatively big coupling. As a result, the Kondo resonance can develop for low temperatures. As we mentioned in section 2.1.1, the ZBA of QDs arises due to a sharp peak in the QD spectral function, the Kondo resonance. This many body state is destroyed by temperature effects, thus this interpretation explains not only the ZBA but also why the conductance grows if temperature is lowered.

Moreover, Cronenwett et al. found that the conductivity follows a universal scaling law. It can be expressed in terms of a single function, $g' = 2e^2/h[1/2f(T/T_K)+1/2]$, where T_K is a free parameter. However g' differs from the one used for QDs, where $g = 2e^2/hf(T/T_K)$.

Motivated by these facts Meir, et al. [7] postulated a quasi-bound state in the dot to introduce a slightly modified Anderson Hamiltonian:

$$
\begin{aligned}
H &= \sum_{\sigma;k \in L,R} \epsilon_{k\sigma} \mathbf{c}_{k\sigma}^\dagger \mathbf{c}_{k\sigma} + \sum_{\sigma} \epsilon_\sigma \mathbf{d}_\sigma^\dagger \mathbf{d}_\sigma + U\mathbf{n}_\uparrow \mathbf{n}_\downarrow \\
&+ \sum_{\sigma;k \in L,R} \left[V_{k\sigma}^{(1)}(1 - \mathbf{n}_{\bar\sigma})\mathbf{c}_{k\sigma}^\dagger \mathbf{d}_\sigma + V_{k\sigma}^{(2)}\mathbf{n}_{\bar\sigma}\mathbf{c}_{k\sigma}^\dagger \mathbf{d}_\sigma + H.c. \right] \quad (2.16)
\end{aligned}
$$

where $\mathbf{c}_{k\sigma}^\dagger (\mathbf{c}_{k\sigma})$ creates (destroys) an electron with momentum k and spin σ in one of the two leads L and R , $\mathbf{d}_\sigma^\dagger(\mathbf{d}_\sigma)$ creates (destroys) a spin-σ electron on the quasi-bound state and $\mathbf{n}_\sigma = \mathbf{d}_\sigma^\dagger \mathbf{d}_\sigma$. $V_{k\sigma}^{(1)}(V_{k\sigma}^{(2)})$ are the hybridization matrix elements for transition between 0 and 1 (1 and 2) electrons on the site. They are taken to be step-like functions with $V_{k\sigma}^{(2)} < V_{k\sigma}^{(1)}$. The idea behind this model can be explained as follows: if one electron is transferred through the quasi-bound state, the probability that a second electron is transferred is reduced due to Coulomb blockade. So the conductance can take any value between $0.5g_0$ and g_0, depending on the parameters. For higher values of the gate voltage, the Coulomb blockade energy decreases below the Fermi energy and the conductance reaches g_0. For temperatures below the Kondo-temperature, the scattering is enhanced due to the Kondo-effect.

Qualitatively this model provides good results for the conductivity, but due to perturbation theory used by Meir, the conductance is not bound by $\frac{2e^2}{h}$ and reduces, at large magnetic fields, to values smaller than $0.5\frac{2e^2}{h}$. His results are shown in figure 2.7, left panel.

Golub et al. [8] used the same model to calculate the shot noise. The results are in qualitative agreement with experiments as can be seen in figure 2.7 right panel.

One point one can retort to this model is that it contains physically not very well motivated, free parameters.

It is worth mentioning that the idea of spin-polarization contradicts to the idea of Kondo related physics. Spin-polarization suppresses the Kondo resonance and as mentioned before, the spin-polarization increases with decreasing temperature.

To conclude, the origin of the 0.7 anomaly appears to be a many-body phenomenon which is not understood yet, but it it probable that some many body state, involving
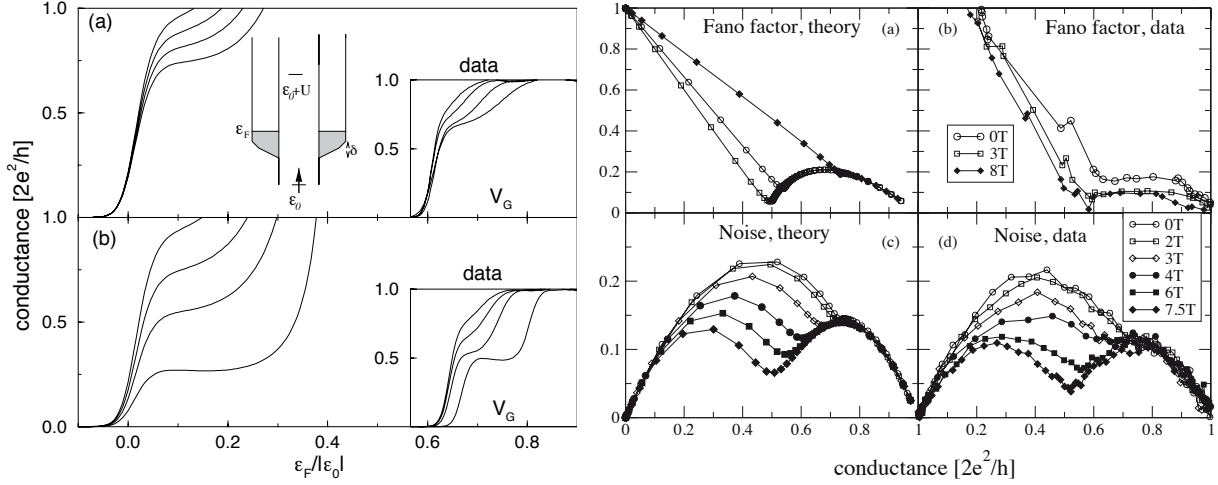
(a)Conductance at temperatures $T = 0.05, 0.1, 0.2, 0.6$ (solid curves, from high to low) as a function of ϵ_F (all energies in units of $|\epsilon_0| = \epsilon_{\uparrow/\downarrow}$). The parameters are $U = 1.45$, $\rho V_1^2 = 0.12$, $\rho V_2^2 = 0.015$, and $\delta = 0.02$. Right inset: experimental conductance of QPC at four different temperatures [4]. Center inset: Schematic of the band structure for the Anderson model (2.16) [7]. (b) Conductance in a magnetic field, for Zeeman splitting $\Delta = 0, 0.07, 0.12, 0.4$ at $T = 0.06$ (solid curves from top to bottom). Inset: experimental conductance of QPC at different magnetic fields [4]

(a) The Fano factor, calculated from the theory, versus zero-bias conductance at different magnetic fields, $g_B B/k_B T = 0$, 4.5, 12, compared to the experimental results of Ref. [17] (b), for $B = 0, 3$, and $8T$. The parameters used in the theory were $eV = k_B T$, $V^{(1)2}/2\pi = 1$, $V^{(2)2}/2\pi = 0.01$. In (c) the noise is calculated for the same parameters as those corresponding to the data of Ref. [18], depicted at (d), with the magnetic field values denoted in the legend, $k_b T = 280 mK$ and $V = 240 \mu V$. The values of $V^{(i)2}$ are the same as in (a). A value of g-factor of 0.44 was used.

Figure 2.7: Results of calculations by Meir et al. [7] (left) and Golub et al. [8](right) using an Anderson-type Hamiltonian (2.16).

strong correlations is created. One reason why methods like bosonisation, which usually provides good results for QWR, is not able to explain the 0.7 anomaly might be that they all assume translation invariant systems. I. e. systems with constant filling over the whole QWR. Considering equation (2.7) makes clear that one has to involve some space dependence, especially in the 0.7 regime where the filling factor changes from zero to some finite value.

To face the challenge describing a non translational invariant interacting quantum wire, we will use a recently developed method, which is known as functional Renormalization Group (fRG). We will set it up in a fashion such that we are able to treat smooth potentials in a non isotropic system. fRG works good for $T = 0$ and zero frequency. An extension to finite temperature and finite frequency is topic of current research. See e.g. Karrasch et al. [19] for a first approach involving some frequency dependence for the SIAM.

Chapter 3

Functional Renormalization Group

Functional Renormalization Group (fRG) is based on the Renormalization Group (RG) idea of Wilson. Renormalization in this context means that one integrates out certain degrees of freedom determined by some parameter b, what leads to model with new effective parameters, i.e. the action is mapped, due to the renormalization, on an effective action. $S \xrightarrow{R} S'$. Iterating these steps leads to a new action which hopefully describes the desired physical situation. Analytically this can be expressed in a differential equation the so called RG flow equation

$$\frac{dS}{db} = R[S] \tag{3.1}$$

It is worth to say that the mapping $S \xrightarrow{R} S'$ does not obey a group structure, in general there does not exist a inverse mapping of R, and thus it is at best a semigroup. Hence the name Renormalization Group is somehow misleading.

In fRG we will not integrate out degrees of freedom, but we will cut off some low energy scales of the interaction. This will lead to a RG flow equation with respect to the parameter that determines the infrared cutoff. Solving the flow equation leads to a model fully containing the interaction.

3.1 Fundamentals

Before introducing functional Renormalization Group (fRG) we recall some fundamentals of functional integrals. This is the common framework to write down the flow equations. Since we want to describe electrons we restrict ourselves to fermions (an introduction to fRG for both fermions and bosons can be found in [11]).

3.1.1 The Partition Function

The grand canonical partition function of a fermionic many-body system can be written in the continuous version of the functional integral. We will use it as a starting point, for

a derivation see [20]. The partition function reads

$$\mathcal{Z} = \int \mathcal{D}\overline{\psi}\psi \exp\left(-\int_0^\beta d\tau \left[\sum_l \overline{\psi}_l(\tau+0)\frac{d\psi_l}{d\tau} + \mathcal{H}\left(\{\overline{\psi}\},\{\psi\}\right)\right]\right) \tag{3.2}$$

with

$$\mathcal{H} = \sum_l \xi_l \overline{\psi}_l(\tau+0)\psi_l(\tau) + \frac{1}{4}\sum_{i,j,k,l} \overline{v}_{i,j,k,l}\overline{\psi}_i(\tau+0)\overline{\psi}_j(\tau+0)\psi_k(\tau)\psi_l(\tau) \tag{3.3}$$

$$(\xi_l = \epsilon_l - \mu)$$

where $\overline{\psi}$ and ψ are Grassmann variables. The summations run over a set of quantum numbers which diagonalizes the interaction-free Hamiltonian. ϵ_l are the corresponding one-particle energies, μ the chemical potential and $\overline{v}_{i,j,k,l}$ the anti-symmetrized matrix elements of the two-particle interaction.

With the inverse temperature β the boundary condition reads

$$\psi_l(\beta) = -\psi_l(0), \qquad \overline{\psi}_l(\beta) = -\overline{\psi}_l(0). \tag{3.4}$$

Consequently it is possible to expand the Grassmann fields in fermionic, i.e. odd Matsubara frequencies $\omega_n = \frac{2n+1}{\beta}\pi$

$$\begin{Bmatrix}\overline{\psi}_l \\ \psi_l\end{Bmatrix}(\tau) = \frac{1}{\sqrt{\beta}}\sum_n e^{\pm i\omega_n\tau}\begin{Bmatrix}\overline{\psi}_l \\ \psi_l\end{Bmatrix}(i\omega_n) \tag{3.5}$$

where

$$\begin{Bmatrix}\overline{\psi}_l \\ \psi_l\end{Bmatrix}(i\omega_n) = \frac{1}{\sqrt{\beta}}\int_0^\beta d\tau\, e^{\mp i\omega_n\tau}\begin{Bmatrix}\overline{\psi}_l \\ \psi_l\end{Bmatrix}(\tau). \tag{3.6}$$

Now we introduce the noninteracting single-particle propagator $\mathcal{G}^0$, and since we are using a basis that diagonalizes $\mathcal{H}^0$ this is also the case for $\mathcal{G}^0$. Thus we have

$$\overline{\psi}_l(i\omega_n)\left[\mathcal{G}_l^0(i\omega_n)\right]^{-1}\psi_l(i\omega_n) = \overline{\psi}_l(i\omega_n)(i\omega_n - \xi_l)\psi_l(i\omega_n) \tag{3.7}$$

and we can write (3.2) in energy-space representation.

$$\frac{\mathcal{Z}}{\mathcal{Z}_0} = \frac{1}{\mathcal{Z}_0}\int \mathcal{D}\overline{\psi}\psi \exp\left(\sum_l \sum_{\omega_n} e^{i\omega 0^+}\overline{\psi}_l(i\omega_n)\left[\mathcal{G}_l^0(i\omega_n)\right]^{-1}\psi_l(i\omega_n)\right.$$

$$\left.-\frac{1}{4}\frac{1}{\beta}\sum_{i,j,k,l}\sum_{n,n',m,m'}\overline{v}_{i,j,k,l}\delta_{m+m',n+n'}\overline{\psi}_i(i\omega_m)\overline{\psi}_j(i\omega_{m'})\psi_k(i\omega_n)\psi_l(i\omega_{n'})\right) \tag{3.8}$$

However equation (3.8) holds for any basis since all properties of the noninteracting problem follow from the Gaussian nature of the functional integral[1]. Using the shorthand notation

---

[1] For more details see [20] chapter 1.5

$(\overline{\psi}, \psi) := \sum_k \psi_k$ respectively $(\overline{\psi}, X\psi) := \sum_{k,k'} \overline{\psi}_k X_{k,k'} \psi_{k'}$, where $k = (\omega_n, l)$, equation (3.8) becomes

$$
\frac{\mathcal{Z}}{\mathcal{Z}_0} = \frac{1}{\mathcal{Z}_0} \int \mathcal{D}\overline{\psi}\psi \exp\left((\overline{\psi}, \left[\mathcal{G}^0\right]^{-1}\psi) - \frac{1}{4} \sum_{k_1', k_2', k_1, k_2} \overline{v}_{k_1', k_2', k_1, k_2} \overline{\psi}_{k_1'} \overline{\psi}_{k_2'} \psi_{k_1} \psi_{k_2} \right)
$$
$$
=: \frac{1}{\mathcal{Z}_0} \int \mathcal{D}\overline{\psi}\psi \exp\left(S_0 - S_{int} \right). \tag{3.9}
$$

Here a factor β^{-1} and the frequency-conserving delta-functions have been absorbed into the two-particle interaction $\overline{v}$. Furthermore we dropped the factor $e^{i\omega 0^+}$ which is one for any finite ω, but will become important for the initial conditions (3.84).

3.1.2   Generating Functionals of Green's Functions

In order to write expectation values for products of fields as functional derivatives with respect to external fields we define the functional [2]

$$
\mathcal{W}\left(\{\overline{\eta}\}, \{\eta\}\right) = \frac{1}{\mathcal{Z}} \int \mathcal{D}\overline{\psi}\psi \exp\left(S_0 - S_{int} - (\overline{\psi}, \eta) - (\overline{\eta}, \psi) \right). \tag{3.10}
$$

Now, we take the functional derivative with respect to the external source fields η and $\overline{\eta}$ and set them to zero. This provides the desired identity for the m-particle Green's Function

$$
G_m(k_1', \ldots, k_m', k_1, \ldots, k_m) := (-1)^m \left\langle \psi_{k_1'} \ldots \psi_{k_m'} \overline{\psi}_{k_1} \ldots \overline{\psi}_{k_m} \right\rangle
$$
$$
= \frac{1}{\mathcal{Z}} \int \mathcal{D}\overline{\psi}\psi \, \psi\overline{\psi} \exp\left(S_0 - S_{int} \right)
$$
$$
= \frac{\delta^m}{\delta\overline{\eta}_{k_1'} \cdots \delta\overline{\eta}_{k_m'}} \frac{\delta^m}{\delta\eta_{k_1} \cdots \delta\eta_{k_m}} \mathcal{W}\left(\{\overline{\eta}\}, \{\eta\}\right) \Bigg|_{\overline{\eta}=0=\eta}. \tag{3.11}
$$

Setting S_{int} equal to zero leads to the well known result for the one-particle Green's function

$$
G_1(l, i\omega_n) = \mathcal{G}_l^0(i\omega_n) = \frac{1}{i\omega_n - \xi_l}. \tag{3.12}
$$

The logarithm of $\mathcal{W}$

$$
\mathcal{W}^c = \ln \mathcal{W} \tag{3.13}
$$

generates the m-particle connected Green's function.

$$
G_m^c(k_1', \ldots, k_m', k_1, \ldots, k_m) := (-1)^m \left\langle \psi_{k_1'} \ldots \psi_{k_m'} \overline{\psi}_{k_1} \ldots \overline{\psi}_{k_m} \right\rangle_c
$$
$$
= \frac{\delta^m}{\delta\overline{\eta}_{k_1'} \cdots \delta\overline{\eta}_{k_m'}} \frac{\delta^m}{\delta\eta_{k_1} \cdots \delta\eta_{k_m}} \mathcal{W}^c\left(\{\overline{\eta}\}, \{\eta\}\right) \Bigg|_{\overline{\eta}=0=\eta} \tag{3.14}
$$

---

[2]This might look very complicated but the idea behind this is in principle the same as the one of a cumulants generating functionals.

3.1.3 Vertex Functions and their Generating Functional

Like the self-energy corresponds to the one-particle Green's function, there exist higher order analoga that correspond to the m-particle Green's functions: the so called m-particle vertex functions. One can define them as the sum of all connected one-particle irreducible diagrams with m amputated external legs.[3] In the literature like [21] the two-particle vertex function is sometimes just called vertex function and is denoted by Γ. Another often used nomenclature is "effective interaction". The existence of different names suggests that we have met with an important object - which we have not defined yet. To do so we first introduce the Grassmann fields

$$\phi_k = -\frac{\delta}{\delta\overline{\eta}_k}\mathcal{W}^c\left(\{\overline{\eta}\},\{\eta\}\right), \qquad \overline{\phi}_k = \frac{\delta}{\delta\eta_k}\mathcal{W}^c\left(\{\overline{\eta}\},\{\eta\}\right) \tag{3.15}$$

which are needed to perform the Legendre transformation of $\mathcal{W}^c$

$$\Gamma\left(\{\overline{\phi}\},\{\phi\}\right) = -\mathcal{W}^c\left(\{\overline{\eta}\},\{\eta\}\right) - \left(\overline{\phi},\eta\right) - \left(\overline{\eta},\phi\right) + \left(\overline{\phi},\left[\mathcal{G}^0\right]^{-1}\phi\right). \tag{3.16}$$

This is the generating functional of the vertex functions

$$\gamma_m(k_1',\ldots,k_m';k_1,\ldots,k_m) = \frac{\delta^m}{\delta\overline{\phi}_{k_1'}\cdots\delta\overline{\phi}_{k_m'}}\frac{\delta^m}{\delta\phi_{k_1}\cdots\delta\phi_{k_m}}\Gamma\left(\{\overline{\phi}\},\{\phi\}\right)\bigg|_{\overline{\phi}=0=\phi}. \tag{3.17}$$

We regard this as a definition of the vertex functions.

Note that in (3.16) we added an extra term to the common definition. This modification does not have any influence on the definition of the vertex functions but it will cancel one term when we will set up the fRG flow equation.

The reader might have got the impression that the self-energy Σ is equal to the one-particle vertex function γ_1. Unfortunately this is not the case. In the next section we show that for fermions we have

$$\Sigma = -\gamma_1. \tag{3.18}$$

This should be kept in mind when checking all the numerous minus signs.

3.1.4 Relation between Vertex and Green's Functions

In this section we will derive some identities which show the relations between vertex and Green's functions. On the one hand this will help to understand the significance of vertex functions. On the other hand it is useful to have already some identities before we face the challenge of setting up the differential equation.

---

[3]Since it is difficult to draw amputated legs the Feynman diagram of m-particle vertex function are often polygons with $2m$ corners.

General Relations

The fields defined in (3.15) satisfy the identities

$$\frac{\delta \phi_{k'}}{\delta \phi_k} = \delta_{k,k'} = \frac{\delta \overline{\phi}_{k'}}{\delta \overline{\phi}_k}$$

$$\frac{\delta \phi_{k'}}{\delta \overline{\phi}_k} = 0 = \frac{\delta \overline{\phi}_{k'}}{\delta \phi_k} \tag{3.19}$$

Differentiating the generating functional of the vertex function with respect to these fields provides

$$\frac{\delta}{\delta \phi_k} \Gamma \left(\{\overline{\phi}\}, \{\phi\} \right) \stackrel{3.16}{=} \sum_q \left[-\frac{\delta \mathcal{W}^c}{\delta \eta_q} \frac{\delta \eta_q}{\delta \phi_k} - \frac{\delta \mathcal{W}^c}{\delta \overline{\eta}_q} \frac{\delta \overline{\eta}_q}{\delta \phi_k} + \overline{\phi}_q \frac{\delta \eta_q}{\delta \phi_k} - \frac{\delta \overline{\eta}_q}{\delta \phi_k} \phi_q - \overline{\phi}_q \left[\mathcal{G}^0 \right]^{-1}_{q,k} \right] + \overline{\eta}_k$$

$$\stackrel{3.15}{=} \overline{\eta}_k - \sum_q \overline{\phi}_q \left[\mathcal{G}^0 \right]^{-1}_{q,k} \tag{3.20}$$

and

$$\frac{\delta}{\delta \overline{\phi}_k} \Gamma \left(\{\overline{\phi}\}, \{\phi\} \right) \stackrel{3.16}{=} \sum_q \left[-\frac{\delta \mathcal{W}^c}{\delta \eta_q} \frac{\delta \eta_q}{\delta \overline{\phi}_k} - \frac{\delta \mathcal{W}^c}{\delta \overline{\eta}_q} \frac{\delta \overline{\eta}_q}{\delta \overline{\phi}_k} + \overline{\phi}_q \frac{\delta \eta_q}{\delta \overline{\phi}_k} - \frac{\delta \overline{\eta}_q}{\delta \phi_k} \phi_q + \overline{\phi}_q \left[\mathcal{G}^0 \right]^{-1}_{q,k} \right] - \eta_k$$

$$\stackrel{3.15}{=} -\eta_k + \sum_q \left[\mathcal{G}^0 \right]^{-1}_{q,k} \phi_q. \tag{3.21}$$

Differentiating (3.20) with respect to $\overline{\phi}_{k'}$ and (3.21) with respect to $\phi_{k'}$ and solving both equations for the first term on the rhs yields

$$\frac{\delta \overline{\eta}_k}{\delta \overline{\phi}_{k'}} = \frac{\delta^2 \Gamma}{\delta \overline{\phi}_{k'} \delta \phi_k} + \left[\mathcal{G}^0 \right]^{-1}_{k',k}$$

$$\frac{\delta \eta_k}{\delta \phi_{k'}} = -\frac{\delta^2 \Gamma}{\delta \phi_{k'} \delta \overline{\phi}_k} + \left[\mathcal{G}^0 \right]^{-1}_{k,k'}. \tag{3.22}$$

Note the different order of k and k' of the free propagator. Using these identities one gets

$$\delta_{k,k'} = \frac{\delta \phi_k}{\delta \phi_{k'}} \stackrel{3.15}{=} -\frac{\delta}{\delta \phi_{k'}} \frac{\delta \mathcal{W}^c}{\delta \overline{\eta}_k} = -\sum_q \left[\frac{\delta \eta_q}{\delta \phi_{k'}} \frac{\delta^2 \mathcal{W}^c}{\delta \eta_q \delta \overline{\eta}_k} + \frac{\delta \overline{\eta}_q}{\delta \phi_{k'}} \frac{\delta^2 \mathcal{W}^c}{\delta \overline{\eta}_q \delta \overline{\eta}_k} \right]$$

$$= \sum_q \left[\left(\frac{\delta^2 \Gamma}{\delta \phi_{k'} \delta \overline{\phi}_q} - \left[\mathcal{G}^0 \right]^{-1}_{q,k'} \right) \frac{\delta^2 \mathcal{W}^c}{\delta \eta_q \delta \overline{\eta}_k} - \frac{\delta^2 \Gamma}{\delta \phi_{k'} \delta \phi_q} \frac{\delta^2 \mathcal{W}^c}{\delta \overline{\eta}_q \delta \overline{\eta}_k} \right] \tag{3.23}$$

and in the same way

$$\delta_{k,k'} = \frac{\delta\overline{\phi}_k}{\delta\overline{\phi}_{k'}} = \sum_q \left[\left(\frac{\delta^2\Gamma}{\delta\overline{\phi}_{k'}\delta\phi_q} + \left[\mathcal{G}^0\right]^{-1}_{k',q} \right) \frac{\delta^2\mathcal{W}^c}{\delta\overline{\eta}_q\delta\eta_k} - \frac{\delta^2\Gamma}{\delta\overline{\phi}_{k'}\delta\overline{\phi}_q} \frac{\delta^2\mathcal{W}^c}{\delta\eta_q\delta\eta_k} \right] \tag{3.24}$$

$$0 = \frac{\delta\overline{\phi}_k}{\delta\phi_{k'}} = \sum_q \left[-\left(\frac{\delta^2\Gamma}{\delta\phi_{k'}\delta\overline{\phi}_q} - \left[\mathcal{G}^0\right]^{-1}_{q,k'} \right) \frac{\delta^2\mathcal{W}^c}{\delta\eta_q\delta\eta_k} - \frac{\delta^2\Gamma}{\delta\phi_{k'}\delta\phi_q} \frac{\delta^2\mathcal{W}^c}{\delta\overline{\eta}_q\delta\eta_k} \right] \tag{3.25}$$

$$0 = \frac{\delta\phi_k}{\delta\overline{\phi}_{k'}} = \sum_q \left[-\left(\frac{\delta^2\Gamma}{\delta\overline{\phi}_{k'}\delta\phi_q} + \left[\mathcal{G}^0\right]^{-1}_{k',q} \right) \frac{\delta^2\mathcal{W}^c}{\delta\overline{\eta}_q\delta\overline{\eta}_k} - \frac{\delta^2\Gamma}{\delta\overline{\phi}_{k'}\delta\overline{\phi}_q} \frac{\delta^2\mathcal{W}^c}{\delta\eta_q\delta\overline{\eta}_k} \right]. \tag{3.26}$$

$$\tag{3.27}$$

We can write the last four equations in one compact form

$$\begin{pmatrix} \frac{\delta^2\Gamma}{\delta\overline{\phi}\delta\phi} + \left[\mathcal{G}^0\right]^{-1} & \frac{\delta^2\Gamma}{\delta\overline{\phi}\delta\overline{\phi}} \\ \frac{\delta^2\Gamma}{\delta\phi\delta\phi} & \frac{\delta^2\Gamma}{\delta\phi\delta\overline{\phi}} - \left[[\mathcal{G}^0]^{-1}\right]^T \end{pmatrix} \cdot \begin{pmatrix} \frac{\delta^2\mathcal{W}^c}{\delta\overline{\eta}\delta\eta} & -\frac{\delta^2\mathcal{W}^c}{\delta\overline{\eta}\delta\overline{\eta}} \\ -\frac{\delta^2\mathcal{W}^c}{\delta\eta\delta\eta} & \frac{\delta^2\mathcal{W}^c}{\delta\eta\delta\overline{\eta}} \end{pmatrix} = 1. \tag{3.28}$$

This identity can be written as

$$\mathcal{V}(\overline{\phi},\phi) := \begin{pmatrix} \frac{\delta^2\mathcal{W}^c}{\delta\overline{\eta}\delta\eta} & -\frac{\delta^2\mathcal{W}^c}{\delta\overline{\eta}\delta\overline{\eta}} \\ -\frac{\delta^2\mathcal{W}^c}{\delta\eta\delta\eta} & \frac{\delta^2\mathcal{W}^c}{\delta\eta\delta\overline{\eta}} \end{pmatrix} = \begin{pmatrix} \frac{\delta^2\Gamma}{\delta\overline{\phi}\delta\phi} + \left[\mathcal{G}^0\right]^{-1} & \frac{\delta^2\Gamma}{\delta\overline{\phi}\delta\overline{\phi}} \\ \frac{\delta^2\Gamma}{\delta\phi\delta\phi} & \frac{\delta^2\Gamma}{\delta\phi\delta\overline{\phi}} - \left[[\mathcal{G}^0]^{-1}\right]^T \end{pmatrix}^{-1} \tag{3.29}$$

where we introduced an abbreviation for this matrix. This equation connects the two generating functionals thus we will need it later on.

Relations for One and Two Particle Vertex Functions

To show relations between vertex and Green's function we set the outer sources to zero and consider we're not in a symmetry braking phase, i.e.

$$\left. \frac{\delta^2\mathcal{W}^c}{\delta\overline{\eta}\delta\overline{\eta}} \right|_{\eta=0=\overline{\eta}} = \left. \frac{\delta^2\mathcal{W}^c}{\delta\eta\delta\eta} \right|_{\eta=0=\overline{\eta}} = \left. \frac{\delta^2\Gamma}{\delta\overline{\phi}\delta\overline{\phi}} \right|_{\phi=0=\overline{\phi}} = \left. \frac{\delta^2\Gamma}{\delta\phi\delta\phi} \right|_{\phi=0=\overline{\phi}} = 0. \tag{3.30}$$

The $(1,1)$ element of $\mathcal{V}$ then provides

$$G_1^c \overset{3.14}{:=} \frac{\delta^2\mathcal{W}^c}{\delta\overline{\eta}\delta\eta} = \left[\frac{\delta^2\Gamma}{\delta\overline{\phi}\delta\phi} + \left[\mathcal{G}^0\right]^{-1} \right]^{-1}. \tag{3.31}$$

If one compares this with the Dyson equation

$$G_1 = \mathcal{G} = \left[\left[\mathcal{G}^0\right]^{-1} - \Sigma \right]^{-1} \tag{3.32}$$

using the fact that for the one-particle propagator the linked cluster theorem provides $G_1^c = G_1$, one gets the identity already mentioned in the last section

$$\gamma_1 = \frac{\delta^2 \Gamma}{\delta\overline{\phi}\delta\phi} = -\Sigma. \tag{3.33}$$

Finally, we want to state the relation between two-particle vertex and Green's function. To this aim we differentiate equation (3.23) twice, first with respect to ϕ_l and second with respect to $\overline{\phi}_{l'}$. Setting the fields to zero yields

$$0 = \sum_q \left[\frac{\delta^4 \Gamma}{\delta\overline{\phi}_{l'}\delta\phi_l\delta\phi_{k'}\delta\overline{\phi}_q} \frac{\delta^2 \mathcal{W}^c}{\delta\eta_q\delta\overline{\eta}_k} + \left(\frac{\delta^2 \Gamma}{\delta\phi_{k'}\delta\overline{\phi}_q} - [\mathcal{G}^0]_{q,k'}^{-1} \right) \sum_{s,s'} \left(\frac{\delta\eta_s}{\delta\phi_l} \frac{\delta\overline{\eta}_{s'}}{\delta\overline{\phi}_{l'}} \frac{\delta^4 \mathcal{W}^c}{\delta\overline{\eta}_{s'}\delta\eta_s\delta\eta_q\delta\overline{\eta}_k} \right) \right]\Bigg|_{\phi=0=\overline{\phi}} \tag{3.34}$$

$$= -\sum_q \gamma_2(l',q,k',l)\mathcal{G}_{k,q} - \sum_{q,s,s'} [\mathcal{G}]_{q,k'}^{-1} [\mathcal{G}]_{s,l}^{-1} [\mathcal{G}]_{l',s'}^{-1} G_2^c(s',k,q,s) \tag{3.35}$$

where we again used that $G_1^c = \mathcal{G}$ and equation (3.22). Solving for the two-particle vertex provides

$$\gamma_2(k_1',k_2',k_1,k_2) = -\sum_{q_1',q_2',q_1,q_2} [\mathcal{G}]_{k_1',q_1'}^{-1} [\mathcal{G}]_{k_2',q_2'}^{-1} [\mathcal{G}]_{q_2,k_2}^{-1} [\mathcal{G}]_{q_1,k_1}^{-1} G_2^c(q_1',q_2',q_1,q_2). \tag{3.36}$$

This proves that the two particle vertex is one-particle irreducible. We get it by cutting all external legs of the connected two-particle Green's function, as mentioned at the beginning of the last section. From equation (3.36) and the definition of the connected Green's function (3.14), it follows that $\gamma_2(k_1',k_2';k_1,k_2)$ is antisymmetric under the exchange k_1' and k_2' or k_1 and k_2 and symmetric under the exchange of the first two with the last two indices

$$\gamma_2(k_1',k_2',k_1,k_2) = -\gamma_2(k_2',k_1',k_1,k_2) = -\gamma_2(k_1',k_2',k_2,k_1)$$
$$= \gamma_2(k_1,k_2,k_1',k_2'). \tag{3.37}$$

3.2 The fRG Flow Equation

We are now ready to use this machinery to set up the flow equation. The goal is to set up a differential equation with respect to some flow-parameter for the vertex function in the following fashion:

$$\frac{d}{d\Lambda}\gamma_m = \mathcal{F}(\gamma_1, \ldots, \gamma_n, \Lambda). \tag{3.38}$$

Since we do not have such a flow parameter yet, we will modify the free propagator so that it depends on Λ:

$$\mathcal{G}^0 \to \mathcal{G}^{0,\Lambda}. \tag{3.39}$$

In order to put the idea across, imagine that for some value $\Lambda_{initial}$ this modified propagator is equal to zero. Expanding the vertex function in a perturbation series gives zero for all summands that contain this propagator. As a consequence at $\Lambda_{initial}$ all vertex functions are zero, with the exception of the two-particle vertex function, that is equal to the bare interaction. Then it is the aim to integrate (3.38) from $\Lambda_{initial}$ to Λ_{final}, for which the free propagator is the ordinary one ($\mathcal{G}^{0,\Lambda_{final}} = \mathcal{G}^0$). This would lead to the exact vertex functions and we could calculate the full propagator from the one-particle vertex function via Dyson's equation.

Note that (3.38) in general is a set of infinitely many coupled differential equations, which is impossible to solve. So the major task is to choose the Λ-dependence in a way that allows us to make some physically motivated simplifications that closes the set of differential equation.

As we will see in the next section, it is not necessary to specify the Λ-dependence to set up the flow equations.

3.2.1 Flow Equation of the Generating Functionals

To get a coupled differential equation as indicated in (3.38) we will set up a differential equation for the generating functional of the vertex functions:

$$\frac{d}{d\Lambda}\Gamma = \tilde{\mathcal{F}}(\Gamma, \phi, \overline{\phi}, \Lambda, \mathcal{G}^0, \ldots). \tag{3.40}$$

Then we will expand Γ on both sides in powers of $\phi\overline{\phi}$ with the vertex functions as coefficients and pull the derivative with respect to Λ on the lhs into the sum. Comparing powers of $\phi\overline{\phi}$ will lead to the desired equation.

Since the generating functional of the vertex function is defined via the generating functional of the connected Green's functions, we will need the following derivative:

$$\frac{d}{d\Lambda}\mathcal{W}^{c,\Lambda} = \frac{d}{d\Lambda}\ln\left[\frac{1}{\mathcal{Z}_0^\Lambda}\int \mathcal{D}\overline{\psi}\psi e^{\left(\left(\overline{\psi},[\mathcal{G}^{0,\Lambda}]^{-1}\psi\right)-S_{int}-(\overline{\psi},\eta^\Lambda)-(\overline{\eta}^\Lambda,\psi)\right)}\right], \tag{3.41}$$

$$\mathcal{Z}_0^\Lambda = \int \mathcal{D}\overline{\psi}\psi \exp\left(\overline{\psi}, \left[\mathcal{G}^{0,\Lambda}\right]^{-1}\psi\right). \tag{3.42}$$

Note that the normalization of the functional differs from the original definition (3.11,3.13). The free propagator now depends on Λ, hence this is also the case for S_0, $\mathcal{Z}_0$, $\mathcal{W}$ and $\mathcal{W}^c$, as indicated by an index. Furthermore we require η and $\overline{\eta}$ to have a Λ-dependence chosen such that the fields ϕ and $\overline{\phi}$, which are the natural variables of Γ, are Λ-independent. As a result η and $\overline{\eta}$ depend on Λ via (3.20) and (3.21).

To decompose the derivative we write it as

$$\frac{d}{d\Lambda}\mathcal{W}^{c,\Lambda} = \sum_{k,k'} \partial_\Lambda \left[\mathcal{G}_0^\Lambda\right]^{-1}_{k,k'} \frac{\delta \mathcal{Z}_0^\Lambda}{\delta \left[\mathcal{G}_0^\Lambda\right]^{-1}_{k,k'}} \frac{\partial \mathcal{W}^{c,\Lambda}}{\partial \mathcal{Z}_0^\Lambda} + \sum_{k,k'} \partial_\Lambda \left[\mathcal{G}_0^\Lambda\right]^{-1}_{k,k'} \frac{\delta \mathcal{W}^{c,\Lambda}}{\delta \left[\mathcal{G}_0^\Lambda\right]^{-1}_{k,k'}}$$
$$+ \sum_k \left[\frac{d\eta_k^\Lambda}{d\Lambda} \frac{\delta \mathcal{W}^{c,\Lambda}}{\delta \eta_k^\Lambda} + \frac{d\overline{\eta}_k^\Lambda}{d\Lambda} \frac{\delta \mathcal{W}^{c,\Lambda}}{\delta \overline{\eta}_k^\Lambda}\right] . \tag{3.43}$$

Here we replaced already $\frac{d\left[\mathcal{G}_0^\Lambda\right]^{-1}}{d\Lambda}$ by $\partial_\Lambda \left[\mathcal{G}_0^\Lambda\right]^{-1}$ since $\mathcal{G}^{0,\Lambda}$ explicitly depends on Λ.

For the last sum we can use the definition (3.15) of the fields - mind the minus sign in the definition of ϕ.

$$\sum_k \frac{d\eta_k^\Lambda}{d\Lambda} \frac{\delta \mathcal{W}^{c,\Lambda}}{\delta \eta_k^\Lambda} = \sum_k \frac{d\eta_k^\Lambda}{d\Lambda} \overline{\phi}_k = -\left(\overline{\phi}_k, \frac{d\eta_k^\Lambda}{d\Lambda}\right) \tag{3.44}$$

$$\sum_k \frac{d\overline{\eta}_k^\Lambda}{d\Lambda} \frac{\delta \mathcal{W}^{c,\Lambda}}{\delta \overline{\eta}_k^\Lambda} = -\sum_k \frac{d\overline{\eta}_k^\Lambda}{d\Lambda} \phi_k = -\left(\frac{d\overline{\eta}_k^\Lambda}{d\Lambda}, \phi_k\right) \tag{3.45}$$

Furthermore it is easy to see from (3.41) that $\frac{\partial \mathcal{W}^{c,\Lambda}}{\partial \mathcal{Z}_0^\Lambda} = -\frac{1}{\mathcal{Z}_0^\Lambda}$ and with

$$\frac{1}{\mathcal{Z}_0^\Lambda} \frac{\delta \mathcal{Z}_0^\Lambda}{\delta \left[\mathcal{G}_0^\Lambda\right]^{-1}_{k,k'}} = \int \frac{\mathcal{D}\overline{\psi}\psi}{\mathcal{Z}_0^\Lambda} \overline{\psi}_k \psi_{k'} e^{S_0^\Lambda} = -\int \frac{\mathcal{D}\overline{\psi}\psi}{\mathcal{Z}_0^\Lambda} \psi_{k'} \overline{\psi}_k e^{S_0^\Lambda} \overset{3.11}{=} \mathcal{G}_{k',k}^{0,\Lambda} \tag{3.46}$$

$$\sum_{k,k'} \partial_\Lambda \left[\mathcal{G}_0^\Lambda\right]^{-1}_{k,k'} \frac{\delta \mathcal{Z}_0^\Lambda}{\delta \left[\mathcal{G}_0^\Lambda\right]^{-1}_{k,k'}} \frac{\partial \mathcal{W}^{c,\Lambda}}{\partial \mathcal{Z}_0^\Lambda} = -\text{Tr}\left(\mathcal{G}^{0,\Lambda} \partial_\Lambda \left[\mathcal{G}^{0,\Lambda}\right]^{-1}\right) \tag{3.47}$$

The minus sign in (3.46) results from interchanging the two fields ψ and $\overline{\psi}$. The same

appears in the following:

$$
\frac{1}{\mathcal{W}^\Lambda} \sum_{k,k'} \partial_\Lambda \left[\mathcal{G}^{0,\Lambda}\right]^{-1}_{k,k'} \frac{\delta}{\delta \left[\mathcal{G}^\Lambda_0\right]^{-1}_{k,k'}} \int \frac{\mathcal{D}\overline{\psi}\psi}{\mathcal{Z}^\Lambda_0} e^{\left(\left(\overline{\psi},\left[\mathcal{G}^{0,\Lambda}\right]^{-1}\psi\right)-S_{int}-(\overline{\psi},\eta^\Lambda)-(\overline{\eta}^\Lambda,\psi)\right)}
$$

$$
= - \frac{1}{\mathcal{W}^\Lambda} \sum_{k,k'} \partial_\Lambda \left[\mathcal{G}^{0,\Lambda}\right]^{-1}_{k,k'} \int \frac{\mathcal{D}\overline{\psi}\psi}{\mathcal{Z}^\Lambda_0} \psi_{k'}\overline{\psi}_k e^{\left(\left(\overline{\psi},\left[\mathcal{G}^{0,\Lambda}\right]^{-1}\psi\right)-S_{int}-(\overline{\psi},\eta^\Lambda)-(\overline{\eta}^\Lambda,\psi)\right)}
$$

$$
= \frac{1}{\mathcal{W}^\Lambda} \mathrm{Tr}\left(\partial_\Lambda \left[\mathcal{G}^{0,\Lambda}\right]^{-1} \frac{\delta}{\delta\overline{\eta}}\frac{\delta}{\delta\eta}\mathcal{W}^\Lambda\right) = \frac{1}{\mathcal{W}^\Lambda}\mathrm{Tr}\left(\partial_\Lambda \left[\mathcal{G}^{0,\Lambda}\right]^{-1} \frac{\delta}{\delta\overline{\eta}}\mathcal{W}^\Lambda\frac{\delta}{\delta\eta}\ln\mathcal{W}^\Lambda\right)
$$

$$
= \frac{1}{\mathcal{W}^\Lambda}\mathcal{W}^\Lambda\left[\mathrm{Tr}\left(\partial_\Lambda\left[\mathcal{G}^{0,\Lambda}\right]^{-1}\frac{\delta}{\delta\overline{\eta}}\mathcal{W}^{c,\Lambda}\frac{\delta}{\delta\eta}\mathcal{W}^{c,\Lambda}\right) + \mathrm{Tr}\left(\partial_\Lambda\left[\mathcal{G}^{0,\Lambda}\right]^{-1}\frac{\delta^2}{\delta\overline{\eta}\delta\eta}\mathcal{W}^{c,\Lambda}\right)\right]
$$

$$
= \left(\overline{\phi}, \partial_\Lambda\left[\mathcal{G}^{0,\Lambda}\right]^{-1}\phi\right) + \mathrm{Tr}\left(\partial_\Lambda\left[\mathcal{G}^{0,\Lambda}\right]^{-1}\frac{\delta^2}{\delta\overline{\eta}\delta\eta}\mathcal{W}^{c,\Lambda}\right) \tag{3.48}
$$

Putting all together provides

$$
\frac{d}{d\Lambda}\mathcal{W}^{c,\Lambda} = -\mathrm{Tr}\left(\mathcal{G}^{0,\Lambda}\partial_\Lambda\left[\mathcal{G}^{0,\Lambda}\right]^{-1}\right) + \mathrm{Tr}\left(\partial_\Lambda\left[\mathcal{G}^{0,\Lambda}\right]^{-1}\frac{\delta^2\mathcal{W}^{c,\Lambda}}{\delta\overline{\eta}\delta\eta}\right)
$$

$$
+ \left(\overline{\phi},\partial_\Lambda\left[\mathcal{G}^{0,\Lambda}\right]^{-1}\phi\right) - \left(\overline{\phi}_k,\frac{d\eta^\Lambda_k}{d\Lambda}\right) - \left(\frac{d\overline{\eta}^\Lambda_k}{d\Lambda},\phi_k\right) \tag{3.49}
$$

This makes it easy to differentiate Γ

$$
\frac{d}{d\Lambda}\Gamma = -\frac{d}{d\Lambda}\mathcal{W}^{c,\Lambda} - \left(\overline{\phi}_k,\frac{d\eta^\Lambda_k}{d\Lambda}\right) - \left(\frac{d\overline{\eta}^\Lambda_k}{d\Lambda},\phi_k\right) + \left(\overline{\phi},\partial_\Lambda\left[\mathcal{G}^{0,\Lambda}\right]^{-1}\phi\right)
$$

$$
= \mathrm{Tr}\left(\mathcal{G}^{0,\Lambda}\partial_\Lambda\left[\mathcal{G}^{0,\Lambda}\right]^{-1}\right) - \mathrm{Tr}\left(\partial_\Lambda\left[\mathcal{G}^{0,\Lambda}\right]^{-1}\frac{\delta^2\mathcal{W}^{c,\lambda}}{\delta\overline{\eta}\delta\eta}\right)
$$

$$
= \mathrm{Tr}\left(\mathcal{G}^{0,\Lambda}\partial_\Lambda\left[\mathcal{G}^{0,\Lambda}\right]^{-1}\right) - \mathrm{Tr}\left(\partial_\Lambda\left[\mathcal{G}^{0,\Lambda}\right]^{-1}\mathcal{V}^{(1,1)}\right) \tag{3.50}
$$

3.2.2   Flow equation for the Vertex Functions

For convenience we leave out the index Λ from now on, but we consider all operators to have a Λ-dependence. To get the $(1,1)$ matrix element of $\mathcal{V}$ we use equation (3.29) and expand the rhs around the full propagator $\mathcal{G}$.

$$
\mathcal{V} = \begin{pmatrix} \frac{\delta^2\Gamma}{\delta\overline{\phi}\delta\phi} + \left[\mathcal{G}^0\right]^{-1} & \frac{\delta^2\Gamma}{\delta\overline{\phi}\delta\overline{\phi}} \\ \frac{\delta^2\Gamma}{\delta\phi\delta\phi} & \frac{\delta^2\Gamma}{\delta\phi\delta\overline{\phi}} - \left[\left[\mathcal{G}^0\right]^{-1}\right]^T \end{pmatrix}^{-1} \tag{3.51}
$$

To get a dependence of the full propagator we insert a fat zero containing the self energy and thus we can use the Dyson equation to bring the full propagator into play:

$$
\frac{\delta^2\Gamma}{\delta\overline{\phi}\delta\phi} + \left[\mathcal{G}^0\right]^{-1} = \frac{\delta^2\Gamma}{\delta\overline{\phi}\delta\phi} - \gamma_1 + \gamma_1 + \left[\mathcal{G}^0\right]^{-1} = \frac{\delta^2\Gamma}{\delta\overline{\phi}\delta\phi} - \gamma_1 + \left[\mathcal{G}\right]^{-1} \tag{3.52}
$$

Since we will use it in the following, it is convenient to define an abbreviation for the first two terms:

$$\mathcal{U} := \frac{\delta^2 \Gamma}{\delta\overline{\phi}\delta\phi} - \gamma_1.$$

Now we can factor out $\mathcal{G}$

$$
\begin{aligned}
\mathcal{V} &= \begin{pmatrix} \mathcal{U} + [\mathcal{G}]^{-1} & \frac{\delta^2 \Gamma}{\delta\overline{\phi}\delta\overline{\phi}} \\ \frac{\delta^2 \Gamma}{\delta\phi\delta\phi} & -\mathcal{U}^T - [[\mathcal{G}]^{-1}]^T \end{pmatrix}^{-1} \\
&= \left[\begin{pmatrix} [\mathcal{G}]^{-1} & 0 \\ 0 & -[[\mathcal{G}]^{-1}]^T \end{pmatrix} + \begin{pmatrix} \mathcal{U} & \frac{\delta^2 \Gamma}{\delta\overline{\phi}\delta\overline{\phi}} \\ \frac{\delta^2 \Gamma}{\delta\phi\delta\phi} & -\mathcal{U}^T \end{pmatrix} \right]^{-1} \\
&= - \left[1 - \begin{pmatrix} -\mathcal{G} & 0 \\ 0 & [\mathcal{G}]^T \end{pmatrix} \begin{pmatrix} \mathcal{U} & \frac{\delta^2 \Gamma}{\delta\overline{\phi}\delta\overline{\phi}} \\ \frac{\delta^2 \Gamma}{\delta\phi\delta\phi} & -\mathcal{U}^T \end{pmatrix} \right]^{-1} \begin{pmatrix} -\mathcal{G} & 0 \\ 0 & [\mathcal{G}]^T \end{pmatrix} \\
&= - \underbrace{\left[1 + \overbrace{\begin{pmatrix} \mathcal{G}\mathcal{U} & \mathcal{G}\frac{\delta^2 \Gamma}{\delta\overline{\phi}\delta\overline{\phi}} \\ -\mathcal{G}^T\frac{\delta^2 \Gamma}{\delta\phi\delta\phi} & \mathcal{G}^T\mathcal{U}^T \end{pmatrix}}^{:=\mathcal{A}} \right]^{-1}}_{=:\tilde{\mathcal{V}}} \begin{pmatrix} -\mathcal{G} & 0 \\ 0 & [\mathcal{G}]^T \end{pmatrix}
\end{aligned}
\tag{3.53}
$$

With this definition $\mathcal{V}^{(1,1)} = \tilde{\mathcal{V}}^{(1,1)}\mathcal{G}$ and we can write the differential equation as

$$\frac{d}{d\Lambda}\Gamma = \text{Tr}\left(\mathcal{G}^{0,\Lambda}\partial_\Lambda \left[\mathcal{G}^{0,\Lambda} \right]^{-1} \right) - \text{Tr}\left(\mathcal{G}\partial_\Lambda \left[\mathcal{G}^{0,\Lambda} \right]^{-1} \tilde{\mathcal{V}}^{(1,1)} \right). \tag{3.54}$$

Now we expand $\tilde{\mathcal{V}}$ into a taylor series around $\mathcal{A} = 0$:

$$[1 + \mathcal{A}]^{-1} = 1 - \mathcal{A} + \mathcal{A}\mathcal{A} - \mathcal{A}\mathcal{A}\mathcal{A} + \dots \tag{3.55}$$

Inserting the definition of $\mathcal{A}$ and taking the $(1,1)$-matrix element provides

$$\tilde{\mathcal{V}}^{(1,1)} = 1 - \mathcal{G}\mathcal{U} + \left(\mathcal{G}\mathcal{U}\mathcal{G}\mathcal{U} - \mathcal{G}\frac{\delta^2 \Gamma}{\delta\overline{\phi}\delta\overline{\phi}}\mathcal{G}^T\frac{\delta^2 \Gamma}{\delta\phi\delta\phi} \right) - \left(\mathcal{G}\mathcal{U}\mathcal{G}\mathcal{U}\mathcal{G}\mathcal{U} + \dots \right) + \dots \tag{3.56}$$

where the brackets group the orders of expansion, and

$$\Gamma = \sum_{m=0}^{\infty} \frac{(-1)^m}{(m!)^2} \sum_{k_1'\dots k_m'} \sum_{k_1\dots k_m} \gamma_m(k_1', \dots, k_m'; k_1, \dots, k_m)\overline{\phi}_{k_1'} \dots \overline{\phi}_{k_m'}\phi_{k_m} \dots \phi_{k_1}. \tag{3.57}$$

Note the minus signs when performing the functional derivative: the factor $(-1)^m$ cancels all minus signs due to permuting the $\overline{\phi}$-derivatives through the ϕ's. Inserted in $\mathcal{U}$ gives

$$\mathcal{U}_{q',q} = \sum_{m=1}^{\infty} \frac{(-1)^m}{(m!)^2} \sum_{k_1'\dots k_m'} \sum_{k_1\dots k_m} \gamma_{m+1}(k_1', \dots, k_m', q'; k_1, \dots, k_m, q)\overline{\phi}_{k_1'} \dots \overline{\phi}_{k_m'}\phi_{k_m} \dots \phi_{k_1}. \tag{3.58}$$

$\mathcal{U}$ is a tensor of rank two what we indicated by the indices q', q. These quantum numbers appear in each vertex. Note that due to the differentiation all indices are shifted by one and the first summand cancels. So $\mathcal{U}$ is at least of second order in the fields and does not depend on γ_0 and γ_1.

The Zero-Particle Vertex Function

For completeness we want to write down the differential equation for γ_0, although we won't need it. To this end we collect all terms off the rhs of (3.54) that do not depend on ϕ or $\overline{\phi}$. For $\tilde{\mathcal{V}}^{(1,1)}$ this is only the constant 1. Thus we get

$$\frac{d}{d\Lambda}\gamma_0 = \mathrm{Tr}\left(\mathcal{G}^{0,\Lambda}\partial_\Lambda\left[\mathcal{G}^{0,\Lambda}\right]^{-1}\right) - \mathrm{Tr}\left(\mathcal{G}\partial_\Lambda\left[\mathcal{G}^{0,\Lambda}\right]^{-1}\right). \tag{3.59}$$

The One-Particle Vertex Function

Now we are in a position to set up the differential equation for the m-particle vertex. The major task, as one could imagine, is to collect all terms with equal powers of $\overline{\phi}\phi$ in the expansion (3.56), in particular for higher powers. Later we will give some hints how one can use Feynman diagrams to facilitate this exercise. We can get by without these for the one-particle vertex, because only the second term in (3.56) is linear in $\overline{\phi}\phi$. This can be seen from the expansion of $\mathcal{U}$ (3.58), noting that $\mathcal{G}\frac{\delta^2\Gamma}{\delta\overline{\phi}\delta\phi}\mathcal{G}^T\frac{\delta^2\Gamma}{\delta\phi\delta\phi}$ contains only quadratic terms in $\overline{\phi}\phi$. We will comment on this term later.

$$\frac{d}{d\Lambda}\gamma_1(k',k) = \sum_{q',q}\left[\mathcal{G}\partial_\Lambda\left[\mathcal{G}^{0,\Lambda}\right]^{-1}\mathcal{G}\right]_{q,q'}\gamma_2(k',q';k,q) \tag{3.60}$$

To make the notation clear we replaced the trace by a sum over all quantum numbers, but in the following we will use the more efficient notation:

$$\left[\gamma_m(k'_1,\ldots,k'_{m-1},\,\cdot\,;k_1,\ldots,k_{m-1},\,\cdot\,)\right]_{q',q} = \gamma_m(k'_1,\ldots,k'_{m-1},q';k_1,\ldots,k_{m-1},q). \tag{3.61}$$

Furthermore, we use the convenient definition

$$\mathcal{S} := \mathcal{G}\partial_\Lambda\left[\mathcal{G}^{0,\Lambda}\right]^{-1}\mathcal{G}, \tag{3.62}$$

so (3.60) becomes

$$\frac{d}{d\Lambda}\gamma_1(k',k) = \mathrm{Tr}\left[\mathcal{S}\,\gamma_2(k',\,\cdot\,;k,\,\cdot\,)\right]. \tag{3.63}$$

Note the beauty of this formula. Now one can say we have done a good job, because the derivative of the vertex contains only two particle irreducible diagrams, as is the case for the vertex itself. However the rhs is not independent of γ_1 since $\mathcal{G}$ and thus $\mathcal{S}$ depends on it.

The Two-Particle Vertex Function

Before writing down the flow equation for γ_2, we consider on the following relations:

$$\frac{\delta^2\Gamma}{\delta\overline{\phi}\delta\overline{\phi}} = \sum_{m=2}^{\infty} \frac{m(m-1)(-1)^m}{(m!)^2} \sum_{k'_1...k'_{m-2}} \sum_{k_1...k_m} \gamma_m(k'_1,\ldots,k'_{m-2},\cdot,\cdot;k_1,\ldots,k_m) \overline{\phi}_{k'_1}\ldots\overline{\phi}_{k'_{m-2}}\phi_{k_{m-2}}\ldots\phi_{k_1} \quad (3.64)$$

$$\frac{\delta^2\Gamma}{\delta\phi\delta\phi} = \sum_{m=2}^{\infty} \frac{m(m-1)(-1)^m}{(m!)^2} \sum_{k'_1...k'_m} \sum_{k_1...k_m} \gamma_m(k'_1,\ldots,k_m;k_1,\ldots,k'_{m-2},\cdot,\cdot) \overline{\phi}_{k'_1}\ldots\overline{\phi}_{k'_m}\phi_{k_{m-2}}\ldots\phi_{k_1}. \quad (3.65)$$

As long as we have not a broken symmetry, all cross-terms in $\mathcal{G}\frac{\delta^2\Gamma}{\delta\overline{\phi}\delta\overline{\phi}}\mathcal{G}^T\frac{\delta^2\Gamma}{\delta\phi\delta\phi}$ that contain a different number of creation and annihilation operators vanish. Note that the flow equation (3.54) with the expansion of $\tilde{\mathcal{V}}$ (3.56) only contains products of (3.64), (3.65) and $\mathcal{U}$ (3.58). Consequently, the derivative of the m-particle vertex contains vertices up to order $m+1$.

To set up the differential equation of γ_2 we need all terms in (3.56) that are proportional to $\overline{\phi}\overline{\phi}\phi\phi$. As one can easily convince oneself they only appear in

$$\mathcal{G}\mathcal{U} - \mathcal{G}\frac{\delta^2\Gamma}{\delta\overline{\phi}\delta\overline{\phi}}\mathcal{G}^T\frac{\delta^2\Gamma}{\delta\phi\delta\phi} + \mathcal{G}\mathcal{U}\mathcal{G}\mathcal{U} \quad (3.66)$$

The first term is proportional to γ_3. The second and third are quadratic in γ_2.

$$\frac{d}{d\Lambda}\gamma_2(k'_1,k'_2;k_1,k_2) = \mathrm{Tr}\left(\mathcal{S}\gamma_3(k'_1,k'_2,\cdot;k_1,k_2,\cdot)\right) \quad (3.67a)$$

$$- \mathrm{Tr}\left(\mathcal{S}\gamma_2(\cdot,\cdot;k_1,k_2)\mathcal{G}^T\gamma_2(k'_1,k'_2;\cdot,\cdot)\right) \quad (3.67b)$$

$$- \mathrm{Tr}(\mathcal{S}\gamma_2(k'_1,\cdot;k_1,\cdot)\mathcal{G}\gamma_2(k'_2,\cdot;k_2,\cdot)) \quad (3.67c)$$

$$- \mathrm{Tr}(\mathcal{S}\gamma_2(k'_2,\cdot;k_2,\cdot)\mathcal{G}\gamma_2(k'_1,\cdot;k_1,\cdot)) \quad (3.67d)$$

$$+ \mathrm{Tr}(\mathcal{S}\gamma_2(k'_2,\cdot;k_1,\cdot)\mathcal{G}\gamma_2(k'_1,\cdot;k_2,\cdot)) \quad (3.67e)$$

$$+ \mathrm{Tr}(\mathcal{S}\gamma_2(k'_1,\cdot;k_2,\cdot)\mathcal{G}\gamma_2(k'_2,\cdot;k_1,\cdot)). \quad (3.67f)$$

Since, in this work, we will set all higher vertices to zero, the equations (3.60) and (3.67) are the major results of this chapter. To understand the structure of the flow equation we want to illustrate terms (b) - (f) in Feynman diagrams. We will represent the two-particle vertex by a wiggly line, where both ends have one ingoing and one outgoing fermionic line. Although normally it is used for the bare interaction, we will use it here for the effective interaction, for reasons that will become obvious. Furthermore we will use a dashed line for the propagator $\mathcal{S}$, but in the first instance one can regard it as a standard fermionic

propagator. Consequently the Feynman diagram of term (3.67 b) looks like

$$(3.68)$$

We call diagrams where two particle are interacting with each other particle-particle diagram. By contrast term (3.67 c) can be illustrated as follows

$$(3.69)$$

Here a virtual particle-hole-pair is created, so this diagram is a particle-hole diagram. In (3.67 d) k_1 and k_2 and k_1' and k_2' are interchanged. This is equivalent to flip the diagram around the horizontal axis and interchange $\mathcal{G}$ and $\mathcal{S}$. Thus the structure is the same as the one of diagram (3.70)

Finally we draw the term in (3.67 e)

$$(3.70a)$$

Pulling on the lower external legs this can be deformed into the following diagram with the same meaning:

$$(3.70b)$$

Finally we rotate the lower line.

$$
\tag{3.70c}
$$

What we get is a diagram where the arrows point in different directions, so again we have a diagram of particle-hole type. For the terms (3.67 e) and (3.67 f) we can make the same symmetry arguments as for (3.67 c) and (3.67 d).

These pictures should be kept in mind when checking conservation laws and other symmetries. For example, when the two-particle vertex is diagonal in spin space, then

$$
\tag{3.71}
$$

$$
\tag{3.72}
$$

Figure 3.1: Feynman graph representation of equation (3.60) and equation(3.67)

in diagram (3.70) the two propagators $\mathcal{G}$ and $\mathcal{S}$ have to be evaluated at the same spin quantum number. This is not the case for the diagrams (3.68) and (3.70). For (3.68) $\mathcal{S}$, k_2 and k_2', respectively $\mathcal{G}$, k_1 and k_1' have the same spin quantum number.

In general one could derive the differential equation of the vertices of arbitrary order from (3.54) combined with (3.56). But it is convenient to define Feynman rules for this task. We only want to sketch them, for details consult [22] and citation in there. The diagrammatic version of the flow equation (3.60) and (3.67) are shown in 3.1.

Although external legs are amputated, we indicated the direction by little arrows. As already mentioned, vertices up to order $m + 1$ enter in the flow equation of the m-particle vertex. The $m + 1$-particle vertex appears only linearly since it follows due to the second term of (3.56) $\mathcal{G}\mathcal{U}$. All other vertices have to form one-loop diagram such that they have m ingoing and outgoing legs.

3.3   Applying fRG on Concrete Problems

To be able to apply the fRG flow equations to physical problems we have to specify the truncation and the explicit Λ-dependence of the free propagator. Furthermore we have to make some approximations.

3.3.1   Truncation

We already mentioned that we will set all m-particle vertices with $m \geq 3$ to zero. This can be justified as follows: At $\Lambda_{initial}$ all vertices except the two particle vertex are zero and all higher vertices are generated by the two-particle vertex at least in third power. So as long as the effective interaction can be regarded as small, all higher vertices can be neglected. If at any value of Λ, the flow equation generates a two particle vertex that can not be regarded as small or even is divergent, this approximation brakes down. If one solves the differential equation numerically one is well advised to implement some "emergency-stop" for this case.

3.3.2   Further Approximations

The quantum numbers in (3.60) and (3.67) contain, in addition to the space or momentum quantum number, Matsubara frequencies. Considering a Hamiltonian that does not depend on time, the vertex functions stay diagonal in frequency space, i.e. the sum of all ingoing is equal to the sum of all outgoing frequencies. For the one particle vertex, this means we can write it as $\gamma_1(k', k, i\omega_n)$. Now k' and k only contain space or momentum quantum numbers. The problem is, there are infinitely many Matsubara frequencies, and thus solving the system of differential equations numerically is impossible. To deal with this problem we will follow the crudest way, i.e. we will neglect the frequency dependence of the bare interaction altogether. This will lead to frequency independent vertex functions and thus a frequency independent self energy. Consequently the self energy can be viewed as an

effective potential. In real space the nonlocal part of the effective potential changes the kinetic energy and thus has an influence on the spectral weight. However we can not hope to obtain an accurate output for nonzero frequency. Only for the limit $\omega \to 0$ this ansatz is meant to lead to the right results. As a consequence, we can only calculate observables like the conductance for the case $T = 0$. This fact reduces our possibilities of analyzing the origin of the 0.7 anomaly of QPCs since it has an interesting behavior for nonzero frequencies, and a major goal of future work will be to to find a way to introduce some frequency dependence.

Although we dropped the frequency dependence of the two-particle vertex, we have to keep track of energy conservation. As a result, the frequencies for which we have to evaluate the propagators $\mathcal{S}$ and $\mathcal{G}$ in equation (3.67) are not independent. Setting the three particle vertex to zero, equation (3.67) becomes:

$$
\frac{d}{d\Lambda}\gamma_2^\Lambda(k_1', k_2'; k_1, k_2) =
$$

$$
\sum_{i\omega_n} \sum_{q,q',s,s'} \Big[-\mathcal{S}_{q,q'}^\Lambda(i\omega_n)\gamma_2^\Lambda(q', s'; k_1, k_2)\mathcal{G}_{s,s'}^\Lambda(-i\omega_n)\gamma_2^\Lambda(k_1', k_2'; s, q)
$$

$$
-\mathcal{S}_{q,q'}^\Lambda(i\omega_n)\gamma_2^\Lambda(k_1', q'; k_1, s)\mathcal{G}_{s,s'}^\Lambda(i\omega_n)\gamma_2^\Lambda(k_2', s'; k_2, q)
$$

$$
-\mathcal{S}_{q,q'}^\Lambda(i\omega_n)\gamma_2^\Lambda(k_2', q'; k_2, s)\mathcal{G}_{s,s'}^\Lambda(i\omega_n)\gamma_2^\Lambda(k_1', s'; k_1, q)
$$

$$
+\mathcal{S}_{q,q'}^\Lambda(i\omega_n)\gamma_2^\Lambda(k_2', q'; k_1, s)\mathcal{G}_{s,s'}^\Lambda(i\omega_n)\gamma_2^\Lambda(k_1', s'; k_2, q)
$$

$$
+\mathcal{S}_{q,q'}^\Lambda(i\omega_n)\gamma_2^\Lambda(k_1', q'; k_2, s)\mathcal{G}_{s,s'}^\Lambda(i\omega_n)\gamma_2^\Lambda(k_1', s'; k_2, q)\Big]. \tag{3.73}
$$

3.3.3 Λ-dependence of the free Propagator

We still have not specified the Λ-dependence of the free propagator. The only restriction we made until now is that there has to exist some $\Lambda_{initial}$ for which the value of all vertices has to be known. E.g. for $\mathcal{G}^{\Lambda_{initial}} = 0$ all vertices except the two-particle vertex are zero. Furthermore there has to be a Λ_{final} were the free propagator is the ordinary one ($\mathcal{G}^{\Lambda_{final}} = \mathcal{G}$).

In low-dimensional interacting systems one often faces the problem that perturbation series are divergent at momentum-transfer zero, i.e. at the Fermi surface[4]. So the idea is to cut off the frequencies around the Fermi surface, i.e. the zero-point of the energy scale, in the following way.

$$
\mathcal{G}^{0,\Lambda} = \Theta(|\omega| - \Lambda)\mathcal{G}^0 \tag{3.74}
$$

where Θ is the usual step-function. In this work we only consider the case $T = 0$. If one wants to treat finite temperature one has to use a smoothed Θ-function. With this choice $\mathcal{G}^\Lambda$ conforms to the requirements with $\Lambda_{initial} = \infty$ and $\Lambda_{final} = 0$.

---

[4]compare e.g. [21] §17

3.3.4   Morris' Lemma

As we will need it in the following, we want to quote the result of Morris' lemma without proof: For a product of a δ and Θ-functions, where both are limits of smoothed functions

$$\delta = \lim_{\epsilon \to 0} \delta_\epsilon, \quad \Theta = \lim_{\epsilon \to 0} \Theta_\epsilon, \tag{3.75}$$

the following holds:

$$\delta_\epsilon f\left(\Theta_\epsilon\right) \to \delta \int_0^1 f(t)dt. \tag{3.76}$$

In equation (3.62) we defined the operator $\mathcal{S}$, which now can be simplified, since we have specified the cutoff. We will put an index Λ if the operators depend on the cutoff, thus if we write $\mathcal{G}^0$ we mean the cutoff-free free propagator.

$$\begin{aligned}
\mathcal{S}^\Lambda &= \mathcal{G}^\Lambda \partial_\Lambda \left[\mathcal{G}^{0,\Lambda}\right]^{-1} \mathcal{G}^\Lambda \\
&= \frac{1}{1 + \Theta\mathcal{G}^0\gamma_1^\Lambda} \Theta\mathcal{G}^0 \left[\mathcal{G}^0\right]^{-1} \frac{1}{\Theta^2}\delta \frac{1}{1 + \Theta\mathcal{G}^0\gamma_1^\Lambda} \Theta\mathcal{G}^0 \\
&= \frac{\delta}{(1 + \Theta\mathcal{G}^0\gamma_1^\Lambda)^2} \mathcal{G}^0 \\
&= \delta\partial_\Theta \frac{1}{1 + \Theta\mathcal{G}^0\gamma_1^\Lambda} \Theta\mathcal{G}^0 \\
&= \delta(|\omega| - \Lambda)\partial_\Theta \mathcal{G}^\Lambda, \tag{3.77}
\end{aligned}$$

where we used (3.74) and

$$\mathcal{G}^\Lambda = \frac{1}{\left[\mathcal{G}^{0,\Lambda}\right]^{-1} + \gamma_1^\Lambda} = \frac{1}{1 + \Theta\mathcal{G}^0\gamma_1^\Lambda} \Theta\mathcal{G}^0. \tag{3.78}$$

3.3.5   Final Version on the flow Equations

Now we are able to carry out the frequency sum in equation (3.60), which in the limit $T = 0$ is an integral.

$$\begin{aligned}
\frac{d}{d\Lambda}\gamma_1(k', k) &= \frac{1}{2\pi} \int d\omega \sum_{q',q} \mathcal{S}^\Lambda_{q,q'}(i\omega)\gamma_2(k', q'; k, q) \\
&= \frac{1}{2\pi} \int d\omega \sum_{q',q} \delta(|\omega| - \Lambda)\partial_\Theta \mathcal{G}^\Lambda_{q,q'}(i\omega)\gamma_2(k', q'; k, q) \\
&= \frac{1}{2\pi} \int d\omega \sum_{q',q} \delta(|\omega| - \Lambda) \int_0^1 dt\partial_t \left.\mathcal{G}^\Lambda_{q,q'}(i\omega)\right|_{\Theta=t} \gamma_2(k', q'; k, q) \\
&= \frac{1}{2\pi} \sum_{\omega=\pm\Lambda} \sum_{q',q} \tilde{\mathcal{G}}^\Lambda_{q,q'}(i\omega)\gamma_2(k', q'; k, q), \tag{3.79}
\end{aligned}$$

where we defined the operator

$$\tilde{\mathcal{G}}^\Lambda = \frac{1}{[\mathcal{G}^0]^{-1} + \gamma_1^\Lambda}.$$ (3.80)

Equation (3.79) now is the final form of the fRG flow equation. This equation and the final flow equation of the two-particle vertex will be the starting point of our calculations. In order to derive the latter we consider the following integral:

$$\frac{1}{2\pi} \int d\omega \mathcal{S}_{q,q'}^\Lambda(i\omega) \mathcal{G}_{s,s'}^\Lambda(\pm i\omega)$$

$$= \frac{1}{2\pi} \int d\omega \delta(|\omega| - \Lambda) \int_0^1 dt \left[\partial_\Theta \mathcal{G}_{q,q'}^\Lambda(i\omega) \right]_{\Theta=t} \left[\mathcal{G}_{s,s'}^\Lambda(\pm i\omega) \right]_{\Theta=t}$$

$$= \frac{1}{2\pi} \int d\omega \delta(|\omega| - \Lambda) \int_0^1 dt \frac{1}{2} \partial_t \left[\mathcal{G}_{q,q'}^\Lambda(i\omega) \mathcal{G}_{s,s'}^\Lambda(\pm i\omega) \right]_{\Theta=t}$$

$$= \frac{1}{4\pi} \int d\omega \delta(|\omega| - \Lambda) \tilde{\mathcal{G}}_{q,q'}^\Lambda(i\omega) \tilde{\mathcal{G}}_{s,s'}^\Lambda(\pm i\omega)$$

$$= \frac{1}{4\pi} \sum_{\omega=\pm\Lambda} \tilde{\mathcal{G}}_{q,q'}^\Lambda(i\omega) \tilde{\mathcal{G}}_{s,s'}^\Lambda(\pm i\omega).$$ (3.81)

This identity, together with (3.73), the symmetries (3.37), and the cyclic invariance of the trace yields:

$$\frac{d}{d\Lambda} \gamma_2^\Lambda(k_1', k_2'; k_1, k_2) =$$

$$\frac{1}{2\pi} \sum_{\omega=\pm\Lambda} \sum_{q,q',s,s'} \left[-\frac{1}{2} \tilde{\mathcal{G}}_{q,q'}^\Lambda(i\omega) \gamma_2^\Lambda(q', s'; k_1, k_2) \tilde{\mathcal{G}}_{s,s'}^\Lambda(-i\omega) \gamma_2^\Lambda(k_1', k_2'; s, q) \right.$$

$$- \tilde{\mathcal{G}}_{q,q'}^\Lambda(i\omega) \gamma_2^\Lambda(k_1', q'; k_1, s) \tilde{\mathcal{G}}_{s,s'}^\Lambda(i\omega) \gamma_2^\Lambda(k_2', s'; k_2, q)$$

$$\left. + \tilde{\mathcal{G}}_{q,q'}^\Lambda(i\omega) \gamma_2^\Lambda(k_2', q'; k_1, s) \tilde{\mathcal{G}}_{s,s'}^\Lambda(i\omega) \gamma_2^\Lambda(k_1', s'; k_2, q) \right].$$ (3.82)

From now on the quantum numbers we use do not contain the frequency.

Note that we did not keep track of the inverse temperature β, since we absorbed it from the beginning into the bare interaction.

3.3.6 Initial Condition

We already mentioned that, since at $\Lambda_{initial} = \infty$ the free propagator is equal to zero and thus an expansion of all vertex function leads zero except for the two-particle vertex. As a result, the initial condition reads:

$$\gamma_2^{\Lambda=\infty}(k_1', k_2'; k_1, k_2) = \bar{v}_{k_1', k_2'; k_1, k_2}$$
$$\gamma_m^{\Lambda=\infty} = 0 \quad (m \neq 2)$$ (3.83)

This is correct for $\Lambda_{initial} = \infty$, however numerically it is not possible to start the flow at infinity. One has to take some Λ_0, which is much bigger than all relevant energies. Although for large values of Λ nothing really happens, since $\tilde{\mathcal{G}}^{\Lambda_0}(i\Lambda_0) \approx \frac{1}{i\Lambda_0} \approx 0$, one has to be careful, because we neglected the convergence factor $e^{i\omega 0^+}$ in our calculations from equation (3.8) on, which can only be done for finite ω. In the limit $\omega \to \infty$ this factor leads to a finite value, which we get by integrating the differential equation of γ_1 (3.79) from infinity down to any finite value $\Lambda = \Lambda_0$:

$$
\begin{aligned}
\gamma_1^{\Lambda_0}(k', k) &= \frac{1}{2\pi} \lim_{\epsilon \to 0} \int_\infty^{\Lambda_0} d\Lambda \sum_{\omega = \pm\Lambda} \sum_{q,q'} e^{i\omega\epsilon} \tilde{\mathcal{G}}_{q,q'}^\Lambda(i\omega) \gamma_2(k', q'; k, q) \\
&= \frac{1}{2\pi} \lim_{\epsilon \to 0} \int_\infty^{\Lambda_0} d\Lambda \sum_{\omega = \pm\Lambda} \sum_{q,q'} e^{i\omega\epsilon} \frac{\delta_{q',q}}{i\omega} \overline{v}_{k',q';k,q} + \mathcal{O}(\Lambda_0^{-1}) \\
&= \frac{1}{\pi} \sum_q \overline{v}_{k',q;k,q} \lim_{\epsilon \to 0} \int_\infty^{\Lambda_0} d\Lambda \frac{\sin\Lambda\epsilon}{\Lambda} + \mathcal{O}(\Lambda_0^{-1}) \\
&= \frac{1}{\pi} \sum_q \overline{v}_{k',q;k,q} \left[\underbrace{\lim_{\epsilon \to 0} \int_0^{\Lambda_0} d\Lambda \frac{\sin\Lambda\epsilon}{\Lambda}}_{=0 \text{ independent of } \Lambda_0} - \underbrace{\lim_{\epsilon \to 0} \int_0^\infty d\Lambda \frac{\sin\Lambda\epsilon}{\Lambda}}_{=\frac{\pi}{2} \text{ independent of } \epsilon} \right] + \mathcal{O}(\Lambda_0^{-1}) \\
&= -\frac{1}{2} \sum_q \overline{v}_{k',q;k,q} + \mathcal{O}(\Lambda_0^{-1}).
\end{aligned}
\tag{3.84}
$$

In the second line we used that

$$
\begin{aligned}
\int_\infty^{\Lambda_0} d\omega \tilde{\mathcal{G}}_{q,q'}^\Lambda(i\omega) &= \int_\infty^{\Lambda_0} d\omega \left[\frac{1}{i\omega - H + \gamma_1^\Lambda} \right]_{q,q'} \\
&= \int_\infty^{\Lambda_0} d\omega \frac{\delta_{q,q'}}{i\omega} + \int_\infty^{\Lambda_0} d\omega \mathcal{O}(\omega^{-2}) \\
&= \int_\infty^{\Lambda_0} d\omega \frac{\delta_{q,q'}}{i\omega} + \mathcal{O}(\Lambda_0^{-1}).
\end{aligned}
\tag{3.85}
$$

Note that we have two limits: The first limit is the integral, since $\int_\infty$ is defined as $\lim_{a \to \infty} \int_a$. We showed that we are not allowed to interchange it with the second limit.

This provides the final version of the initial condition.

$$
\gamma_1^{\Lambda_0}(k', k) = -\frac{1}{2} \sum_q \overline{v}_{k',q;k,q}
$$

$$
\gamma_2^{\Lambda_0}(k_1', k_2'; k_1, k_2) = \overline{v}_{k_1',k_2';k_1,k_2}
$$

$$
\gamma_m^{\Lambda_0} = 0 \quad (m > 2)
\tag{3.86}
$$

Chapter 4

fRG in one Dimension

4.1 Microscopic Model

Our intention is to describe a QPC in the 0.7 region, i.e. in the transition between zero and one open channel. This makes it plausible to consider only the lowest mode. The lowest mode is a true one dimensional QWR, which can be described by a one dimensional tight binding chain. Such a description is reasonable for two reasons: First, we want to describe a semiconductor where we have a finite bandwidth, with a cosine-like dispersion relation inside the first Brillouin zone. So we have to associate the lattice spacing with the distance of two sites. The second reason is a practical one. In order to handle the flow equation numerically we have to discretize the real space.

As discussed in section 2.2.1 the width of the QPC produces an effective potential which has to be added to the actual potential. Both have to be extracted from the potential generated by the top gate geometry considering many body effects like screening and dielectric properties of the materials. This has been done for example by Siddiki and Marquardt [23].

In order to take into account the effect of interaction we will use the extended Hubbard model, i.e. the bare interaction ranges up to nearest neigbours. This may sound like a crude simplification, since the bare interaction decays with $\frac{1}{|r|}$. However using a $\frac{1}{|r|}$ interaction would be wrong as well, since our method only takes into account one dimensional screening, not the screening that is caused by the material and the top gate. The latter is expected to have the greatest influence, since it is made up of metal which has a much higher mobility than semiconductors. A discussion about influences of metallic top gates was given by Guinea [24].

On both sides the contact is coupled to semi infinite non-interacting tight binding chains describing the baths - see figure (4.1). So the Hamiltonian reads

$$H = H_c + H_{lc} + H_l + H_{int} \tag{4.1a}$$
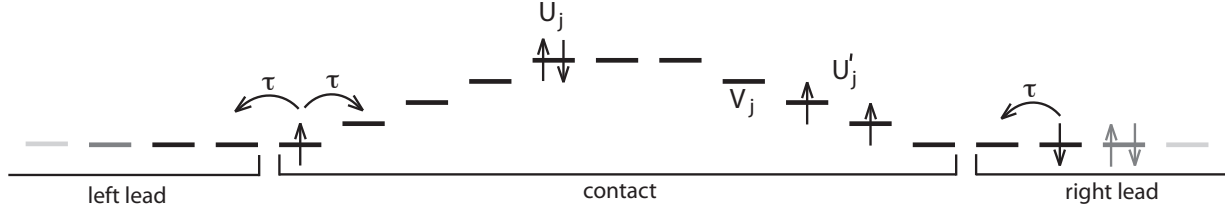
Figure 4.1: Microscopic Model

where

$$
H_c = \sum_{\sigma=\uparrow,\downarrow} \left[\sum_{j=-\frac{N}{2}+1}^{\frac{N}{2}} \left(V_j - \mu - \frac{\sigma h_j}{2} \right) d_{j,\sigma}^\dagger d_{j,\sigma} - \sum_{j=-\frac{N}{2}+1}^{\frac{N}{2}-1} \tau_j \left(d_{j+1,\sigma}^\dagger d_{j,\sigma} + h.c. \right) \right]. \qquad (4.1b)
$$

N is the numbers of sites belonging to the contact region, $d_{j,\sigma}$ ($d_{j,\sigma}^\dagger$) annihilates (creates) an electron with spin σ at site j of the contact. μ is the chemical and V_j the space-dependent potential, h_j a space dependent magnetic field and τ_j the hopping-matrix element. In most cases τ_j will be chosen independent of j.

$$
H_l = -\sum_{\sigma=\uparrow,\downarrow} \sum_{s=L,R} \sum_{j=1}^{\infty} \left[\mu\, c_{j,s,\sigma}^\dagger c_{j,s,\sigma} + \tau_l \left(c_{j+1,s,\sigma}^\dagger c_{j,s,\sigma} + h.c. \right) \right] \qquad (4.1c)
$$

$c_{j,s,\sigma}$ ($c_{j,s,\sigma}^\dagger$) annihilates (creates) an electron with spin σ on the left ($s = L$) respectively right ($s = R$) lead at site j. On both sides, site 1 is the one next to the contact. The bandwidth of these leads is equal to 4τ. Thus we will set $\tau := 1$ to define the energy scale. All other energies are measured in units of τ.

$$
H_{lc} = -\tau_{lc} \sum_{\sigma=\uparrow,\downarrow} \left(c_{1,L,\sigma}^\dagger d_{-\frac{N}{2}+1,\sigma} + d_{\frac{N}{2},\sigma}^\dagger c_{1,R,\sigma} + h.c. \right) \qquad (4.1d)
$$

couples the leads with the contact.

$$
H_{int} = \sum_{j=-\frac{N}{2}+1}^{\frac{N}{2}} U_j\, n_{j,\uparrow} n_{j,\downarrow} + \sum_{\sigma,\sigma'=\uparrow,\downarrow} \sum_{j=-\frac{N}{2}+1}^{\frac{N}{2}-1} U_j'\, n_{j,\sigma} n_{j+1,\sigma'} \qquad (4.1e)
$$

with $n_{j,\sigma} = d_{j,\sigma}^\dagger d_{j,\sigma}$ the local density operator. U_j is the charging energy when two electrons are on site j. U_j' is the energy of two electrons being on the neighbouring sited j and $j+1$.

4.1.1 Fundamentals of the Tight-Binding Model

First we want to discuss some details of the noninteracting tight binding chain. Therefore we want to diagonalize a infinite long tight binding chain with $V_j = 0$. It is convenient to

write the Hamiltonian in bra-ket notation

$$H_{TB} = -\mu \sum_j |j\rangle\langle j| - \tau \sum_j \left(|j\rangle\langle j+1| + |j+1\rangle\langle j| \right). \tag{4.2}$$

The diagonalization is an easy application of Bloch's theorem, which tells us that the eigenstate has the form

$$|\psi_k\rangle = \sum_j e^{ikj}|j\rangle. \tag{4.3}$$

Note that we can not normalize this state.

$$H_{TB}|\psi_k\rangle = \left[-\mu \sum_j |j\rangle\langle j| - \tau \sum_j \left(|j\rangle\langle j+1| + |j+1\rangle\langle j| \right) \right] \sum_j e^{ikj}|j\rangle$$

$$= \left[-\mu - \tau \left(e^{ik} + e^{-ik} \right) \right] \sum_j e^{ikj}|j\rangle$$

$$= \left[-\mu - 2\tau \cos k \right] |\psi_k\rangle \tag{4.4}$$

This proves that $|\psi_k\rangle$ in fact is an eigenstate of H_{TB} with eigenvalue

$$\omega_k = -\mu - 2\tau \cos k. \tag{4.5}$$

Thus, the density of states is given by:

$$A(\omega_k) = \frac{dk}{d\omega_k} = \frac{1}{\frac{d\omega_k}{dk}} = \frac{1}{2\tau \sin k} = \frac{1}{\sqrt{4\tau^2 - \omega_k^2}}. \tag{4.6}$$
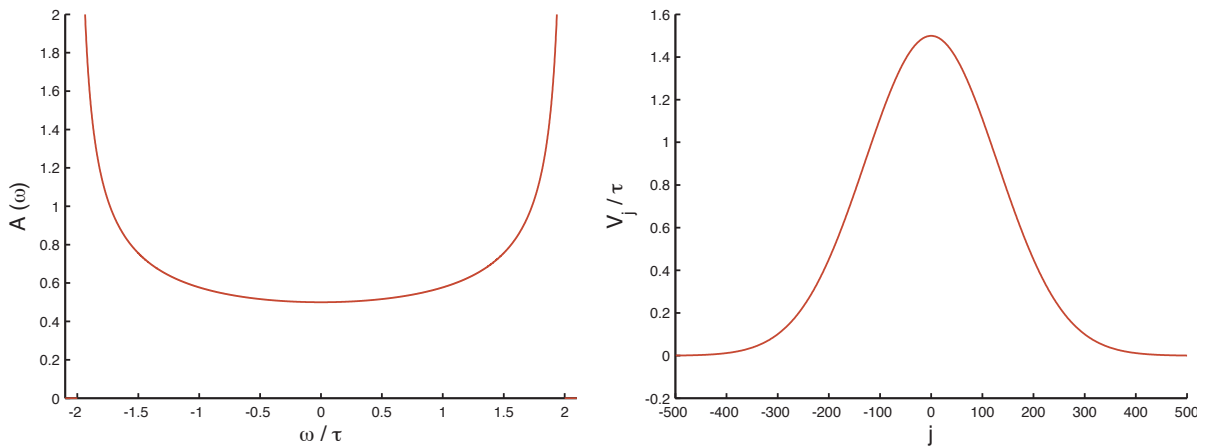
Figure 4.2: Left: Spectral function of an infinite long translationally invariant tight-binding chain. Right: Potential used to illustrate the band geometry of a tight-binding chain (see figure 4.3).

A plot of the spectral function with $\mu = 0$ is shown in figure 4.2, left panel. Note that the tight binding chain creates a band, which reaches from $\mu - 2\tau$ to $\mu + 2\tau$. If the length of the chain is finite, with length N, the spectral function consists of N delta peaks with equal weight. We get the eigenenergies and thus the position of the peaks by applying the quantization condition on k, namely $k_n = \pm n \frac{\pi}{N}$

$$\omega_n = -\mu - 2\tau \cos\left(\pm n \frac{\pi}{N}\right). \tag{4.7}$$

To obtain a smooth spectral function, the peaks have to be broadened by hand to with some value bigger than the typical energy spacing.

We now consider a tight binding chain with a smooth potential. We use a potential of gaussian shape, shown in figure 4.2, right panel. The smoothed spectral function as a function of ω and j is shown in figure 4.3. Note that the band looks like a tube where the center is defined by the local potential (blue line in figure 4.3). The band is filled up to the Fermi energy (red line in figure 4.3) which we shall take to define the zero point of the energy scale. For temperatures much smaller than the Fermi temperature, which is the only case that we shall consider, only states around the Fermi energy are of physical interest. As a result the conductance is one in units of $\frac{e^2}{h}$ (compare section 2.2.1) if the maximum of the potential is smaller than $-\mu + 2\tau$, so that the bottom of the shifted band always lie below zero, ensuring that there are always states available for carrying the current. Conversely, the conductance is zero if the potential maximum is larger than $-\mu + 2\tau$ (compare for example figure 5.8).

If we now consider a system with $\mu = 0$, i.e., a system, that for $V = 0$ is at half filling, and a potential defining some plateau, then in the region of the plateau we locally have a lower filling factor. Consequently we can always set μ to zero and adding an appropriate potential inside the contact region, to achieve the desired filling factor.
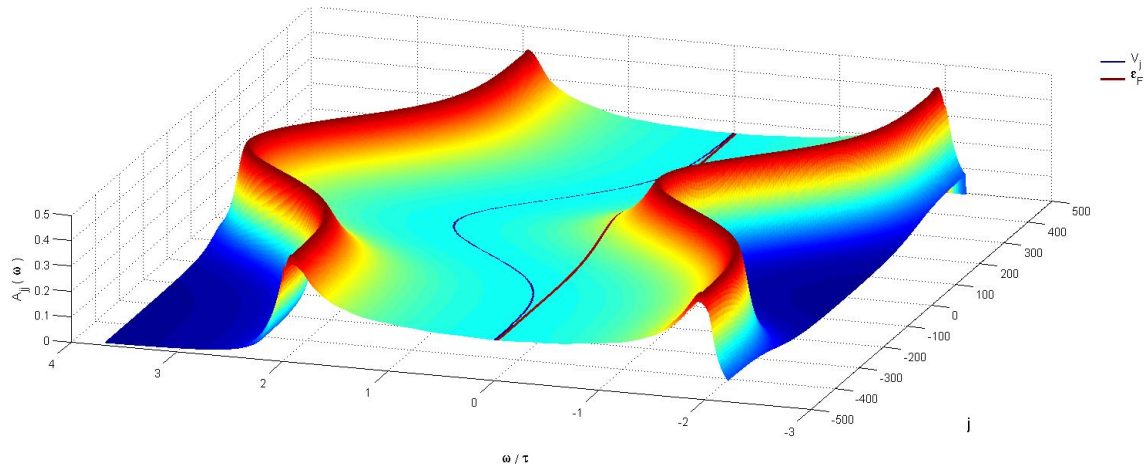
Figure 4.3: Smoothed (with $\delta = \tau/10$) spectral function (see equation (4.36)) as a function of ω and j for the potential shown in figure 4.2, right panel.

4.1.2 Influence of the Leads: The Projection Method

The model Hamiltonian (4.1) lives on an infinite-dimensional Hilbert space, which is impossible to threat numerically. But we are not interested in the details of the leads. The flow equations won't affect this part, since there is no interaction present. One effect of the two leads is, they produce a finite lifetime on the end of the contact, thus electrons are not reflected and boundary interference effects are suppressed. The second consequence is, since there is an infinite number of electrons on the lead, the number of electrons is not conserved. The electron-density at the end of the contact is fixed by the chemical potential. Electrons that are pushed away (drawn forward) by a potential can escape to (enter from) infinity.

To get a finite dimensional Hilbert space, we define a projection operator P that projects on the states inside the contact and a projector Q, perpendicular to P, that projects on the infinite-dimensional Hilbert space of the leads.

$$P + Q = 1, \qquad P^2 = P, \qquad Q^2 = Q \tag{4.8}$$

We only need the part of the propagator that connects states where the two-particle vertex functions are nonzero. This applies only inside the contact. Consequently we need $P\mathcal{G}P$. We define $PHP = H_{PP}$ etc., and with the above definition of P and Q obviously

$$H_{PP} = H_c + H_{int}, \qquad H_{PQ} + H_{QP} = H_{lc}, \qquad H_{QQ} = H_l. \tag{4.9}$$

$$\mathcal{G}_{PP}(\omega) = P\left[\omega - \begin{pmatrix} H_{PP} & H_{PQ} \\ H_{QP} & H_{QQ} \end{pmatrix}\right]^{-1} P = \left[\begin{pmatrix} \omega P - H_{PP} & -H_{PQ} \\ -H_{QP} & \omega Q - H_{QQ} \end{pmatrix}^{-1}\right]_{1,1}$$

$$= \frac{1}{\omega P - H_{PP} - H_{PQ}\frac{1}{\omega Q - H_{QQ}}H_{QP}} \tag{4.10}$$

Furthermore we define

$$\Sigma_{PP}(\omega) := -H_{PQ}\frac{1}{\omega Q - H_{QQ}}H_{QP}$$

$$= -\tau^2 \sum_{\sigma=\uparrow,\downarrow}\ \left[|1,\sigma\rangle\langle 1,\sigma,L|\tfrac{1}{\omega-H_{QQ}}|1,\sigma,L\rangle\langle 1,\sigma|\right.$$

$$\left. +|N,\sigma\rangle\langle 1,\sigma,R|\tfrac{1}{\omega-H_{QQ}}|1,\sigma,R\rangle\langle N,\sigma|\right]$$

$$= -\tau^2 \sum_{\sigma=\uparrow,\downarrow} \left[|1,\sigma\rangle g_{L,\sigma}(\omega)\langle 1,\sigma| +|N,\sigma\rangle g_{R,\sigma}(\omega)\langle N,\sigma|\right] \tag{4.11}$$

In the last line we defined the functions $g_{s,\sigma}$ $(s = L/R)$ which in our case are independent of s and σ due to symmetry, thus we will omit the indices. To calculate g we consider a infinite long chain, i.e. a chain that goes from $-\infty$ to ∞, with chemical potential μ. We

pick out one single site randomly, which then provides

$$G_{PP,\uparrow} = \frac{1}{\omega + \mu - \tau^2(g_{L,\uparrow}(\omega) + g_{R,\uparrow}(\omega))}$$

$$= \frac{1}{\omega + \mu - 2\tau^2 g(\omega)} \overset{!}{=} -i\frac{dk}{d\omega},$$

$$\Rightarrow g(\omega) = \frac{1}{2\tau^2}\left(\omega + \mu - i\frac{d\omega(k)}{dk}\right), \tag{4.12}$$

with $\omega(k)$ being the dispersion relation. This holds in general. Using the dispersion relation of a tight binding chain with hopping matrix-element τ,

$$\omega(k) = -2\tau\cos k - \mu, \qquad k = -\arccos\frac{\omega + \mu}{2\tau} \tag{4.13}$$

we get

$$\frac{d\omega}{dk} = 2\tau\sin k = \pm 2\tau a\sqrt{1 - \cos^2 k}$$

$$= \pm\sqrt{4\tau^2 - (\omega + \mu)^2}$$

$$\Rightarrow g(\omega) = \begin{cases} \frac{1}{2\tau^2}\left(\omega + \mu - i\sqrt{4\tau^2 - (\omega + \mu)^2}\right) & \Im(\omega) \geq 0 \\ \frac{1}{2\tau^2}\left(\omega + \mu + i\sqrt{4\tau^2 - (\omega + \mu)^2}\right) & \Im(\omega) < 0 \end{cases} \tag{4.14}$$

Note that the method we described here is exact. We now can thread the subspace of the contact, which has $2N$ dimensions (the 2 is due to spin), separately.

4.2 The fRG-flow equations

4.2.1 Spinless Fermions

First we will consider the case of spinless fermions on the grounds that we have less terms to keep track of, but all concepts can be illustrated. The spinfull case is more complicated, but no new ideas enter. The second reason is, that we can separate spin-effects like the Kondo resonance from other interaction-effects.

In the case of spinless fermions we have no sum over spins. Furthermore we have no onside-interactions, since the Pauli principle forbids that two electrons are on the same site. Consequently the different parts of our Hamiltonian (4.1) read

$$H_c = \left[\sum_{j=-\frac{N}{2}+1}^{\frac{N}{2}} (V_j - \mu)\, d_j^\dagger d_j - \sum_{j=-\frac{N}{2}+1}^{\frac{N}{2}-1} \left(\tau_j d_{j+1}^\dagger d_j + h.c.\right)\right] \tag{4.15a}$$

$$H_l = -\sum_{s=L,R}\sum_{k=1}^{\infty}\left[\mu\, c_{k,s}^\dagger c_{k,s} + \tau_l\left(c_{k+1,s}^\dagger c_{k,s} + h.c.\right)\right]. \tag{4.15b}$$

$$H_{lc} = -\tau_{lc} \left(c_{1,L}^\dagger d_1 + d_N^\dagger c_{1,R} + h.c. \right) \tag{4.15c}$$

and

$$H_{int} = \sum_{j=-\frac{N}{2}+1}^{\frac{N}{2}-1} U_j' n_j n_{j+1} \tag{4.15d}$$

This defines our system completely. So in principle one could solve the coupled flow equations for γ_1 and γ_2 numerically. But the number of variables is huge. The dimensionality of the Hilbert space, as mentioned, is N (for the spinless case), and thus γ_1 has N^2 and γ_2 N^4 independent variables. With a computer with around $10GB$ of memory N is bounded by 100. Using a computer with more memory does not really help, to push N one order of magnitude up means we need 10^4 times more memory, i.e. $100TB$!! This makes clear that we need to make more approximations. Taking all independent variables of γ_2 is absolutely unnecessary, since, due to screening-effects, the range of the interaction is bounded. This is a physical argument. One could also argue in the fRG scheme: the $\gamma_2(j, j+2; j, j+2)$ is generated in power of two by $\gamma_2(j, j+1; j, j+1)$, which is regarded as being small; $\gamma_2(j, j+4; j, j+4)$ is generated in second power by $\gamma_2(j, j+2; j, j+2)$, and so on, thus the effective interaction decays strongly with the distance. A good approximation would be

$$\gamma_2(j, j+l_1; j+l_2, j+l_3) = 0 \qquad \forall \, |l_1|, |l_2|, |l_3| > l \tag{4.16}$$

This reduces the number of independent variables to $N \cdot (2l+1)^3$. Also the independent variables of γ_1 are reduced to $N \cdot (2l+1)$, since γ_1 is generated by γ_2. Thus the total number of independent variables grows linearly with the system size. This is the best we can expect.

We will set l to 1, implying that the range of interaction, to be called the "numerical screening length" is only one lattice spacing. Although this is significantly smaller than the physical screening length (typically $50nm$), we expect that this will nevertheless capture the essential effect of interactions correctly, as long as the wavelength of relevant excitations is larger than the physical screening length. This will be the case if the potential varies smoothly on the scale of the physical screening length, and temperature is low enough.

With this choice of l, the only independent nonzero matrix element of the two-particle vertex is $\gamma_2(j, j+1, j, j+1)$. All other matrix elements containing j and $j+1$ can be expressed by this using the symmetries of the two-particle vertex (3.37). By consequence γ_2 reduces to a vector and we use the abbreviation

$$U_j^\Lambda = \gamma_2^\Lambda(j, j+1; j, j+1). \tag{4.17}$$

Before we write down the flow equation of U^Λ we make some considerations on the one-particle vertex. Because of computational technical reasons we do not use γ_1 as operand, instead we define a effective Λ-dependent Hamiltonian

$$H_{eff}^\Lambda = H_c - \gamma_1^\Lambda. \tag{4.18}$$

The flow equation for this effective Hamiltonian simply reads

$$\frac{d}{d\Lambda}H_{eff}^{\Lambda} = -\frac{d}{d\Lambda}\gamma_1^{\Lambda} \tag{4.19}$$

and its initial conditions

$$H_{eff}^{\Lambda_0} = H_c - \gamma_1^{\Lambda_0} = H_c + \frac{1}{2}\sum_q \overline{v}_{k',q;k,q} \tag{4.20}$$

where we used the initial condition of the vertices (3.86). With (3.79) equation (4.19) takes the form

$$\frac{d}{d\Lambda}H_{j,j}^{\Lambda} = -\frac{1}{2\pi}\sum_{\omega=\pm\Lambda}\sum_{q,q}\tilde{\mathcal{G}}_{q',q}^{\Lambda}(i\omega)\gamma_2(j,q';j,q)$$

$$= -\frac{1}{2\pi}\sum_{\omega=\pm\Lambda}\left(\tilde{\mathcal{G}}_{j+1,j+1}(i\omega)U_j^{\Lambda} + \tilde{\mathcal{G}}_{j-1,j-1}^{\Lambda}(i\omega)U_{j-1}^{\Lambda}\right) \tag{4.21}$$

$$\frac{d}{d\Lambda}H_{j,j+1}^{\Lambda} = -\frac{1}{2\pi}\sum_{\omega=\pm\Lambda}\sum_{q,q}\tilde{\mathcal{G}}_{q',q}^{\Lambda}(i\omega)\gamma_2(j,q';j+1,q)$$

$$= \frac{1}{2\pi}\sum_{\omega=\pm\Lambda}\tilde{\mathcal{G}}_{j,j+1}(i\omega)U_j^{\Lambda} \tag{4.22}$$

$$\frac{d}{d\Lambda}H_{j+1,j}^{\Lambda} = \frac{1}{2\pi}\sum_{\omega=\pm\Lambda}\tilde{\mathcal{G}}_{j+1,j}(i\omega)U_j^{\Lambda} \tag{4.23}$$

$$\frac{d}{d\Lambda}H_{j,j+l}^{\Lambda} = 0 \qquad (|l| > 1). \tag{4.24}$$

We dropped the index "*eff*" to make room for the quantum numbers. Consequently the effective Hamiltonian stays tridiagonal. Furthermore it stays real - if it is real in the beginning. This is not obvious since the propagator is complex. Using the definition of $\tilde{\mathcal{G}}$ (3.80) together with (4.10) we get

$$\tilde{\mathcal{G}}^{\Lambda}(-i\Lambda) = \frac{1}{-i\Lambda - H_{eff}^{\Lambda} - 2\tau^2 g(-i\Lambda)\left(|1,\sigma\rangle\langle 1,\sigma| + |N,\sigma\rangle\langle N,\sigma|\right)} = \left[\tilde{\mathcal{G}}^{\Lambda}(i\Lambda)\right]^* \tag{4.25}$$

where the star denotes the complex conjugate. Thus the sum

$$\sum_{\omega=\pm\Lambda}\tilde{\mathcal{G}}_{i,j}(i\omega) = 2\,\Re\left(\tilde{\mathcal{G}}_{i,j}(i\Lambda)\right). \tag{4.26}$$

is real and H_{eff}^{Λ} is real as long as U^{Λ} is real. This property implies, that H_{eff}^{Λ} is symmetric, since it is hermitian, and thus $\tilde{\mathcal{G}}^{\Lambda}$ is symmetric which is consistent with (4.22) and (4.23).

We use the fact that the propagator is symmetric to simplify the flow-equation of U. We get

$$
\begin{aligned}
\frac{d}{d\Lambda} U_j^\Lambda = \frac{1}{2\pi} \sum_{\omega=\pm\Lambda} \Big[&\tilde{\mathcal{G}}_{j,j}^\Lambda(i\omega)\tilde{\mathcal{G}}_{j+1,j+1}^\Lambda(-i\omega) \left(U_j^\Lambda\right)^2 \\
&- \tilde{\mathcal{G}}_{j,j+1}^\Lambda(i\omega)\tilde{\mathcal{G}}_{j+1,j}^\Lambda(-i\omega) \left(U_j^\Lambda\right)^2 \\
&- \left(\tilde{\mathcal{G}}_{j-1,j}^\Lambda(i\omega)\right)^2 U_j^\Lambda U_{j-1}^\Lambda \\
&- \left(\tilde{\mathcal{G}}_{j,j+1}^\Lambda(i\omega)\right)^2 \left(U_j^\Lambda\right)^2 \\
&- \left(\tilde{\mathcal{G}}_{j-1,j+2}^\Lambda(i\omega)\right)^2 U_{j-1}^\Lambda U_{j+1}^\Lambda \\
&- \left(\tilde{\mathcal{G}}_{j+1,j+2}^\Lambda(i\omega)\right)^2 U_j^\Lambda U_{j+1}^\Lambda \\
&+ \tilde{\mathcal{G}}_{j,j}^\Lambda(i\omega)\tilde{\mathcal{G}}_{j+1,j+1}^\Lambda(i\omega)U_j^\Lambda U_j^\Lambda \Big]
\end{aligned}
\tag{4.27}
$$

4.2.2 Spin $\frac{1}{2}$-Fermions

For the spin $\frac{1}{2}$-fermions we make the same approximations as for the spinless case. Our system is not isotropic, since a magnetic field is present, furthermore it is not translationally invariant. Consequently we have 11 independent matrix elements for each site in the two-particle vertex

$$
\begin{aligned}
U_j &= \gamma_2(j\uparrow, j\downarrow; j\uparrow, j\downarrow) \\
U_{j,\uparrow}' &= \gamma_2(j\uparrow, j+1\uparrow; j\uparrow, j+1\uparrow) & U_{j\downarrow}' &= \gamma_2(j\downarrow, j+1\downarrow; j\downarrow, j+1\downarrow) \\
U_{j,\uparrow\downarrow}' &= \gamma_2(j\uparrow, j+1\downarrow; j\uparrow, j+1\downarrow) & U_{j,\downarrow\uparrow}' &= \gamma_2(j\downarrow, j+1\uparrow; j\downarrow, j+1\uparrow) \\
P_j &= \gamma_2(j\uparrow, j\downarrow; j+1\uparrow, j+1\downarrow) & V_j &= \gamma_2(j\uparrow, j+1\downarrow; j+1\uparrow, j\downarrow) \\
W_j^{(1)} &= \gamma_2(j\uparrow, j\downarrow; j\uparrow, j+1\downarrow) & W_j^{(2)} &= \gamma_2(j\uparrow, j\downarrow; j+1\uparrow, j\downarrow) \\
W_j^{(3)} &= \gamma_2(j\uparrow, j\downarrow; j\uparrow, j-1\downarrow) & W_j^{(4)} &= \gamma_2(j\uparrow, j\downarrow; j-1\uparrow, j\downarrow)
\end{aligned}
\tag{4.28}
$$

One could argue that if the local potential does not change too fast in space and the magnetic field is not too strong we can make the approximation $W^{(1)} \approx W^{(2)} \approx W^{(3)} \approx W^{(4)}$, but we will go even further. If we are in the Hubbard model, i.e. in equation (4.1e) we set $U' = 0$, W is generated only in second order, so one can neglect these terms. To go even further we will neglect it even in the extended Hubbard model. This can be done with the same arguments if one sets $U' \ll U$. This reduces the number of independent variables to seven. Since we want to be able to treat problems that strongly depend on space we won't make the approximation $U_{j,\uparrow\downarrow}' \approx U_{j,\downarrow\uparrow}'$.

For the spin $\frac{1}{2}$-fermions we also define an effective Λ-dependent Hamiltonian

$$
H_{i,j,\sigma}^\Lambda = H_c - \gamma_1(i\sigma, j\sigma)
\tag{4.29}
$$

where we already implied that the Hamiltonian stays diagonal in spin-space, which is the case since it is in the beginning of the flow and so is $\bar{v}$. By consequence the propagator is also diagonal in spin space. Thus the flow equation reads

$$
\begin{aligned}
\frac{d}{d\Lambda} H^{\Lambda}_{j,j,\sigma} &= -\frac{1}{2\pi} \sum_{\omega=\pm\Lambda} \sum_{q,q} \tilde{\mathcal{G}}^{\Lambda}_{q',q}(i\omega) \gamma_2(j\sigma, q'; j\sigma, q) \\
&= -\frac{1}{2\pi} \sum_{\omega=\pm\Lambda} \left(\tilde{\mathcal{G}}^{\Lambda}_{j,j,\bar{\sigma}}(i\omega) U_j + \tilde{\mathcal{G}}^{\Lambda}_{j+1,j+1,\bar{\sigma}}(i\omega) U'_{j,\sigma\bar{\sigma}} \right. \\
&\qquad\qquad + \tilde{\mathcal{G}}^{\Lambda}_{j-1,j-1,\bar{\sigma}}(i\omega) U'_{j-1,\bar{\sigma}\sigma} + \tilde{\mathcal{G}}^{\Lambda}_{j+1,j+1,\sigma}(i\omega) U'_{j,\sigma} \\
&\qquad\qquad \left. + \tilde{\mathcal{G}}^{\Lambda}_{j-1,j-1,\sigma}(i\omega) U'_{j-1,\sigma} \right) \\
\frac{d}{d\Lambda} H^{\Lambda}_{j,j+1,\sigma} &= -\frac{1}{2\pi} \sum_{\omega=\pm\Lambda} \left(-\tilde{\mathcal{G}}^{\Lambda}_{j,j+1,\sigma}(i\omega) U'_{j\sigma} + \tilde{\mathcal{G}}^{\Lambda}_{j,j+1,\bar{\sigma}}(i\omega) P_j \right. \\
&\qquad\qquad \left. + \tilde{\mathcal{G}}^{\Lambda}_{j,j+1,\bar{\sigma}} V_j \right)
\end{aligned}
$$

$$(4.30)$$

$$(4.31)$$

The flow equation of the two-particle vertex is quite long, so we put it in the appendix.

4.3   Interpreting Results

As discussed in section 3.3.2, the vertex functions that we get out of the fRG flow equation are frequency independent. Consequently we can interpret the self energy as a renormalized potential, leading to a noninteracting effective Hamiltonian

$$
\mathcal{H}^{\mathit{eff}} = \mathcal{H}^{\Lambda=0}. \tag{4.32}
$$

The diagonal part, i.e. the local potential, keeps track of energy shifts due to charging effects, screening etc. The nonlocal part, which in our approximation scheme is only the first off-diagonal renormalizes the hopping, and thus the dispersion relation. Since the bandwidth for constant hopping is equal to 4τ, it can change due to interaction. From the effective Hamiltonian we can calculate the Green' s function

$$
G_{i,j}(\omega) = \left[\omega - \mathcal{H}^{\mathit{eff}} \right]^{-1} \tag{4.33}
$$

The Green's function in turn can be used to calculate observables.

4.3.1   Spectral Function

The diagonal part of the spectral function can be obtained directly from the Green's function [25],

$$
A_{i,i}(\omega) = -\frac{1}{\pi} \Im G_{i,i}(\omega). \tag{4.34}
$$

and is nothing but the local density of states. In the zero temperature case for finite dimensional systems, $A_{ii}(\omega)$ is a series of delta peaks

$$A_{ii}(\omega) = \sum_m |\langle m|i\rangle|^2 \, \delta(\omega - \omega_m) \tag{4.35}$$

Here m labels the energy eigenstates and i the position eigenstates. However since our system is infinitely extended the energy spectrum is continuous inside the band and consequently so is the spectral function. This does not apply to states lying outside the band. Their spectral weight is δ-shaped, since they have an infinite life-time. In order to make them visible one can broaden them by a small but finite complex constant $i\delta$ which shifts the poles away from the real axis.

$$A_{ii}(\omega) = -\frac{1}{\pi} Im \left[\omega - \mathcal{H}^{\text{eff}} - i\delta\right]^{-1} \tag{4.36}$$

As already mentioned in section 3.3.2, we cannot expect to get reliable results for nonzero frequency a priori, consequently we can trust the spectral function only in the limit $\lim_{\omega \to 0} A_{i,i}(\omega)$. Nevertheless Andergassen et al. [26, 27] showed that the method yields good results not only for the zero frequency behavior but for the low frequency behavior of the spectral function for Luttinger liquids with a single impurity.

4.3.2 Local Density

The expectation value at zero temperature for the local density operator is simply the local density of states summed up to the Fermi energy.

$$n_i = \int_{-\infty}^{0} d\omega A_{ii}(\omega). \tag{4.37}$$

Here we already implemented the fact that the Fermi energy is per definition equal to zero. Now in the last section, we mentioned that the method we use does not provide reliable results for the local density of states for nonzero frequencies, so why should we trust the local density? In fact, in the standard RG terminology n_i is a composite operator [28], and one should renormalize it separately. Nevertheless, it turns out that calculating n_i with equation (4.37) provides surprisingly good results (for the SIAM at zero magnetic field the occupation n and the conductivity G are not independent: $G = \frac{e^2}{h} \sin^2 \frac{n}{\pi}$, this could be used to check the validity of (4.37)). This fact can be explained as follows. In equation (4.37) only the spectral weight below the Fermi surface enters, which is expected to be adequate, since it is proportional to the charging energy.

For more careful analysis of the local density profile, one ought to renormalize the density operator separately, as done by Andergassen et al. [27].

4.3.3 Conductivity

Since fRG maps the interacting one dimensional system onto a noninteracting one-dimensional system we can use Landauer-Büttiger formalism to describe transport. One could say that this is not clear, since we are dealing with an interacting system and calculating conductivity with the effective noninteracting Hamiltonian involves further approximations, but it turns out that this is not the case as showed for example by Enss et al.[22]. In linear response theory, only the zero frequency part of the transmission contributes to the conductivity, for which this method is expected to provide reliable results.

A detailed derivation of the conductance in the fRG scheme can be found in [29]. Here we only want to quote the final result for the zero temperature conductivity for linear response applied for a one dimensional chain.

$$G_\sigma = \frac{e^2}{h} \mathcal{T}_\sigma \tag{4.38}$$

where $\mathcal{T}_\sigma$ is the transmission for spin σ

$$\mathcal{T}_\sigma = \left| 2\pi \rho_{lead}(\mu) \tau^2 \mathcal{G}_{N,1}^\sigma(\mu) \right|^2 \tag{4.39}$$

4.3.4 Shot Noise

The shot noise in a mesoscopic system at zero temperature and zero frequency is [30]

$$S(\omega = 0) = \frac{e^3 |V_{SD}|}{\pi \hbar} \sum_n \mathcal{T}_n (1 - \mathcal{T}_n) \tag{4.40}$$

where $\mathcal{T}_n$ is the transmission of the nth channel. The shot noise vanishes in the limit $V_{SD} \to 0$, thus it is convenient to define a shot noise factor

$$\mathcal{N} = \sum_n \mathcal{T}_n (1 - \mathcal{T}_n) \tag{4.41}$$

Chapter 5

Numerical Results

In this chapter we will present numerical results of the fRG flow equations in one dimension set up in the last chapter. As already mentioned, we will use τ_l as an energy scale and set it to one. When we do not specify the interaction explicitly, it will be taken as constant over the whole contact region, with a smooth decay on both ends to avoid interference effects. We pointed out that U has to be small to justify the truncation scheme; nevertheless, in most cases we will set $U = \tau$, which is not really small in comparison, e.g., to the bandwidth $4\tau_l$. While we did not systematically analyze the reliability of fRG for such a choice of U, its use is justified by the results of Andergassen et al. [27]. They made a quantitative comparison with exact results, for the method used here applied to Luttinger liquids with impurities. To give an example, they calculated the effective decay exponent of long range Friedel oscillations. The error for spinless fermions was within a range of about 5% for $U = \tau$.

In systems for which we are using the extended Hubbard model we set $U' = U/10$, which should be sufficient small to justify neglecting the vertices of type $\gamma_2(j\sigma, j\bar{\sigma}; j\sigma, j+1\bar{\sigma})$.

5.1   Main Effects of the Interaction

As already mentioned, the fRG flow equations map the interacting system onto a non-interacting system with renormalized local potential and renormalized nonlocal potential or effective hopping. Before applying the system to concrete models we want to analyze the main effects of the interaction. Therefore we calculate the effective potential with the method described in section 4.2.2 with $U = \tau$ and $U' = 0.1\tau$. The region of interaction is bounded and decays smoothly to zero (see figure 5.1 blue line). Furthermore we consider a bare potential of gaussian shape with maximum τ in the middle of the wire (see figure 5.1 red line).

The effective potential emerging from the RG flow is shown in figure 5.1 green line. In the region with nonzero interaction it is shifted, due to the charging energy. Consequently we have a lower density, since the electrons are displaced out of this region to infinity. The effective potential follows in general the bare potential, but since the density in regions
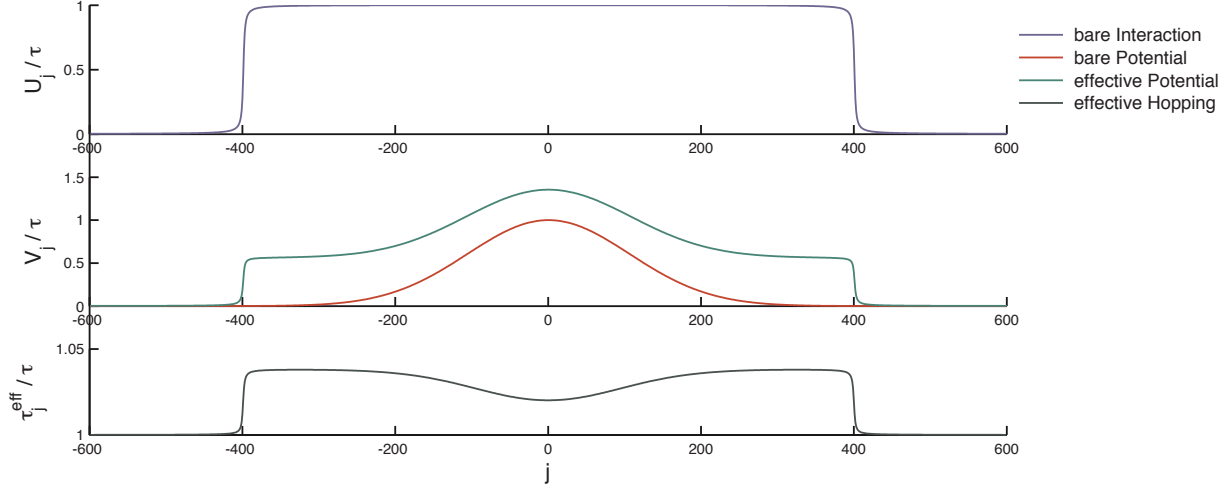
Figure 5.1: Prototype of a QWR with interacting region and a gaussian potential.

with higher potential is lower, so is the charging energy. As a result in regions with higher potential the effective potential is less shifted by renormalization than in the region with zero potential.

Furthermore, the effective hopping is slightly bigger than the bare hopping. Since the bandwidth is equal to $4\tau^{eff}$, this results in a bigger bandwidth.

5.2   Quantum Dots

5.2.1   The Single Impurity Anderson Model

Before we try to model a QWR, let us study a zero dimensional system, in order to gain intuition for the types of results that are to be expected. These systems are physically well understood and there exist numerous exact results, obtained with various methods, to which we can compare our results. The simplest model of a QD is the SIAM (2.4). Translated to our model (4.1) reads

$$H_c = \sum_{\sigma=\uparrow,\downarrow} \left(\epsilon_d - \frac{\sigma h}{2} \right) d_\sigma^\dagger d_\sigma \tag{5.1a}$$

$$H_{lc} = -\tau_d \sum_{\sigma,\sigma'=\uparrow,\downarrow} \left(c_{1,L,\sigma}^\dagger d_\sigma + d_{\sigma'}^\dagger c_{1,R,\sigma'} + h.c. \right) \tag{5.1b}$$

$$H_{int} = U\, n_\uparrow n_\downarrow. \tag{5.1c}$$

Since the length of the contact region $N = 1$, the contact operators d_σ and $d_\sigma^\dagger$ as well as n_σ have no site index. ϵ_d is the dot energy controlled by the gate voltage V_g. It is convenient
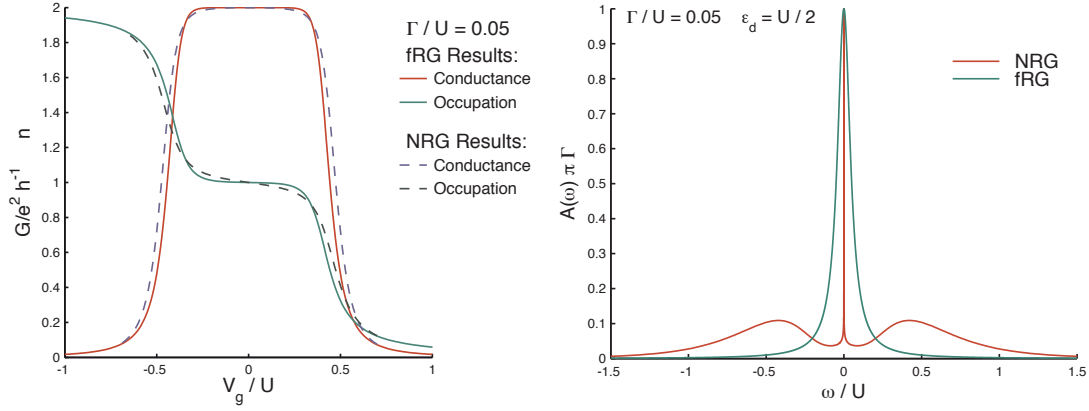
Figure 5.2: Comparison of fRG results with exact NRG results of the SIAM with $\Gamma/U = 0.05$. Left: Conductance and occupation versus gate voltage. Right: Spectral function versus frequency for the particle hole symmetric point ($V_g = 0$).

to measure the gate voltage with respect to the particle hole symmetric point, and thus

$$V_g = \epsilon_d + \frac{U}{2}. \tag{5.2}$$

The determining quantity for QDs is not the coupling τ_d of the dot to the reservoir but the total hybridization $\Gamma = \Gamma_R + \Gamma_L$ (again the indices R/L stands for the right/left reservoir) with

$$\Gamma_s = \pi\rho_s(0)\tau_d^2 \tag{5.3}$$

where $\rho_s(0)$ is the density of states at the Fermi energy of the left ($s = L$) and the right ($s = R$) lead. Using $\pi\rho_s(\omega) = -\Im g_s(\omega)$ and the fact that our system is symmetric, i.e. $\Gamma_R = \Gamma_L$ we get

$$\tau_d = \sqrt{-\frac{\Gamma}{2\Im g_s(0)}} = \sqrt{\frac{\Gamma\tau_l}{2}}. \tag{5.4}$$

Furthermore, the absolute value of U does not have influence on the physics of the system, provided that it is much larger than Γ. That means, since U is measured in units of τ_l, the absolute value of τ_l has no influence on the physics neither, and is not useful to determine the energy scale. The important quantity is the ratio $\frac{\Gamma}{U}$. Consequently it is convenient to use U as energy scale for the SIAM. We calculated the conductivity and the occupation for $\Gamma/U = 0.05$, $T = 0$, $V_{sd} = 0$ and $h = 0$ with fRG as well as with NRG. A comparison of both are shown in figure 5.2 left panel. This looks quiet good, but as mentioned before the conductivity only depends on the zero frequency results. What is about nonzero frequency? A comparison of the spectral function of NRG and fRG results for the particle hole symmetric point, i.e. $e_d = -\frac{U}{2}$, can be found in figure 5.2 right panel. For $\omega = 0$ both are the same, but the shapes are totally different. The shape of the fRG spectral function is the one of a single noninteracting level with hybridization Γ, whereas
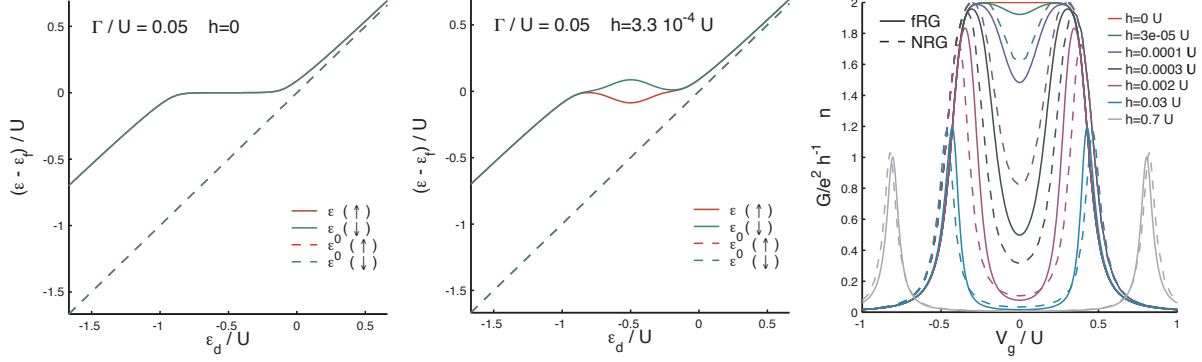
Figure 5.3: Effective level position as a function level energy ϵ_d without interaction (dashed lines) and with $U = 0.3\tau$ (solid lines) at zero magnetic field (left) and with Zeeman splitting (middle). Conductance versus gate voltage for different magnetic fields (right), for both fRG (solid lines) and NRG (dashed lines).

the correct spectral function has a narrow central peak of width T_K and two broad side peaks, of width Γ. In fact the fRG method is not able to produce a spectral function of a different shape, since the self energy is frequency independent. Only the position of the level is shifted due to interaction. That means that there exist only one level, although in the interacting case the spectral function is supposed to have two maxima, one for the singe occupied level and the second for the double occupied one (compare figure 5.2 left panel NRG results).

In figure 5.3, left panel, one can see the effective level position as a function of ϵ_d. For $\epsilon_d \ll \epsilon_f$ where the level is doubly occupied it is shifted up by U due to the charging energy. In the case $\epsilon_d \gg \epsilon_f$ the level is empty, and thus it stays unchanged during the flow. The interesting physics happens between these two cases. The level is pinned at the Fermi surface for a range of gate voltages mimicking the Kondo resonance. Upon switching on a magnetic field by adding a corresponding Zeeman energy, the levels are pushed apart, as can be seen in figure 5.3 middle panel. Note that the repulsion of the effective levels is about 10^3 times larger then the Zeeman splitting, although the splitting of the Kondo resonances are known be of order of the Zeeman energy. To be precise, one expects the levelspacing ΔE to be for $h \ll T_K$, $\Delta E = \frac{4}{3}h$ [31] and for $h \gg T_K$, $\Delta E = 2h \left(1 - \frac{1}{2\ln h/T_K}\right)$ [32]. However within the presented fRG scheme (with its frequency independent self energy) the large repulsion is necessary to lead to the right zero frequency results: Since the level width is equal to the hybridization, the splitting has to be of order Γ to reproduce the exact local density of states at zero frequency. A comparison of the linear conductance with NRG for different magnetic fields are shown in figure 5.3 right panel. We want to mention that NRG is not expected to provide reliable results for Zeeman energies in the order of T_K (for $\epsilon_d = U/2$ $T_K = 3.4 \; 10^{-8}U$).

5.2.2 A More Realistic Modeling of QDs

A QD in general is a small island where electrons are trapped in a potential. The potential can be regarded as a box, thus the energies are quantized. In the SIAM one picks out one of these energy levels, namely the one that is the closest to the Fermi energy. Since we set up a method in one dimension, we can extend our system in one dimension, and directly model the potential with two barriers. In the zero dimensional model the potential barriers around the dot are replaced by small coupling constants.

The one dimensional model reflects in addition the following properties of the real situation. First, we have a number of discrete levels, that are obtained from the diagonalisation of the dot region. Second, the strength of coupling of the levels to the bath depends on the energy. Electrons with higher energy can tunnel through the barriers more easily. For energies above the barrier, the transmission becomes one and thus the spectrum continuous.

The starting point of this description is a continuous system, i.e. the coupling $\tau_j = \tau_l = \tau$ is constant within the whole system. The interaction is constant in the contact region and smoothly decays at both ends, so the system continuously merges into the leads, which are noninteracting. The potential is chosen to consist of two gaussian peaks, separated by a distance d. The bottom of the valley inside the dot can be controlled by a parameter called V_g. The potential landscape is shown in figure 5.4, left panel. Note that V_g has to be associated with the negative gate voltage because a higher bottom means that electrons are suppressed, which is done by a lower voltage.

Figure 5.4, right panel, shows the spectral function for each site inside the dot. The spectral function reproduces the density distribution of the square well eigenfunctions. To
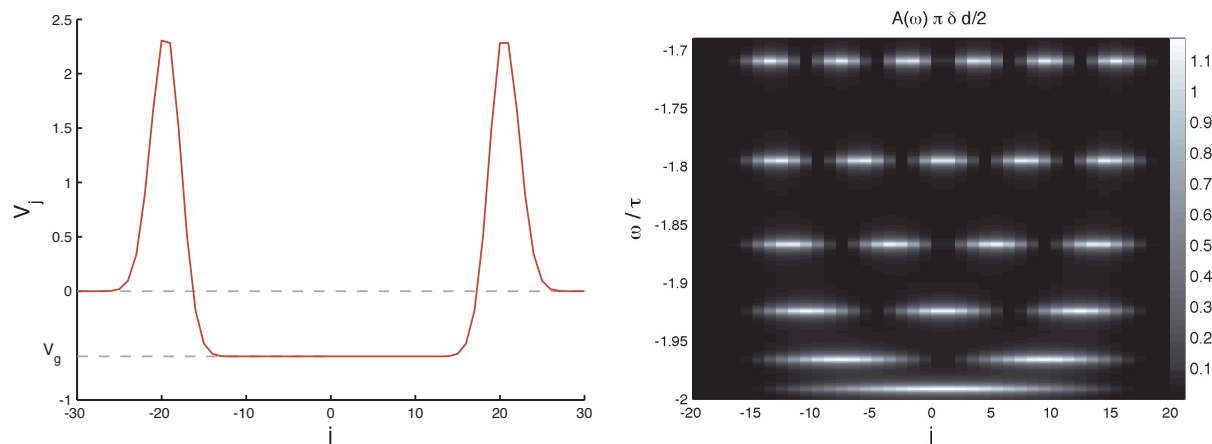
Figure 5.4: Left: Shape of the potential that we are using for ore model. The bottom between the two barriers is controlled via V_g. Right: Spectral function versus site number and frequency for the potential shown in the left panel with $V_g = 0$, the levels are broadened by a finite value of $\delta = 0.002\tau$.
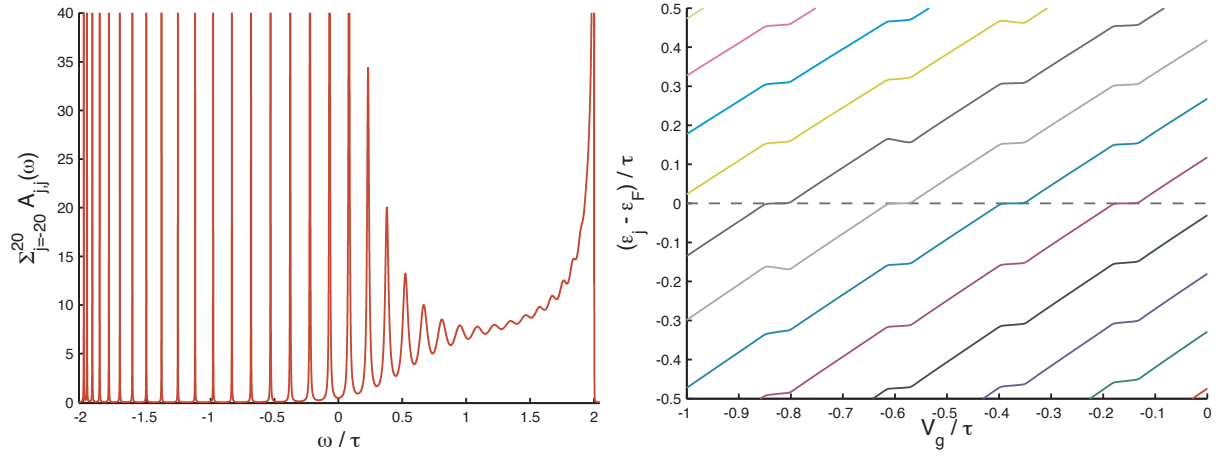
Figure 5.5: Results for the potential shown in figure 5.4. Left: Dot-spectral function versus frequency for the noninteracting system $(U = 0)$ and $V_g = 0$; the levels are broadened by a finite value of $\delta = 5 \ 10^{-5}\tau$ and the spectral function is cropped at $A(\omega) = 40$. Right: Effective level position versus V_g for the interacting system $U = 2\tau$ and $U' = U/10$.

get a spectral function of the dot one has to integrate the local spectral function over the whole dot region.

$$A_d(\omega) = \sum_{j=-d/2}^{d/2} A_{j,j}(\omega) \tag{5.5}$$

This dot-spectral function for $U = 0$ and $V_g = 0$ can be seen in figure 5.5 left panel. As one can see there are a number of discrete states inside the dot, which are, in the noninteracting case, doubly occupied. So we expect to get a Kondo-plateau for each of these levels.

The occupation of the dot can be calculated using equation (4.37) with the dot spectral function $A_d(\omega)$ instead of the local spectral function.

In order to make a rough estimate of the dot-charging energy U_d, we describe the dot in the continuous space by an infinite square well with parabolic dispersion relation. Furthermore we neglect the nearest neighbor interaction, in other words we take the interaction to be proportional to the Kronecker delta. In the continuum limit the Kronecker delta becomes a Dirac delta $\delta_{\text{Kronecker}} \rightarrow a\delta_{\text{Dirac}}$ (where a is the lattice spacing and $d/a = const$).

This makes it easy to calculate U_d from the eigenfunctions $\psi_n(x) = \sqrt{\frac{2}{d}} \cos \frac{n\pi x}{d}$

$$
\begin{aligned}
U_d &\approx a \int_{-d/2}^{d/2} dx \int_{-d/2}^{d/2} dx' \psi_n^2(x) \psi_n^2(x') U \delta(x - x') \\
&= a \frac{4U}{d^2} \int_{-d/2}^{d/2} dx \cos^4 \frac{n\pi x}{d} \\
&= a \frac{4U}{d^2} \int_{-d/2}^{d/2} dx \left[\frac{1}{4} + \cos \frac{2n\pi x}{d} + \frac{1}{4} \cos^2 \frac{2n\pi x}{d} \right] \\
&= a \frac{3}{2} \frac{U}{d} \approx 0.04U.
\end{aligned}
\tag{5.6}
$$

In the last step we inserted the distance $d/a = 40$ that we used in our calculations. The hybridization can be read off the dot-spectral function. At the Fermi energy we get for the full width at half maximum $2\Gamma_f = 7\ 10^{-3}\tau$ and consequently

$$
\frac{U_d}{\Gamma_f} \approx 11 \frac{U}{\tau}
\tag{5.7}
$$

In our calculations $\tau = U = 1$, $U' = 0.1$ and $d = 40$ as mentioned before, in other words, our parameter choice ensures that $U_d/\Gamma_f \gg 1$, s needed to see Kondo physics. We are now able to scan the dot for its Kondo resonances. Since the dot consists of 40 sites we expect just as many resonances. We picked out four of them, and calculated in addition to the conductivity at zero magnetic field the occupation and transition phase. The absolute value of the transition phase depends on the details of the potential outside the dot,
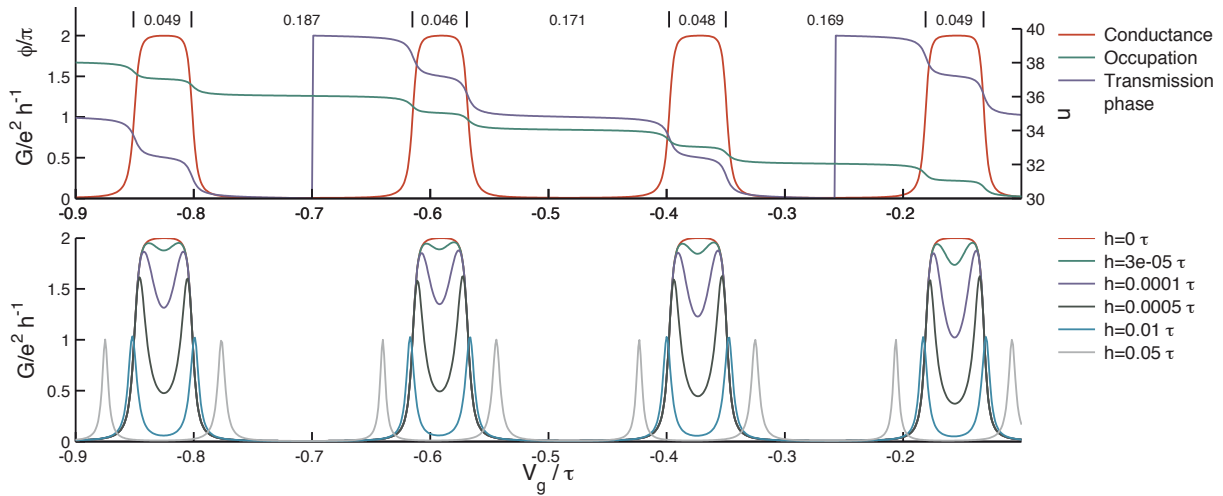
Figure 5.6: Results for the potential shape shown in figure 5.4 with $U = 2\tau$ and $U' = \frac{U}{10}$ Upper panel: Conductance, occupation, and transmission phase versus V_g. Lower panel: Conductance versus V_g for different Zeeman energies.

however the absolute value of a phase has no physical meaning. Only relative phases can be measured, and consequently we randomly choose two neighboring resonances and set the phase between these two resonances to zero, i.e. we plot the phase relative to this point. Furthermore we calculated the conductivity for several magnetic fields. The results are shown in figure 5.6. Note that all important features of the Kondo resonance are reproduced. In the region of the resonance the number of electrons on the dot is odd, the phase is pinned at $\frac{\pi}{2}$ and the conductance is one. Applying a magnetic field leads to a suppression of the conductance, the plateaus develop into two peaks.

We are now able to read off the dot-charging energy U_d, from the width of the plateaus. It is between 0.045 and 0.05, which is in the order of magnitude of our estimation. Note that additionally the distance of the plateau is of order $U_d + \delta E$. A plot of the effective level positions – defined by the maxima of the spectral function – as a function of V_g is shown in figure 5.5 right panel. All levels are expected to increase uniformly with V_g. This is not the case. Since all level spacings are more or less fixed, each time one level is pinned at the Fermi surface, all other level have to stand still as well. This again is an artifact of neglecting the frequency dependence of the self energy.

5.3 Quantum Point Contacts

In the last section we showed that our method is able to reproduce a number of physical relevant observables of the Kondo problem, for both a more cartoon like model – the SIAM – and a more realistic model set up in one dimensional real space. Thus we are now in a position to set up a model for the QPC. Since we are restricted to zero temperature, we do not expect to see the 0.7 anomaly. However we are able to treat magnetic field, which in the Kondo problem has a similar influence like temperature, in that it reduces the linear conductance.

We showed that we cannot trust the nonzero frequency results provided by this model, thus we will only use the linear response conductance, which only depends on zero frequency, to analyze the data.

As discussed in section 4.1, we will describe the QPC by its lowest mode, with the bare potential substantially determined by equation (2.7) and all screening effects outside the QWR. Furthermore, one could adopt the same considerations as in equation (5.6) for the transverse direction of the point contact. This would mean that the interaction gets stronger with decreasing width, and thus depends on the position x. However, we will refrain from incorporating the latter complication, since we do not want to use too many independent variables. We are interested in properties of interacting QWRs with a local potential, but need to keep U reasonably small to ensure that fRG remains reliable. According to Andergassen et al. [27], this is still the case for $U = \tau$, which is the choice we shall adopt here (unless specified otherwise).

With this (somewhat) arbitrary choice we will analyze the physics of a interacting QWR where the electrons are totally squeezed out of a region by an external potential. To do so we will mainly use a potential of the shape shown for example in figure 5.7, which is

essentially a product of two arc-tangent functions with the maximum set to V_g and the infimum set to zero

$$V_j = V_g \frac{\arctan\left(a\left(j + \frac{b}{2}\right)\right)\arctan\left(a\left(-j + \frac{b}{2}\right)\right) + \frac{\pi^2}{4}}{\arctan^2(a\frac{b}{2}) + \frac{\pi^2}{4}} \tag{5.8}$$

here b determines the width of the barrier and a the sharpness of the borders.

We have not (yet) tried to determine realistic values for the parameters a and b, or of the Zeeman field h from a detailed modeling of the 3-dimensional electrostatic environment of the QPC. This will be a topic of future work. However we have checked that a wide range of choices for these parameters yields qualitatively similar behavior for the conductance.

For large values of a the potential changes strongly in space, and thus the approximation of short ranged interactions is questionable. Calculations where a is large should thus not be taken too seriously.

5.3.1   Spinless Point Contact

First we will take a brief look at the QPC for the spinless model set up in section 4.2.1. The length of the region with interaction $U = \tau$ is equal to $N = 100$, where the interaction smoothly decays at both ends. The width of the potential barrier is equal to $b = 40$. In figure 5.7 left panel one can see the potential for $U = 0$ as well as $U = \tau$, for $V_g = 2\tau$. Since the bandwidth is equal to 4τ this value of V_g is the point where the barrier breaks
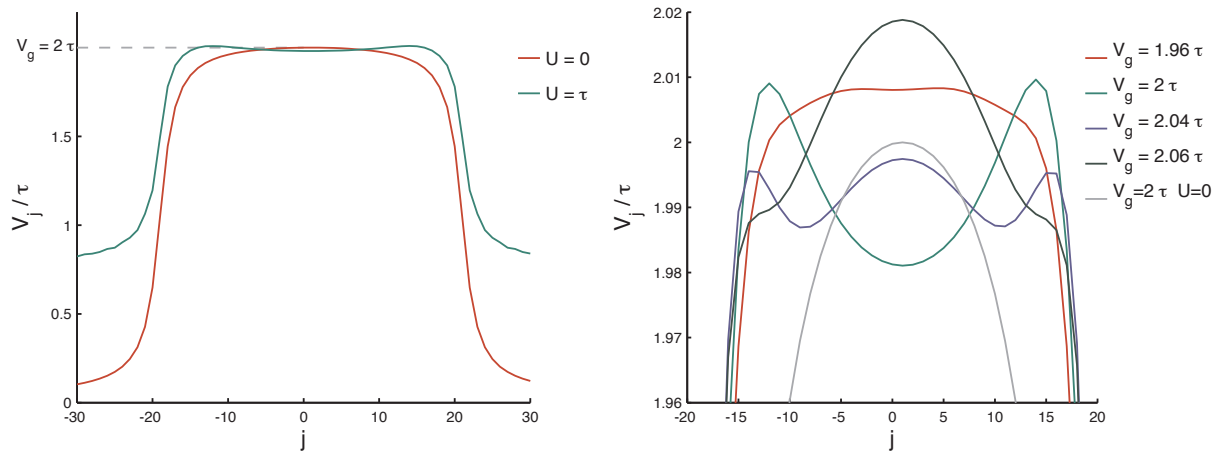
Figure 5.7: Left: Shape of the bare potential (5.8) with $V_g = 2\tau$, $b = 50$, and $a = 0.7$ (red line) and effective potential for the interacting system with $U = \tau$ at zero frequency and the same parameters (green line). Right: Detail screen of the effective potential at zero frequency for different values of V_g showing the emergence of a potential minimum for V_g values near 2τ; for comparison: the bare potential for $V_g = 2\tau$ (grey line)
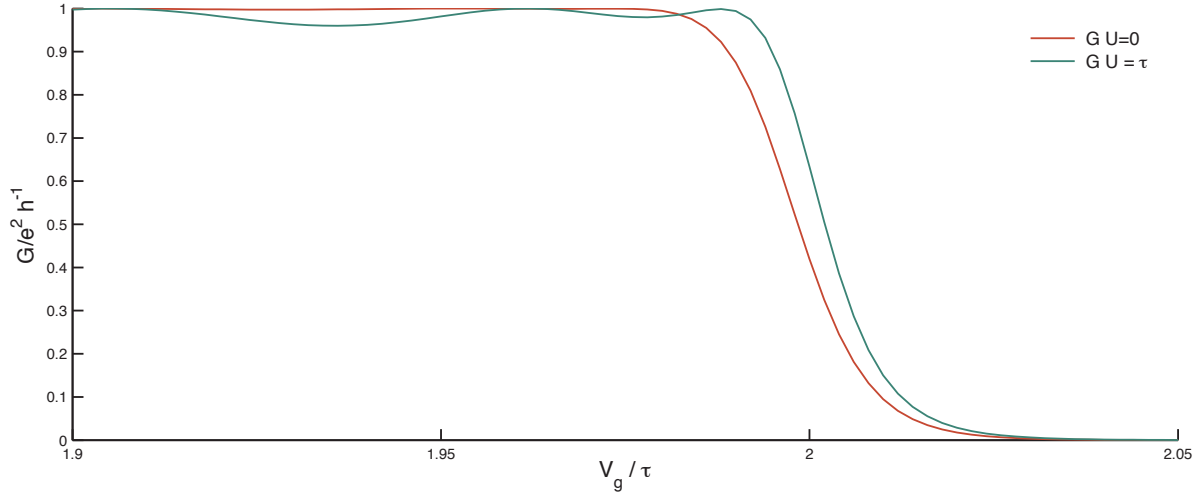
Figure 5.8: Conductance as a function of V_g for the spinless point contact, for the potential shown in figure 5.7 left panel.

through the Fermi surface. In the noninteracting case at $V_g = 2\tau$ the transmission changes from one to zero as can be seen in figure 5.8.

Note that due to the interaction (see figure 5.7 left panel) the width of the barrier increases and the walls become steeper. Furthermore a small valley is formed inside the dot. This is a first indication that a bounded state develops inside the dot. This does not happen for every gate voltage as can be seen in figure 5.7 right panel, where the potential is plotted for different values of V_g in a zoom-in onto the plateau region. The local minimum in the effective potential arises for V_g near the Fermi energy ($V_g = 2\tau$) and disappears for higher gate voltages. Figure 5.8 shows how this affects the conductivity. In the noninteracting case the transmission decreases uniformly to zero, while in the QWR where interaction is present the conductivity oscillates as a function of V_g before it goes to zero as well, in a way reminiscent of a square potential with infinitely sharp borders.

5.3.2 Spin $\frac{1}{2}$ Contact

The next step is to implement the spin degree of freedom, and thus we use the model of section 4.2.2 to describe the contact. We use a potential of the same shape as for the spinless case. The width of the barrier is chosen equal to $b = 150$, and again the steepness of its walls as $a = 0.7$ (see figure 5.9 left panel), and the length of the region where the interaction $U = \tau$ and $U' = 0.1\tau$ is present is equal to $N = 300$. Again on both ends the interaction decays smoothly to zero to suppress interference effects. The effective potential in the spinfull case shown in figure 5.9 left panel for $V_g = 2\tau$ indicates the same characteristics as for the spinless case, i.e the barrier gets broadened and the borders get sharpened. Furthermore inside the contact a small valley develops.

As we already argued in section 2.2.2 we do not expect to see the 0.7 anomaly within the
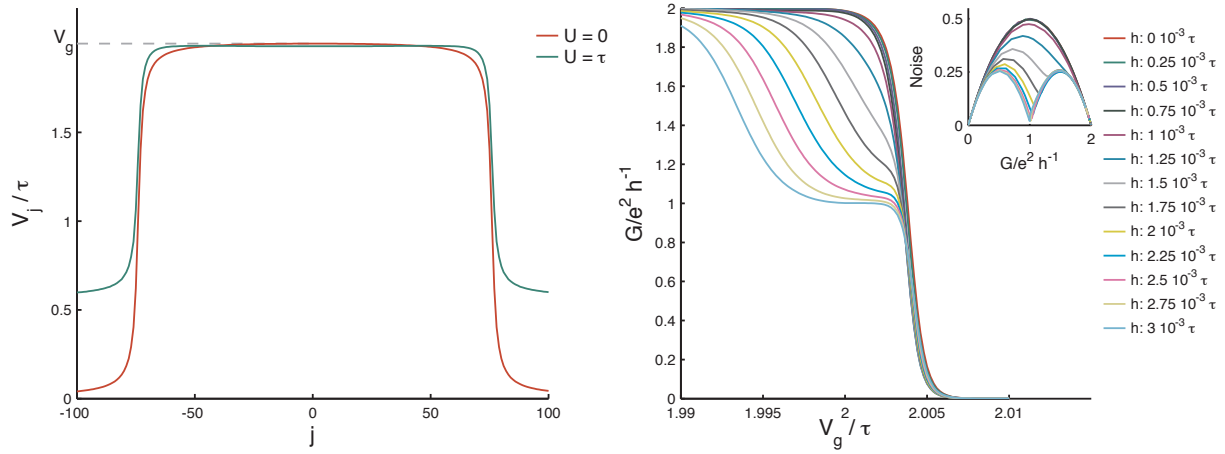
Figure 5.9: Left: Shape of the bare potential (redline) and effective potential at zero frequency for $V_g = 2\tau$ (green line). Right: Conductance as a function of V_g for different magnetic fields. right inset: shot noise factor versus conductance.

method we use here, since it is restricted to zero temperature. Thus it comes as no surprise that the conductance as a function of V_g for zero Zeeman energy $h = 0$ (see figure 5.9 right panel) does not show an additional feature. However there is another important feature associated with the 0.7 anomaly, namely the magnetic field dependence of the conductance. The spin resolved conductivity step due to magnetic field develops from above, as can be seen in figure 2.5 left panel. Our method nicely reproduces this feature, as can be seen in figure 5.9. Furthermore this leads to an asymmetric shot noise factor as a function of conductivity, as can be seen in the inset of figure 2.5 left panel. The agreement with the measurements (compare figure 2.7 right panel (d)) is remarkable.

In order to make a deeper analysis of the magnetic field dependence, we plotted the total and spin-resolved conductance for both the noninteracting case ($U = 0$ figure 5.10 (a-c)) and the interacting case ($U = \tau$, $U' = 0.1\tau$ figure 5.10 (d-f)). In the noninteracting case, all lines of the total conductance go through the point $G = \frac{1}{2}g_0$ at $V_g = 2\tau$. The graphs are symmetric with respect to this point. In the interacting case as well as in measurements, we do not observe such a behavior. This is due to the fact that the conductivity of the spin direction with lower energy (namely spin ↓) is strongly suppressed (compare 5.10 (f)) while the other spin direction is hardly affected by the magnetic field (compare 5.10 (e)). Note that due to the latter the pinch-off value of V_g is hardly changed by magnetic field, in agreement with experiment.

Furthermore, the step in the total conductivity at high magnetic field is much bigger than the Zeeman splitting. This was also reported by Koop et al. [9]. They plotted the separation between the maxima of $\frac{dG}{dV_g}$ versus the applied magnetic field B. For high magnetic fields this curve tends to a straight line, whose gradient is associated with an effective g-factor (compare figure 5.11). The offset of this straight line is called ΔE_{hfo}
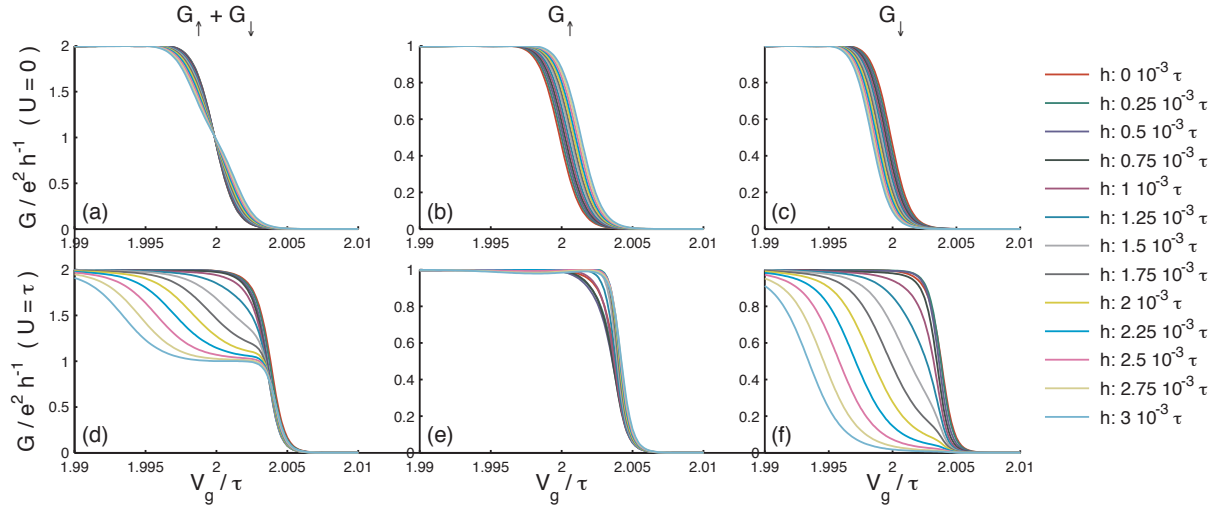
Figure 5.10: Conductance as a function of V_g for different magnetic fields of the noninteracting system for both spin direction (a), spin up (b) and spin down (c), and in the interacting case, i.e. $U = \tau$, $U' = 0.1\tau$, of both spin direction (d), spin up (e) and spin down (f).

(where "hfo" stands for high frequency offset). Doing the same analysis we get a g factor of $g^* = 3.15$ (compare figure 5.11, middle panel) in agreement with Koop et al., who reported a g-factor up to three times higher than in bulk 2DEG. For low magnetic fields the curve extracted of the experimental data saturates at some value called $\Delta E_{0.7}$. We do not observe such a behavior, since this has to be associated with the 0.7 anomaly at zero magnetic fields, and thus can only be observed at nonzero temperature. We find the
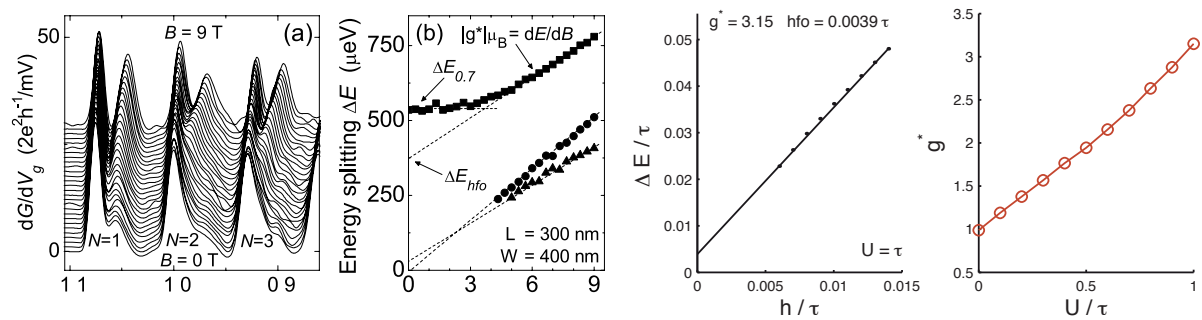
Figure 5.11: Left: Measurements on a QPC: $\frac{dG}{dV_g}$ as a function of gate voltage (right) [9] and distance of the maxima of $\frac{dG}{dV_g}$ versus applied magnetic field (middle left) [9]. Right: calculations with a potential shape shown in figure 5.9: distance of the maxima of $\frac{dG}{dV_g}$ versus Zeeman splitting h (middle right) and effective g-factor g^* versus interaction U (right).
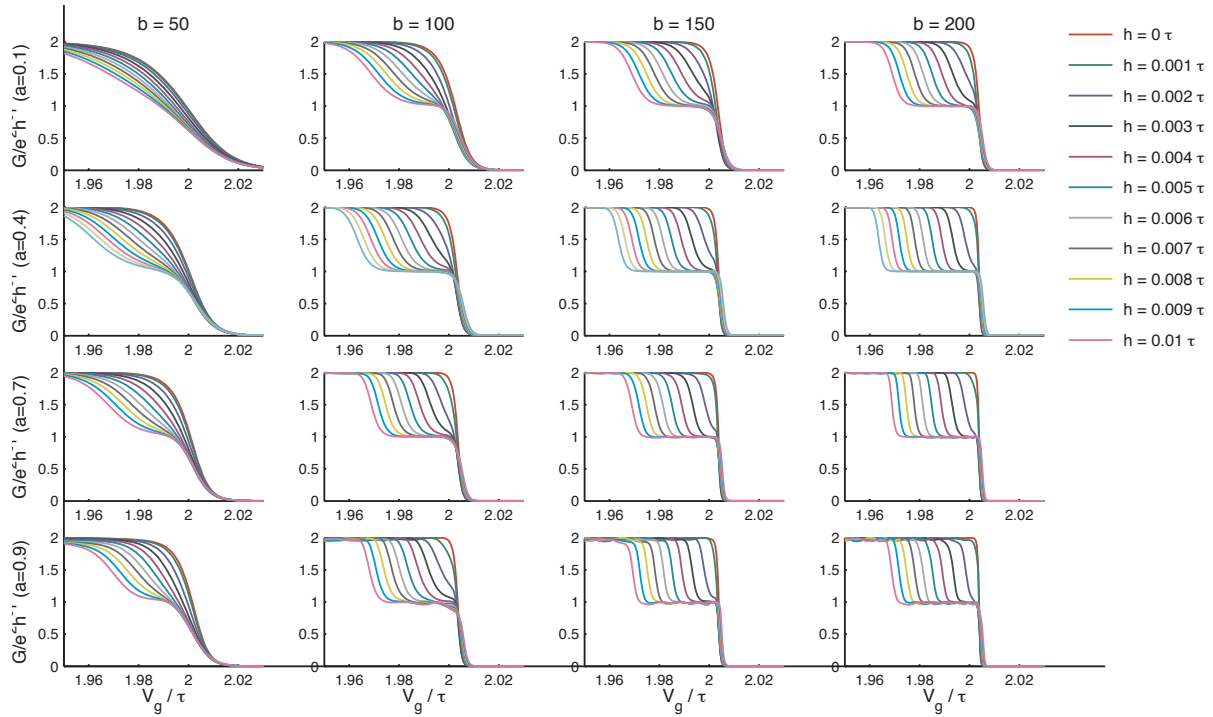
Figure 5.12: Conductance for different values of Zeeman energy h using the potential (5.8) with different values of a and b.

g-factor to be only weakly dependent on the shape of the one-dimensional potential and the width of the barrier, but significantly on the strength of the interaction U. Recall that we argued that the value of U depends on the effective width w of the contact, and thus in this fashion the g-factor does depends on the details of the geometry. This fact is confirmed by experimental data of Koop et al. [9], who found a correlation between g^* and the sublevel spacing ω_{12}. Both U and ω_{12} depend on the effective width w of the QWR. Figure 5.11, right panel, shows the U dependence of the g-factor. For $U = 0$ it is equal to one, as it should be. The g-factor increases linearly with the interaction with gradient approximately equal to $2\frac{1}{\tau}$. As a consequence the effective g-factor can be used to determine the strength of the interaction U in our model. Fortunately the experimentally observed value of $g^* \lesssim 3$ corresponds to a choice $U \lesssim \tau$ which is still small enough for the fRG approach to be fairly reliable.

To illustrate the geometry dependence of the conductance curves we calculated the conductance for different values of Zeeman energies and the potential of equation (5.8), for four different values of a, and for each value of a for four different values of b. The results are shown in figure 5.12. The step around $0.7g_0$ for low magnetic fields gets less pronounced if the length of the contact b is smaller, in agreement with measurements of very short contacts around $50nm$ [33]. It gets more pronounced if the sharpness of the borders, which is controlled via a, increases, i.e. if the width where the potential changes
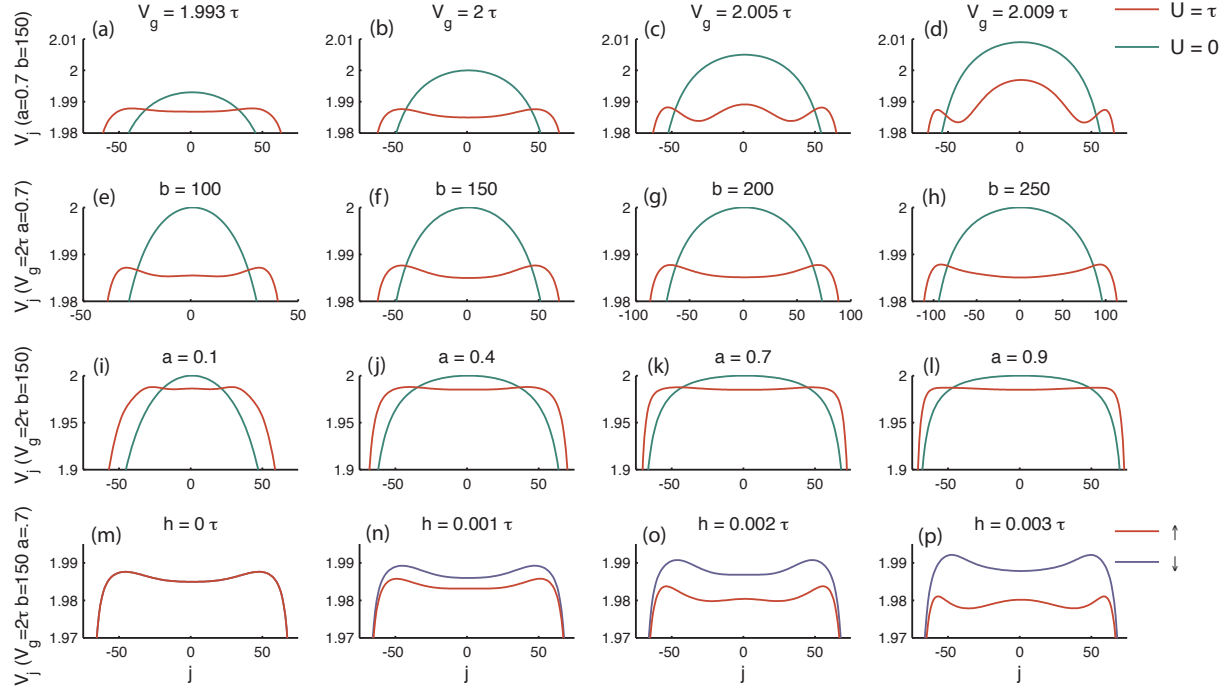
Figure 5.13: a-l: Effective potential for different values of V_g, a and b, for the noninteracting case ($U = 0$) (green lines) as well as for $U = \tau$ (red lines) m-p: Effective potential for different values of Zeeman energies h withe the parameters $U = \tau$, $V_g = 2\tau$, $a = 0.7$ and $b = 150$, for spin up (red lines) and spin down electrons (blue lines).

from 0 to V_g is smaller. For high values of a (i.e. very sharp walls), the conductivity starts to oscillate as can be seen in the last line of figure 5.12.

To get a deeper understanding of how the geometry influences the properties of the QPC we plotted the effective potential for several different parameter choices. The effective potential for the noninteracting case ($U = 0$) as well as for $U = \tau$ for $a = 0.7$ and $b = 150$ and different values of V_g is shown in figure 5.13 (a-d). Qualitatively we see the same behavior as for the spinless case shown in figure 5.7, right panel. As the bottom of the band is pushed upward past the Fermi energy, a valley arises in the middle of the contact. For higher values of V_g a hump emerges in the middle of the valley which grows rapidly with increasing V_g. We next fix V_g to 2τ and a to 0.7 and calculate the effective potential for different values of b. The results are shown in 5.13 (e-h). The valley length scales with the width of the barrier, while the borders remain unchanged, i.e. in comparison to the width, the borders get sharper. Note that for the most narrow barrier the valley is less pronounced than for the wider ones. Finally, we calculate the effective potential for different values of a while V_g is fixed to 2τ and b to 150. We plotted the results in figure 5.13 (i-l), where we showed a larger range for the y-axis than for the figures (a-h). For the smallest value of $a = 0.1$ the valley is less pronounced, as in the case of the smallest value

of b. The borders get steeper with increasing a, as expected. To conclude we can say, that the important quantity for the formation of the valley, and thus for the 0.7 anomaly, is the length of the low density regime inside the dot, where screening is weaker and the effect of interaction more pronounced.

Furthermore we want to mention that the step around $0.7g_0$ for low magnetic fields, as well as the valley inside the dot for $V_g \approx 2\tau$, gets more pronounced if the nearest neighbor interaction U' is bigger, but it does not vanish when we set $U' = 0$, since the nearest neighbor interaction is generated during the flow. A lowering of U' can be compensated by increasing the length b. In the spinless case the nearest neighbor interaction is dominant, since there is no onsite interaction. Thus for the spinless contact the formation of a valley is stronger.

Moreover, we calculated the effective potential for different values of Zeeman energies h. The results are shown in figure 5.13 (m-p), whereas we chose the parameters $U = \tau$, $V_g = 2\tau$, $a = 0.7$ and $b = 150$. Note that the difference in the effective potential for spin up and spin down electrons is about three times bigger than the Zeeman energy.

To conclude we can say that we have some indications that the formation of a step around $0.7g_0$ for nonzero magnetic field is associated with a formation of a quasi-bound state inside the dot. This lends support to a Kondo-related scenario like that advocated by Meir and collaborators [7], although we take a somewhat critical view of models like (2.16), since the details of the bound state change strongly for different V_g (compare figure 5.13), and it does not form for every value of V_g. On the other hand, our results also indicate that the physics of field-induced interaction-enhanced spin polarization is relevant for the 0.7 anomaly: At $T = 0$, the breaking of spin symmetry by magnetic field, leads to a misbalance of the spin density in the point contact region, that is strongly enhanced by presence of interactions, which are not well screened, due to the low density inside the QPC. Thus based on our current fRG calculations, it appears that the 0.7 anomaly involves some combination of Kondo type physics and spin-polarization physics. To investigate these issues in more detail, our calculations will have to be extended to finite temperatures and to finite frequency spectral information.

Chapter 6

Conclusion and Outlook

In QPCs the conductance is quantized in units of $g_0 = \frac{2e^2}{h}$. In addition, at intermediate temperature scales a shoulder-like step at around $0.7g_0$ develops, which has become known as the so-called 0.7 anomaly. This anomaly depends, in a very particular manner, on temperature, source-drain voltage and magnetic fields (chapter 2).

In this thesis we studied dependence on gate voltage and magnetic field of the conductance of QPCs, in the limit $T = 0$. The intention was to get a better understanding of (geometry-dependent) many-body effects in QPC and their possible relevance for the 0.7 anomaly.

We used fRG, a powerful tool, to keep track of the effects of interactions. The presented computation scheme extends previous work for translational independent filling factor and isotropic Luttinger liquids [27], to arbitrary potential landscapes in non-isotropic systems with short-ranged interactions. The fRG method treats the interaction by introducing an energy cutoff as a flow parameter in the free propagator. Solving coupled flow equation in the vertex functions, where we neglected the frequency dependence, leads to an effective model for zero frequency. Due to the flow, the model covers all energy scales of the microscopic model.

The restriction to zero frequency yields reliable results only in the limit $T = 0$. However in this limit many important features of the Kondo resonance in quantum dots are recovered. We showed this by applying the fRG scheme to the SIAM as well as to a more realistic model of a QD, based on a one-dimensional potential with two barriers representing the tunnel contacts. But we also observed, that we can trust the method only in the limit $\omega = 0$, and thus we are restricted to the linear response conduction as the only observable that can be used to interpret the generated results.

This brought us in the position to calculate the conductance for QPCs, where we represented the contact by a potential barrier. We reproduced all features that could be expected within our scheme: (i) The pinch-off value of the gate voltage is hardly affected by magnetic fields, (ii) an enhanced electron g-factor is observed for high magnetic fields, (iii) the noise factor as a function of conductance for different values of magnetic fields is in qualitatively agreement with measurements and (iv) the non-spin degenerated conductance develops "from above" for low magnetic field, whereby a small step at around $0.7g_0$

emerges for some intermediate value of the Zeeman energy. Although we did not attempt to relate the used potential shape to a realistically-modelled three-dimensional potential landscape, we showed that main qualitative features of the phenomenon are robust, in that they are obtained within a wide range of parameters.

Based on our work, several further questions suggest themselves for future study:

(i) Do a self consistent calculation, containing the screening effects of the 2DEG and the metallic top-gate, to get a realistic potential landscape for the QPC. This would be a very important step for comparing our data quantitatively to experiments, but we do not expect to get qualitatively new features.

(ii) Calculate the temperature dependence of the conductance. To this end, one has to modify the cutoff dependence of the free propagator, since one deals with discrete Matsubara frequencies. But this is not the major task. One also has to consider finite frequencies, since they play an important role for finite temperatures. This will lead to a far higher dimensionality of the Hilbert space, and also much more complicated flow equations. Due to these facts the length of the region defining the contact will have to be restricted to a much smaller value than is the case for the calculations presented in this thesis (where the restrictions, to $N = 10^7$ sites, were not severe).

(iii) Study spectral properties (such as $A_{j,j}(\omega)$ of the system in the point contact region. In particular, try to establish more conclusively whether a quasi-bound state forms, and if yes, under what conditions.

(iv) Calculate the dependence of the conductance on a finite source-drain voltage. To this end, the fRG formalism must be extended to deal with non-equilibrium steady-state transport.

(v) For (ii) to (iv), study the geometric crossover between the geometries of a quantum point contact and a quantum dot, in order to investigate to what extent the 0.7 anomaly is related (or smoothly crosses over) to the Kondo effect that occurs for quantum dots. To this end, reliable information on spectral quantities would be particularly useful.

(vi) Apart from the work on QPCs, it would be intruiging to apply the fRG to Wigner crystals. Since Wigner crystals arise only for long-ranged interactions, one would have to extend the range of the effective two-particle vertex to include very many sites, at the cost of not allowing it to flow (else the number of flowing parameters would become prohibitively large, compare discussion on independent variables in section 4.2.1).

Appendix A

Flow Equation of the Spin-$\frac{1}{2}$ Two-Particle Vertex

Here we present the flow equation of the two-particle vertex for the one dimensional spin $\frac{1}{2}$ tight-binding chain of section 4.2.2. Starting from equation (3.82) using the condition (4.16) with the nomenclature (4.28), and setting vertices of the type $\gamma_2(j\sigma, j\bar{\sigma}; j\sigma, j+1\bar{\sigma})$ to zero one gets

$$
\frac{d}{d\Lambda}U_j = \frac{1}{2\pi}\sum_{\omega=\pm\Lambda}\Big(
\begin{array}{llll}
\tilde{\mathcal{G}}_{j-1,j-1\uparrow}^{\Lambda,i\omega} & P_{j-1} & \tilde{\mathcal{G}}_{j-1,j-1\downarrow}^{\Lambda,-i\omega} & P_{j-1}
\end{array}
$$

$$
\begin{array}{lllll}
+2 & \tilde{\mathcal{G}}_{j,j-1\uparrow}^{\Lambda,i\omega} & P_{j-1} & \tilde{\mathcal{G}}_{j,j-1\downarrow}^{\Lambda,-i\omega} & U_j \\
+ & \tilde{\mathcal{G}}_{j,j\uparrow}^{\Lambda,i\omega} & U_j & \tilde{\mathcal{G}}_{j,j\downarrow}^{\Lambda,-i\omega} & U_j \\
+ & \tilde{\mathcal{G}}_{j+1,j+1\uparrow}^{\Lambda,i\omega} & P_j & \tilde{\mathcal{G}}_{j+1,j+1\downarrow}^{\Lambda,-i\omega} & P_j \\
- & \tilde{\mathcal{G}}_{j-1,j-1\uparrow}^{\Lambda,i\omega} & U'_{j-1,\uparrow} & \tilde{\mathcal{G}}_{j-1,j-1\uparrow}^{\Lambda,i\omega} & U'_{j-1,\uparrow\downarrow} \\
- & \tilde{\mathcal{G}}_{j-1,j+1\downarrow}^{\Lambda,i\omega} & U'_{j,\uparrow\downarrow} & \tilde{\mathcal{G}}_{j+1,j-1\downarrow}^{\Lambda,i\omega} & U'_{j-1,\downarrow} \\
- & \tilde{\mathcal{G}}_{j,j-1\uparrow}^{\Lambda,i\omega} & U'_{j-1,\uparrow} & \tilde{\mathcal{G}}_{j-1,j\uparrow}^{\Lambda,i\omega} & U_j \\
- & \tilde{\mathcal{G}}_{j+1,j-1\downarrow}^{\Lambda,i\omega} & U'_{j-1,\downarrow\uparrow} & \tilde{\mathcal{G}}_{j-1,j+1\downarrow}^{\Lambda,i\omega} & U'_{j,\downarrow} \\
- & \tilde{\mathcal{G}}_{j+1,j\downarrow}^{\Lambda,i\omega} & U_j & \tilde{\mathcal{G}}_{j,j+1\downarrow}^{\Lambda,i\omega} & U'_{j,\downarrow} \\
- & \tilde{\mathcal{G}}_{j+1,j+1\uparrow}^{\Lambda,i\omega} & U'_{j,\uparrow} & \tilde{\mathcal{G}}_{j+1,j+1\uparrow}^{\Lambda,i\omega} & U'_{j,\downarrow\uparrow} \\
+2 & \tilde{\mathcal{G}}_{j-1,j\uparrow}^{\Lambda,i\omega} & U_j & \tilde{\mathcal{G}}_{j,j-1\downarrow}^{\Lambda,i\omega} & V_{j-1} \\
+ & \tilde{\mathcal{G}}_{j,j\uparrow}^{\Lambda,i\omega} & U_j & \tilde{\mathcal{G}}_{j,j\downarrow}^{\Lambda,i\omega} & U_j \\
+ & \tilde{\mathcal{G}}_{j+1,j+1\uparrow}^{\Lambda,i\omega} & V_j & \tilde{\mathcal{G}}_{j+1,j+1\downarrow}^{\Lambda,i\omega} & V_j)
\end{array}
$$

$$
\begin{array}{lllll}
 & \tilde{\mathcal{G}}_{j-1,j-1\downarrow}^{\Lambda,-i\omega} & P_{j-1} & & \\
+2 & \tilde{\mathcal{G}}_{j+1,j-1\uparrow}^{\Lambda,i\omega} & P_{j-1} & \tilde{\mathcal{G}}_{j+1,j-1\downarrow}^{\Lambda,-i\omega} & P_j \\
+2 & \tilde{\mathcal{G}}_{j+1,j\uparrow}^{\Lambda,i\omega} & U_j & \tilde{\mathcal{G}}_{j+1,j\downarrow}^{\Lambda,-i\omega} & P_j \\
- & \tilde{\mathcal{G}}_{j-1,j-1\downarrow}^{\Lambda,i\omega} & U'_{j-1,\downarrow\uparrow} & \tilde{\mathcal{G}}_{j-1,j-1\downarrow}^{\Lambda,i\omega} & U'_{j-1,\downarrow} \\
- & \tilde{\mathcal{G}}_{j-1,j\downarrow}^{\Lambda,i\omega} & U_j & \tilde{\mathcal{G}}_{j,j-1\downarrow}^{\Lambda,i\omega} & U'_{j-1,\downarrow} \\
- & \tilde{\mathcal{G}}_{j-1,j+1\uparrow}^{\Lambda,i\omega} & U'_{j,\uparrow} & \tilde{\mathcal{G}}_{j+1,j-1\uparrow}^{\Lambda,i\omega} & U'_{j-1,\uparrow\downarrow} \\
- & \tilde{\mathcal{G}}_{j,j+1\uparrow}^{\Lambda,i\omega} & U'_{j,\uparrow} & \tilde{\mathcal{G}}_{j+1,j\uparrow}^{\Lambda,i\omega} & U_j \\
- & \tilde{\mathcal{G}}_{j+1,j-1\uparrow}^{\Lambda,i\omega} & U'_{j-1,\uparrow} & \tilde{\mathcal{G}}_{j-1,j+1\uparrow}^{\Lambda,i\omega} & U'_{j,\downarrow\uparrow} \\
- & \tilde{\mathcal{G}}_{j+1,j+1\downarrow}^{\Lambda,i\omega} & U'_{j,\uparrow\downarrow} & \tilde{\mathcal{G}}_{j+1,j+1\downarrow}^{\Lambda,i\omega} & U'_{j,\downarrow} \\
+ & \tilde{\mathcal{G}}_{j-1,j-1\uparrow}^{\Lambda,i\omega} & V_{j-1} & \tilde{\mathcal{G}}_{j-1,j-1\downarrow}^{\Lambda,i\omega} & V_{j-1} \\
+2 & \tilde{\mathcal{G}}_{j-1,j+1\uparrow}^{\Lambda,i\omega} & V_j & \tilde{\mathcal{G}}_{j+1,j-1\downarrow}^{\Lambda,i\omega} & V_{j-1} \\
+2 & \tilde{\mathcal{G}}_{j,j+1\uparrow}^{\Lambda,i\omega} & V_j & \tilde{\mathcal{G}}_{j+1,j\downarrow}^{\Lambda,i\omega} & U_j
\end{array}
$$

(A.1)

$$
\begin{array}{rllll rllll}
\multicolumn{10}{c}{\dfrac{d}{d\Lambda}U'_{j,\sigma} = \dfrac{1}{2\pi}\sum_{\omega=\pm\Lambda}\Big(\tilde{\mathcal{G}}^{\Lambda,i\omega}_{j+1,j+1\sigma}\ \ U'_{j,\sigma}\ \ \tilde{\mathcal{G}}^{\Lambda,-i\omega}_{j,j\sigma}\ \ U'_{j,\sigma}}\\[4pt]
-&\tilde{\mathcal{G}}^{\Lambda,i\omega}_{j,j+1\sigma}&U'_{j,\sigma}&\tilde{\mathcal{G}}^{\Lambda,-i\omega}_{j+1,j\sigma}&U'_{j,\sigma}
&-&\tilde{\mathcal{G}}^{\Lambda,i\omega}_{j,j-1\overline{\sigma}}&U'_{j-1,\overline{\sigma}\sigma}&\tilde{\mathcal{G}}^{\Lambda,-i\omega}_{j-1,j\overline{\sigma}}&U'_{j,\overline{\sigma}\sigma}\\[3pt]
-&\tilde{\mathcal{G}}^{\Lambda,i\omega}_{j,j-1\sigma}&U'_{j-1,\sigma}&\tilde{\mathcal{G}}^{\Lambda,-i\omega}_{j-1,j\sigma}&U'_{j,\sigma}
&-&\tilde{\mathcal{G}}^{\Lambda,i\omega}_{j,j\overline{\sigma}}&U_j&\tilde{\mathcal{G}}^{\Lambda,-i\omega}_{j,j\overline{\sigma}}&U'_{j,\overline{\sigma}\sigma}\\[3pt]
-&\tilde{\mathcal{G}}^{\Lambda,i\omega}_{j,j+1\overline{\sigma}}&U'_{j,\sigma\overline{\sigma}}&\tilde{\mathcal{G}}^{\Lambda,-i\omega}_{j+1,j\overline{\sigma}}&U'_{j,\overline{\sigma}\sigma}
&-&\tilde{\mathcal{G}}^{\Lambda,i\omega}_{j,j+1\sigma}&U'_{j,\sigma}&\tilde{\mathcal{G}}^{\Lambda,-i\omega}_{j+1,j\sigma}&U'_{j,\sigma}\\[3pt]
-&\tilde{\mathcal{G}}^{\Lambda,i\omega}_{j+1,j-1\overline{\sigma}}&U'_{j-1,\overline{\sigma}\sigma}&\tilde{\mathcal{G}}^{\Lambda,-i\omega}_{j-1,j+1\overline{\sigma}}&U_{j+1}
&-&\tilde{\mathcal{G}}^{\Lambda,i\omega}_{j+1,j\overline{\sigma}}&U_j&\tilde{\mathcal{G}}^{\Lambda,-i\omega}_{j,j+1\overline{\sigma}}&U_{j+1}\\[3pt]
-&\tilde{\mathcal{G}}^{\Lambda,i\omega}_{j+1,j+1\overline{\sigma}}&U'_{j,\sigma\overline{\sigma}}&\tilde{\mathcal{G}}^{\Lambda,-i\omega}_{j+1,j+1\overline{\sigma}}&U_{j+1}
&-&\tilde{\mathcal{G}}^{\Lambda,i\omega}_{j+2,j-1\overline{\sigma}}&U'_{j-1,\overline{\sigma}\sigma}&\tilde{\mathcal{G}}^{\Lambda,-i\omega}_{j-1,j+2\overline{\sigma}}&U'_{j+1,\sigma\overline{\sigma}}\\[3pt]
-&\tilde{\mathcal{G}}^{\Lambda,i\omega}_{j+2,j-1\sigma}&U'_{j-1,\sigma}&\tilde{\mathcal{G}}^{\Lambda,-i\omega}_{j-1,j+2\sigma}&U'_{j+1,\sigma}
&-&\tilde{\mathcal{G}}^{\Lambda,i\omega}_{j+2,j\overline{\sigma}}&U_j&\tilde{\mathcal{G}}^{\Lambda,-i\omega}_{j,j+2\overline{\sigma}}&U'_{j+1,\sigma\overline{\sigma}}\\[3pt]
-&\tilde{\mathcal{G}}^{\Lambda,i\omega}_{j+2,j+1\overline{\sigma}}&U'_{j,\sigma\overline{\sigma}}&\tilde{\mathcal{G}}^{\Lambda,-i\omega}_{j+1,j+2\overline{\sigma}}&U'_{j+1,\sigma\overline{\sigma}}
&-&\tilde{\mathcal{G}}^{\Lambda,i\omega}_{j+2,j+1\sigma}&U'_{j,\sigma}&\tilde{\mathcal{G}}^{\Lambda,-i\omega}_{j+1,j+2\sigma}&U'_{j+1,\sigma}\\[3pt]
+&\tilde{\mathcal{G}}^{\Lambda,i\omega}_{j+1,j+1\overline{\sigma}}&P_j&\tilde{\mathcal{G}}^{\Lambda,-i\omega}_{j,j\overline{\sigma}}&P_j
&+2&\tilde{\mathcal{G}}^{\Lambda,i\omega}_{j+1,j\overline{\sigma}}&V_j&\tilde{\mathcal{G}}^{\Lambda,-i\omega}_{j+1,j\overline{\sigma}}&P_j\\[3pt]
+&\tilde{\mathcal{G}}^{\Lambda,i\omega}_{j,j\overline{\sigma}}&V_j&\tilde{\mathcal{G}}^{\Lambda,-i\omega}_{j+1,j+1\overline{\sigma}}&V_j
&+&\tilde{\mathcal{G}}^{\Lambda,i\omega}_{j,j\sigma}&U'_{j,\sigma}&\tilde{\mathcal{G}}^{\Lambda,-i\omega}_{j+1,j+1\sigma}&U'_{j,\sigma}\Big)
\end{array}
\tag{A.2}
$$

$$
\begin{array}{rllll rllll}
\multicolumn{10}{c}{\dfrac{d}{d\Lambda}U'_{j,\sigma\overline{\sigma}} = \dfrac{1}{2\pi}\sum_{\omega=\pm\Lambda}\Big(\tilde{\mathcal{G}}^{\Lambda,i\omega}_{j+1,j+1\sigma}\ \ V_j\ \ \tilde{\mathcal{G}}^{\Lambda,-i\omega}_{j,j\overline{\sigma}}\ \ V_j}\\[4pt]
+&\tilde{\mathcal{G}}^{\Lambda,i\omega}_{j+1,j+1\overline{\sigma}}&U'_{j,\sigma\overline{\sigma}}&\tilde{\mathcal{G}}^{\Lambda,-i\omega}_{j,j\sigma}&U'_{j,\sigma\overline{\sigma}}
&+2&\tilde{\mathcal{G}}^{\Lambda,i\omega}_{j,j+1\sigma}&V_j&\tilde{\mathcal{G}}^{\Lambda,-i\omega}_{j+1,j\overline{\sigma}}&U'_{j,\sigma\overline{\sigma}}\\[3pt]
-&\tilde{\mathcal{G}}^{\Lambda,i\omega}_{j,j-1\overline{\sigma}}&U'_{j-1,\overline{\sigma}\sigma}&\tilde{\mathcal{G}}^{\Lambda,-i\omega}_{j-1,j\overline{\sigma}}&U'_{j,\overline{\sigma}}
&-&\tilde{\mathcal{G}}^{\Lambda,i\omega}_{j,j-1\sigma}&U'_{j-1,\sigma}&\tilde{\mathcal{G}}^{\Lambda,-i\omega}_{j-1,j\sigma}&U'_{j,\sigma\overline{\sigma}}\\[3pt]
-&\tilde{\mathcal{G}}^{\Lambda,i\omega}_{j,j\overline{\sigma}}&U_j&\tilde{\mathcal{G}}^{\Lambda,-i\omega}_{j,j\overline{\sigma}}&U'_{j,\overline{\sigma}}
&-&\tilde{\mathcal{G}}^{\Lambda,i\omega}_{j,j+1\overline{\sigma}}&U'_{j,\sigma\overline{\sigma}}&\tilde{\mathcal{G}}^{\Lambda,-i\omega}_{j+1,j\overline{\sigma}}&U'_{j,\overline{\sigma}}\\[3pt]
-&\tilde{\mathcal{G}}^{\Lambda,i\omega}_{j,j+1\sigma}&U'_{j,\sigma}&\tilde{\mathcal{G}}^{\Lambda,-i\omega}_{j+1,j\sigma}&U'_{j,\sigma\overline{\sigma}}
&-&\tilde{\mathcal{G}}^{\Lambda,i\omega}_{j+1,j-1\sigma}&U'_{j-1,\sigma}&\tilde{\mathcal{G}}^{\Lambda,-i\omega}_{j-1,j+1\sigma}&U_{j+1}\\[3pt]
-&\tilde{\mathcal{G}}^{\Lambda,i\omega}_{j+1,j+1\sigma}&U'_{j,\sigma}&\tilde{\mathcal{G}}^{\Lambda,-i\omega}_{j+1,j+1\sigma}&U_{j+1}
&-&\tilde{\mathcal{G}}^{\Lambda,i\omega}_{j+2,j-1\overline{\sigma}}&U'_{j-1,\overline{\sigma}\sigma}&\tilde{\mathcal{G}}^{\Lambda,-i\omega}_{j-1,j+2\overline{\sigma}}&U'_{j+1,\overline{\sigma}}\\[3pt]
-&\tilde{\mathcal{G}}^{\Lambda,i\omega}_{j+2,j-1\sigma}&U'_{j-1,\sigma}&\tilde{\mathcal{G}}^{\Lambda,-i\omega}_{j-1,j+2\sigma}&U'_{j+1,\overline{\sigma}\sigma}
&-&\tilde{\mathcal{G}}^{\Lambda,i\omega}_{j+2,j\overline{\sigma}}&U_j&\tilde{\mathcal{G}}^{\Lambda,-i\omega}_{j,j+2\overline{\sigma}}&U'_{j+1,\overline{\sigma}}\\[3pt]
-&\tilde{\mathcal{G}}^{\Lambda,i\omega}_{j+2,j+1\overline{\sigma}}&U'_{j,\sigma\overline{\sigma}}&\tilde{\mathcal{G}}^{\Lambda,-i\omega}_{j+1,j+2\overline{\sigma}}&U'_{j+1,\overline{\sigma}}
&-&\tilde{\mathcal{G}}^{\Lambda,i\omega}_{j+2,j+1\sigma}&U'_{j,\sigma}&\tilde{\mathcal{G}}^{\Lambda,-i\omega}_{j+1,j+2\sigma}&U'_{j+1,\overline{\sigma}\sigma}\\[3pt]
+&\tilde{\mathcal{G}}^{\Lambda,i\omega}_{j+1,j+1\sigma}&P_j&\tilde{\mathcal{G}}^{\Lambda,-i\omega}_{j,j\overline{\sigma}}&P_j
&+2&\tilde{\mathcal{G}}^{\Lambda,i\omega}_{j+1,j\sigma}&U'_{j,\sigma\overline{\sigma}}&\tilde{\mathcal{G}}^{\Lambda,-i\omega}_{j+1,j\overline{\sigma}}&P_j\\[3pt]
+&\tilde{\mathcal{G}}^{\Lambda,i\omega}_{j,j\sigma}&U'_{j,\sigma\overline{\sigma}}&\tilde{\mathcal{G}}^{\Lambda,-i\omega}_{j+1,j+1\overline{\sigma}}&U'_{j,\sigma\overline{\sigma}}\Big)
\end{array}
\tag{A.3}
$$

$$
\begin{array}{rllll rllll}
\multicolumn{10}{c}{\dfrac{d}{d\Lambda}P_j = \dfrac{1}{2\pi}\sum_{\omega=\pm\Lambda}\Big(\tilde{\mathcal{G}}^{\Lambda,i\omega}_{j,j-1\uparrow}\ \ P_{j-1}\ \ \tilde{\mathcal{G}}^{\Lambda,-i\omega}_{j,j-1\downarrow}\ \ P_j}\\[4pt]
+&\tilde{\mathcal{G}}^{\Lambda,i\omega}_{j+1,j-1\uparrow}&P_{j-1}&\tilde{\mathcal{G}}^{\Lambda,-i\omega}_{j+1,j-1\downarrow}&U_{j+1}
&+&\tilde{\mathcal{G}}^{\Lambda,i\omega}_{j+2,j-1\uparrow}&P_{j-1}&\tilde{\mathcal{G}}^{\Lambda,-i\omega}_{j+2,j-1\downarrow}&P_{j+1}\\[3pt]
+&\tilde{\mathcal{G}}^{\Lambda,i\omega}_{j,j\uparrow}&U_j&\tilde{\mathcal{G}}^{\Lambda,-i\omega}_{j,j\downarrow}&P_j
&+&\tilde{\mathcal{G}}^{\Lambda,i\omega}_{j+1,j\uparrow}&U_j&\tilde{\mathcal{G}}^{\Lambda,-i\omega}_{j+1,j\downarrow}&U_{j+1}\\[3pt]
+&\tilde{\mathcal{G}}^{\Lambda,i\omega}_{j+2,j\uparrow}&U_j&\tilde{\mathcal{G}}^{\Lambda,-i\omega}_{j+2,j\downarrow}&P_{j+1}
&+&\tilde{\mathcal{G}}^{\Lambda,i\omega}_{j,j+1\uparrow}&P_j&\tilde{\mathcal{G}}^{\Lambda,-i\omega}_{j,j+1\downarrow}&P_j\\[3pt]
+&\tilde{\mathcal{G}}^{\Lambda,i\omega}_{j+1,j+1\uparrow}&P_j&\tilde{\mathcal{G}}^{\Lambda,-i\omega}_{j+1,j+1\downarrow}&U_{j+1}
&+&\tilde{\mathcal{G}}^{\Lambda,i\omega}_{j+2,j+1\uparrow}&P_j&\tilde{\mathcal{G}}^{\Lambda,-i\omega}_{j+2,j+1\downarrow}&P_{j+1}\\[3pt]
+&\tilde{\mathcal{G}}^{\Lambda,i\omega}_{j+1,j+1\downarrow}&P_j&\tilde{\mathcal{G}}^{\Lambda,i\omega}_{j,j\downarrow}&U'_{j,\downarrow}
&+&\tilde{\mathcal{G}}^{\Lambda,i\omega}_{j+1,j\downarrow}&V_j&\tilde{\mathcal{G}}^{\Lambda,i\omega}_{j+1,j\downarrow}&U'_{j,\downarrow}\\[3pt]
+&\tilde{\mathcal{G}}^{\Lambda,i\omega}_{j+1,j\uparrow}&U'_{j,\uparrow}&\tilde{\mathcal{G}}^{\Lambda,i\omega}_{j+1,j\uparrow}&V_j
&+&\tilde{\mathcal{G}}^{\Lambda,i\omega}_{j,j\uparrow}&U'_{j,\uparrow}&\tilde{\mathcal{G}}^{\Lambda,i\omega}_{j+1,j+1\uparrow}&P_j\\[3pt]
+&\tilde{\mathcal{G}}^{\Lambda,i\omega}_{j+1,j+1\uparrow}&P_j&\tilde{\mathcal{G}}^{\Lambda,i\omega}_{j,j\downarrow}&U'_{j,\downarrow\uparrow}
&+&\tilde{\mathcal{G}}^{\Lambda,i\omega}_{j+1,j\uparrow}&U'_{j,\uparrow\downarrow}&\tilde{\mathcal{G}}^{\Lambda,i\omega}_{j+1,j\downarrow}&U'_{j,\downarrow\uparrow}\\[3pt]
+&\tilde{\mathcal{G}}^{\Lambda,i\omega}_{j,j+1\uparrow}&P_j&\tilde{\mathcal{G}}^{\Lambda,i\omega}_{j,j+1\downarrow}&P_j
&+&\tilde{\mathcal{G}}^{\Lambda,i\omega}_{j,j\uparrow}&U'_{j,\uparrow\downarrow}&\tilde{\mathcal{G}}^{\Lambda,i\omega}_{j+1,j+1\downarrow}&P_j\Big)
\end{array}
\tag{A.4}
$$

$$\frac{d}{d\Lambda}V_j = \frac{1}{2\pi}\sum_{\omega=\pm\Lambda}\Big(\tilde{\mathcal{G}}^{\Lambda,i\omega}_{j+1,j+1\uparrow}\,V_j\quad\tilde{\mathcal{G}}^{\Lambda,-i\omega}_{j,j\downarrow}\,U'_{j,\downarrow\uparrow}$$

$$
\begin{aligned}
&+\ \tilde{\mathcal{G}}^{\Lambda,i\omega}_{j+1,j+1\downarrow}\,U'_{j,\uparrow\downarrow}\,\tilde{\mathcal{G}}^{\Lambda,-i\omega}_{j,j\uparrow}\,V_j
&&+\ \tilde{\mathcal{G}}^{\Lambda,i\omega}_{j,j+1\uparrow}\,V_j\,\tilde{\mathcal{G}}^{\Lambda,-i\omega}_{j+1,j\downarrow}\,V_j\\
&+\ \tilde{\mathcal{G}}^{\Lambda,i\omega}_{j,j+1\downarrow}\,U'_{j,\uparrow\downarrow}\,\tilde{\mathcal{G}}^{\Lambda,-i\omega}_{j+1,j\uparrow}\,U'_{j,\downarrow\uparrow}
&&+\ \tilde{\mathcal{G}}^{\Lambda,i\omega}_{j+1,j\uparrow}\,U'_{j,\uparrow}\,\tilde{\mathcal{G}}^{\Lambda,i\omega}_{j+1,j\uparrow}\,P_j\\
&+\ \tilde{\mathcal{G}}^{\Lambda,i\omega}_{j,j+1\downarrow}\,P_j\,\tilde{\mathcal{G}}^{\Lambda,i\omega}_{j,j+1\downarrow}\,U'_{j,\downarrow}
&&+\ \tilde{\mathcal{G}}^{\Lambda,i\omega}_{j,j\downarrow}\,V_j\,\tilde{\mathcal{G}}^{\Lambda,i\omega}_{j+1,j+1\downarrow}\,U'_{j,\downarrow}\\
&+\ \tilde{\mathcal{G}}^{\Lambda,i\omega}_{j,j\uparrow}\,U'_{j,\uparrow}\,\tilde{\mathcal{G}}^{\Lambda,i\omega}_{j+1,j+1\uparrow}\,V_j
&&+\ \tilde{\mathcal{G}}^{\Lambda,i\omega}_{j,j-1\uparrow}\,V_{j-1}\,\tilde{\mathcal{G}}^{\Lambda,i\omega}_{j-1,j\downarrow}\,V_j\\
&+\ \tilde{\mathcal{G}}^{\Lambda,i\omega}_{j,j\uparrow}\,U_j\,\tilde{\mathcal{G}}^{\Lambda,i\omega}_{j,j\downarrow}\,V_j
&&+\ \tilde{\mathcal{G}}^{\Lambda,i\omega}_{j,j+1\uparrow}\,V_j\,\tilde{\mathcal{G}}^{\Lambda,i\omega}_{j+1,j\downarrow}\,V_j\\
&+\ \tilde{\mathcal{G}}^{\Lambda,i\omega}_{j+1,j-1\uparrow}\,V_{j-1}\,\tilde{\mathcal{G}}^{\Lambda,i\omega}_{j-1,j+1\downarrow}\,U_{j+1}
&&+\ \tilde{\mathcal{G}}^{\Lambda,i\omega}_{j+1,j\uparrow}\,U_j\,\tilde{\mathcal{G}}^{\Lambda,i\omega}_{j,j+1\downarrow}\,U_{j+1}\\
&+\ \tilde{\mathcal{G}}^{\Lambda,i\omega}_{j+1,j+1\uparrow}\,V_j\,\tilde{\mathcal{G}}^{\Lambda,i\omega}_{j+1,j+1\downarrow}\,U_{j+1}
&&+\ \tilde{\mathcal{G}}^{\Lambda,i\omega}_{j+2,j-1\uparrow}\,V_{j-1}\,\tilde{\mathcal{G}}^{\Lambda,i\omega}_{j-1,j+2\downarrow}\,V_{j+1}\\
&+\ \tilde{\mathcal{G}}^{\Lambda,i\omega}_{j+2,j\uparrow}\,U_j\,\tilde{\mathcal{G}}^{\Lambda,i\omega}_{j,j+2\downarrow}\,V_{j+1}
&&+\ \tilde{\mathcal{G}}^{\Lambda,i\omega}_{j+2,j+1\uparrow}\,V_j\,\tilde{\mathcal{G}}^{\Lambda,i\omega}_{j+1,j+2\downarrow}\,V_{j+1}\Big)
\end{aligned}
$$

(A.5)

Bibliography

[1] Yigal Meir, Ned S. Wingreen, and Patrick A. Lee. Transport through a strongly interacting electron system: Theory of periodic conductance oscillations. *Phys. Rev. Lett.*, 66(23):3048–3051, Jun 1991.

[2] D. Goldhaber-Gordon, Hadas Shtrikman, D. Mahalu, David Abusch-Magder, U. Meirav, and M. A. Kastner. Kondo effect in a single-electron transistor. *Nature*, 391:156–159, 1998.

[3] W. G. van der Wiel, S. De Franceschi, T. Fujisawa, J. M. Elzerman, S. Tarucha, and L. P. Kouwenhoven. The kondo effect in the unitary limit. *Science*, 289(5487):2105–2108, 2000.

[4] S. M. Cronenwett, H. J. Lynch, D. Goldhaber-Gordon, L. P. Kouwenhoven, C. M. Marcus, K. Hirose, N. S. Wingreen, and V. Umansky. Low-temperature fate of the 0.7 structure in a point contact: A kondo-like correlated state in an open system. *Phys. Rev. Lett.*, 88(22):226805, May 2002.

[5] B. J. van Wees, H. van Houten, C. W. J. Beenakker, J. G. Williamson, L. P. Kouwenhoven, D. van der Marel, and C. T. Foxon. Quantized conductance of point contacts in a two-dimensional electron gas. *Phys. Rev. Lett.*, 60(9):848–850, Feb 1988.

[6] K. J. Thomas, J. T. Nicholls, M. Y. Simmons, M. Pepper, D. R. Mace, and D. A. Ritchie. Possible spin polarization in a one-dimensional electron gas. *Phys. Rev. Lett.*, 77(1):135–138, Jul 1996.

[7] Yigal Meir, Kenji Hirose, and Ned S. Wingreen. Kondo model for the "0.7 anomaly" in transport through a quantum point contact. *Phys. Rev. Lett.*, 89(19):196802, Oct 2002.

[8] A. Golub, T. Aono, and Yigal Meir. Suppression of shot noise in quantum point contacts in the "0.7 regime". *Physical Review Letters*, 97(18):186801, 2006.

[9] E. J. Koop, A. I. Lerescu, J. Liu, B. J. van Wees, D. Reuter, A. D. Wieck, and C. H. van der Wal. The influence of device geometry on many-body effects in quantum point contacts: Signatures of the 0.7 anomaly, exchange and kondo. *Journal of Superconductivity Incorporating Novel Magnetism*, 20:433, 2007.

[10] D. A. Wharam, T. J. Thornton, R. Newbury, M. Pepper, H. Ahmed, J. E. F. Frost, and G. A. C. Jones. One-dimensional transport and the quantisation of the ballistic resistance. *Journal of Physics C*, 21:L209, 1988.

[11] Volker Meden. Funktionale renormierungsgruppe. Technical report, Georg-August Universität Göttingen, 2002.

[12] D. J. Reilly, T. M. Buehler, J. L. O'Brien, A. R. Hamilton, A. S. Dzurak, R. G. Clark, B. E. Kane, L. N. Pfeiffer, and K. W. West. Density-dependent spin polarization in ultra-low-disorder quantum wires. *Phys. Rev. Lett.*, 89(24):246801, Nov 2002.

[13] W. J. de Haas, J. H. de Boer, and G. J. van den Berg. The electrical resistance of gold, copper, and lead at low temperatures. *Physica (Ultrecht)*, 1:1115, 1934.

[14] Jun Kondo. Resistance minimum in dilute magnetic alloys. *Prog. Theor. Phys.*, 32:37–49, 1964.

[15] Anders Mathias Lunde, Alessandro De Martino, Reinhold Egger, and Karsten Flensberg. Electron-electron interaction effects in quantum point contacts. arXiv:0707.1989v1, Juli 2007.

[16] L. P. Rokhinson, L. N. Pfeiffer, and K. W. West. Spontaneous spin polarization in quantum point contacts. *Phys. Rev. Lett.*, 96(15):156602, 2006.

[17] P. Roche, J. Ségala, D. C. Glattli, J. T. Nicholls, M. Pepper, A. C. Graham, K. J. Thomas, M. Y. Simmons, and D. A. Ritchie. Fano factor reduction on the 0.7 conductance structure of a ballistic one-dimensional wire. *Physical Review Letters*, 93(11):116602, 2004.

[18] L. DiCarlo, Y. Zhang, D. T. McClure, D. J. Reilly, C. M. Marcus, L. N. Pfeiffer, and K. W. West. Shot-noise signatures of 0.7 structure and spin in a quantum point contact. *Physical Review Letters*, 97(3):036810, 2006.

[19] C. Karrasch, R. Hedden, R. Peters, Th Pruschke, K. Schonhammer, and V. Meden. A finite-frequency functional rg approach to the single impurity anderson model. *CONDENSED MATTER*, 20:345205, 2008.

[20] Henri Orland John W. Negele. *Quantum Many-Particle Systems*. Eddison-Wesley, 1988.

[21] L.P. Pitajewski E.M. Lifschitz. *L.D. Landau E.M. Lifschitz IX: Statistische Physik Teil 2 - Theorie des kondensierten Zustandes*. Akademie Verlag, 1992.

[22] Tilman Enss. *Renormalization, Conservation Laws and Transport in Correlated Electron Systems*. PhD thesis, University of Stuttgart, 2005. arXiv:cond-mat/0504703v1.

[23] A. Siddiki and F. Marquardt. Self-consistent calculation of the electron distribution near a quantum point contact in the integer quantum hall effect. *Physical Review B (Condensed Matter and Materials Physics)*, 75(4):045325, 2007.

[24] Francisco Guinea. Electronic dephasing in wires due to metallic gates. *Physical Review B (Condensed Matter and Materials Physics)*, 71(4):045424, 2005.

[25] G. Rickayzen. *Green's Function and Condensed Matter.* Academic Press Inc., 1980.

[26] S. Andergassen, T. Enss, V. Meden, W. Metzner, U. Schollwöck, and K. Schönhammer. Functional renormalization group for luttinger liquids with impurities. *Phys. Rev. B*, 70(7):075102, Aug 2004.

[27] S. Andergassen, T. Enss, V. Meden, W. Metzner, U. Schollwöck, and K. Schönhammer. Renormalization-group analysis of the one-dimensional extended hubbard model with a single impurity. *Physical Review B (Condensed Matter and Materials Physics)*, 73(4):045125, 2006.

[28] J. Zinn-Justin. *Quantum Field Theory and Critical Thenomena - 2nd ed.* Oxford University Press Inc., 1993.

[29] Christoph Karrasch. Transport through correlated quantum dots – a functional renormalization group approach. Master's thesis, Georg-August Universität Göttingen, 2006. arXiv:cond-mat/0612329v1.

[30] Ya. M. Blanter and M. Bttiker. Shot noise in mesoscopic conductors. *Physics Reports*, 336(1-2):1–166, September 2000.

[31] A. Rosch, T. A. Costi, J. Paaske, and P. Wölfle. Spectral function of the kondo model in high magnetic fields. *Phys. Rev. B*, 68(1):014430, Jul 2003.

[32] Joel E. Moore and Xiao-Gang Wen. Anomalous magnetic splitting of the kondo resonance. *Phys. Rev. Lett.*, 85(8):1722–1725, Aug 2000.

[33] Yunchul Chung, Sanghyun Jo, Dong-In Chang, Hu-Jong Lee, M. Zaffalon, V. Umansky, and M. Heiblum. Tunable 0.7 conductance plateau in quantum dots. *Physical Review B (Condensed Matter and Materials Physics)*, 76(3):035316, 2007.

Acknowledgements

First of all I want to thank my advisor Jan von Delft, who gave me the opportunity to work on this interesting topic in an open atmosphere at his chair. He understands it to let one work independently and giving the right advise at the right time. Thanks to his guidance I always found the right way to proceed with my work. Whenever I had the feeling to got stuck within the development of my work he was the one who encouraged me to keep on going and he always was right after all.

Special thanks goes to Andreas Weichselbaum, who helped me with all my Matlab problems. Furthermore he left his NRG code to me. Theresa Hecht was the one who helped me to produce data with this NRG code. Thanks for that. At this place I also want to thank Peter Fritsch who generously left his ODE-solver, written in c, to me, which I used to implement the fRG flow equations. He also helped me writing an efficient numeric code in c. Furthermore he made my PowerBook printing on the network printer. Thanks a lot, Peter.

An important role in gaining understanding of the essential physics played the senior members of our chair. Florian Marquardt, who gave an excellent lecture in mesoscopic physics. Due to him I was fascinated of this field, so I finally decided that I want to work within this field. Oleg Yevtushenko, who always had time for my questions. Here I again want to thank Theresa Hecht, she was the one, beside Jan, who taught me a good intuition for Kondo physics.

Special thanks goes also to Jan Heyder, for finding all the wrong minus signs and all the other mistakes in my thesis. I am looking forward to proceed my work on fRG with him. I thank Markus Hanl, who produced NRG data for my thesis in the last minute.

Thanks goes to Barbara Englert for the good Lindt chocolate, Alex "da Pirat" Buchner for "good" indian food, Max Treiber for buying always new milk, Pei Wang my office mate for giving me a little understanding for the Chinese culture, Markus Heyl my office mate for discussing mathematical problems, Wolfgang Münder for being married now, Korbinian Paul for conquering the Habicht with me, Björn Kubala, Max Ludwig and Clemens Neuenhahn for playing with me in the CeNS football team and of course to all the other group members Stefan Kehrein, Alexandre Faribault, Vitaly Golovach, Jiang Qian, Jerome Rech, Afif Siddiki, Benjamin Abel, Cheng Guo, Georg Heinrich, Ferdinand Helmer, Alexan-